

**Signalübertragungswege und  
Präventionsmöglichkeiten der kardialen  
Hypertrophie:**

**Conditional overexpression of neuronal nitric oxide  
synthase is cardioprotective in ischemia-reperfusion**

Dissertation zur Erlangung des  
naturwissenschaftlichen Doktorgrades  
der Bayerischen Julius-Maximilians-Universität Würzburg

vorgelegt von

Natalie Burkard

aus Würzburg

Würzburg 2010

eingereicht am: .....

Mitglieder der Promotionskommission:

Vorsitzender:

Gutachter:

Gutachter:

Tag des Promotionskolloquiums:

Doktorurkunde ausgehändigt am:

*To my husband Martin*

The present study was performed under the supervision of PD Dr. med. Oliver Ritter in the laboratory of Molecular Cardiology, Medicine Clinic and Policlinic I (Director Prof. Dr. G. Ertl) at the Julius-Maximilians-University of Würzburg.

**Erklärung gemäß § 4 Abs. 3 Promotionsordnung:**

Hiermit erkläre ich ehrenwörtlich, dass ich die vorliegende Arbeit selbständig angefertigt und keine anderen als die von mir angegebenen Quellen und Hilfsmittel benutzt habe.

Die Dissertation hat weder in gleicher noch in ähnlicher Form in einem anderen Prüfungsverfahren vorgelegen.

Ich habe bisher, außer den mit dem Zulassungsgesuch urkundlich vorgelegten Graden, keine weiteren akademischen Grade erworben oder zu erwerben versucht.

Würzburg, den

(Natalie Burkard)

## TABLE OF CONTENTS

Cover	1
Committee of Dissertation	2
Dedication	3
Declaration	4
Table of contents	5
Figures	10
Summary	12
Zusammenfassung	14
1. Introduction	16
1.1. Nitric oxide	16
1.2. Nitric oxide synthases (NOS)	17
1.2.1. Structure and catalysed reaction of NOS	18
1.2.2. The reductase and oxygenase domains	19
1.3. NOS isoforms	21
1.4. Neuronal nitric oxide synthase (nNOS)	23
1.5. Myocardial ischemia-reperfusion injury	25
1.6. Mitochondria	29
1.6.1. Mitochondria and ROS	29
1.6.2. Mitochondria and NO	32
1.7. Reduced nicotinamide adenine dinucleotide phosphate	

(NADPH) oxidase and xanthine oxidoreductase (XOR)	34
1.7.1. NADPH oxidase	34
1.7.2. XOR	37
1.8. Conditional nNOS overexpression impairs myocardial contractility	42
1.9. Aim of the study	51
2. Material	52
2.1. Equipment	52
2.2. Consumable material	53
2.2.1. Common consumable material	53
2.2.2. Chemicals	53
2.2.3. Enzymes	53
2.3. Working Kits	54
2.4. Solutions and buffers	54
2.4.1. DNA Electrophoresis	54
2.4.2. Western blotting	55
2.4.3. Electron microscopy	57
2.4.4. Immunofluorescence staining of isolated adult cardiac myocytes	57
2.4.5. Mitochondria isolation	60

2.4.6. Isolation of neonatal rat cardiomyocytes	61
2.4.7. O <sub>2</sub> -consumption	62
2.4.8. NADPH oxidase activity	63
2.5. Vectors	63
2.6. Oligonucleotides	64
2.7. Antibodies	65
2.8. Mouse strains	65
3. Methods	67
3.1. Animal model	67
3.2. Genotyping of double transgenic mice	68
3.3. Infarct size measurement after ischemia-reperfusion <i>in vivo</i>	70
3.4. <i>In vitro</i> ischemia-reperfusion experiments with isolated hearts (Langendorff)	71
3.5. Electron microscopy with immunogold labeling	71
3.6. Immunofluorescence staining of isolated adult cardiac myocytes	72
3.6.1. Preparation of adult cardiac myocytes	72
3.6.2. Immunostaining of cardiac myocytes	73
3.7. nNOS protein expression in isolated mitochondria	74
3.8. Coimmunoprecipitation experiments	75
3.9. Transfection of neonatal cardiomyocytes and treatment with geldanamycin	76
3.9.1. Isolation of neonatal cardiomyocytes	76

3.9.2. Transfection and treatment of neonatal cardiomyocytes	76
3.10. Nitrite level measurement	77
3.11. Cytochrome c oxidase activity	77
3.12. Myocardial O <sub>2</sub> -consumption	78
3.13. O <sub>2</sub> <sup>-</sup> production in isolated mitochondria	79
3.14. Reactive oxygen free radical (ROS)-concentration	80
3.15. NADPH oxidase and xanthine oxidoreductase activity	81
3.16. NADPH oxidase and XOR protein expression	81
3.17. Statistics	83
4. Results	84
4.1. nNOS overexpression reduced infarct size <i>in vivo</i> after ischemia-reperfusion injury	84
4.2. Recovery of left ventricular developed pressure (LVDP) after ischemia-reperfusion injury in isolated hearts (Langendorff)	86
4.3. nNOS protein expression in the mitochondria	88
4.4. Translocation of nNOS to mitochondria	98
4.5. nNOS impairs cytochrome c oxidase activity and nitrite levels	101
4.6. Myocardial oxygen consumption (MVO <sub>2</sub> )	104
4.7. Generation of reactive oxygen species (ROS) and O <sub>2</sub> <sup>-</sup> production	105
4.8. NADPH oxidase activity and XOR activity	108
4.9. NADPH oxidase subunits and XOR protein expression levels	110
5. Discussion	115



6. References	123
7. Abbreviations	143
8. Acknowledgements	146
9. Curriculum Vitae	147
10. Publications	149

**Figures:**

Figure 1	Domain structure of human nNOS, eNOS and iNOS	18
Figure 2	Two step synthesis of NO	19
Figure 3	Electron transfer in NOS reaction	21
Figure 4	Genomic organisation of human nNOS	24
Figure 5	Major mediator of lethal reperfusion injury	27
Figure 6	Main mechanism for mitochondrial ROS generation	31
Figure 7	Structure of the neutrophil NADPH oxidase	35
Figure 8	The purine degradation pathway	38
Figure 9	Gene structure of XOR, AO, SO	39
Figure 10	Crystal structure of bovine XOR homodimer	39
Figure 11	Mechanism of generation of ROS in ischemia-reperfusion injury	42
Figure 12	nNOS protein expression	43
Figure 13	NOS activity	44
Figure 14	Hemodynamics	45
Figure 15	Coimmunoprecipitation experiments	46
Figure 16	Calcium current density	47
Figure 17	Intracellular calcium transients	48
Figure 18	Fractional shortening	49
Figure 19	Scheme of gene regulation in the Tet-Off system	68
Figure 20	Oxygen measurement setup	79
Figure 21	Representative heart sections	85
Figure 22	Infarct area within AAR [%]	85
Figure 23	Area at risk [%]	86
Figure 24	Ischemia-reperfusion injury	87
Figure 25	Electron microscopy of mouse myocardium	89
Figure 26	Electron microscopy with two different antibodies	91
Figure 27	Immunofluorescence staining of isolated adult cardiac myocytes	92
Figure 28	nNOS protein expression in isolated mitochondria	93
Figure 29	Representative Western Blot of nNOS protein expression in isolated mitochondria	93
Figure 30	Protein expression of L-type Ca <sup>2+</sup> -channel	94
Figure 31	Protein expression of SERCA2a	94

Figure 32	Porin protein expression	95
Figure 33	Representative Western Blot of porin protein expression	95
Figure 34	Cytochrome c protein expression	96
Figure 35	Representative Western Blot of cytochrome c protein expression	96
Figure 36	nNOS protein expression in isolated mitochondria of WT mice after ischemia-reperfusion	97
Figure 37	Representative Western Blot of nNOS protein expression in isolated mitochondria of WT mice after ischemia-reperfusion	97
Figure 38	Coimmunoprecipitation of nNOS and HSP90	98
Figure 39	Coimmunoprecipitation of iNOS and HSP90	99
Figure 40	Coimmunoprecipitation of eNOS and HSP90	99
Figure 41	HSP90 dependency of mitochondrial nNOS translocation	100
Figure 42	Representative Western Blot of HSP90 dependency of mitochondrial nNOS translocation	100
Figure 43	Nitrite-level of isolated mitochondria	101
Figure 44	Cytochrome c oxidase activity	102
Figure 45	Cytochrome c oxidase rate of nNOS overexpressing mice	102
Figure 46	Cytochrome c oxidase rate of non-induced mice	103
Figure 47	Myocardial oxygen consumption at rest	104
Figure 48	Myocardial oxygen consumption at work	105
Figure 49	O <sub>2</sub> <sup>-</sup> production in isolated mitochondria	106
Figure 50	ROS concentration	107
Figure 51	ROS concentration in non-induced animals	107
Figure 52	ROS concentration in nNOS overexpressing animals	108
Figure 53	NADPH oxidase activity	109
Figure 54	Xanthine oxidoreductase activity	109
Figure 55	rac 1 protein expression	111
Figure 56	Representative Western Blot of rac 1 protein expression	111
Figure 57	p47 <sup>PHOX</sup> protein expression	112
Figure 58	Representative Western Blot of p47 <sup>PHOX</sup> protein expression	112
Figure 59	p67 <sup>PHOX</sup> protein expression	113
Figure 60	Representative Western Blot of p67 <sup>PHOX</sup> protein expression	113
Figure 61	XOR protein expression	114
Figure 62	Representative Western Blot of XOR protein expression	114

---

**Summary:**

I previously demonstrated that conditional overexpression of the neuronal nitric oxide synthase (nNOS) inhibited L-type  $\text{Ca}^{2+}$ -channels and decreased myocardial contractility<sup>1</sup> (Burkard N. et al. (2007). *Circ Res* 100, 32-44). However, nNOS has multiple targets within the cardiac myocyte and it is possible that interesting biological functions of this protein remain to be elucidated. In this study, I showed that nNOS overexpression has a cardioprotective effect after ischemia-reperfusion injury by inhibiting mitochondrial function and reducing the generation of reactive oxygen species (ROS).

The effect of conditional nNOS overexpression in cardiac myocytes in ischemia-reperfusion injury was assessed. Ischemia-reperfusion injury in WT mice resulted in nNOS accumulation in the mitochondria. Similarly, transgenic nNOS overexpression caused nNOS abundance in mitochondria. Electron microscopy of mouse myocardium from nNOS overexpressing mice showed that after induction of its expression, nNOS is additionally localised in mitochondria. nNOS translocation into mitochondria was dependent on HSP90. Ischemia-reperfusion experiments in isolated hearts showed a cardioprotective effect of nNOS overexpression (30min post-ischemia, LVDP  $27.0 \pm 2.5$  mmHg in non-induced animals vs.  $45.2 \pm 1.9$  mmHg in nNOS overexpressing mice,  $n=12$ ,  $p < 0.05$ ). Consistently with this finding, *in vivo* the infarct size within the area at risk was significantly decreased in nNOS overexpressing mice compared to non-induced animals ( $36.6 \pm 8.4$  relative % vs.  $61.1 \pm 2.9$  relative %,  $n=12$ ,  $p < 0.05$ ). nNOS overexpression also caused a significant increase in mitochondrial nitrite levels accompanied by a decrease of cytochrome c oxidase activity ( $72.0 \pm 8.9$  units/ml in nNOS overexpressing mice vs.  $113.2 \pm 17.1$  units/ml in non-induced mice,  $n=12$ ,  $p < 0.01$ ) resulting in an inhibition of mitochondrial function. Accordingly,  $\text{O}_2$ -consumption ( $\text{MVO}_2$ ) in isolated heart muscle stripes was decreased in nNOS overexpressing mice, already under resting conditions ( $0.016 \pm 0.0015$  vs.  $0.024 \pm 0.006$  ml $[\text{O}_2]$  x  $\text{mm}^{-3}$  x  $\text{min}^{-1}$ ,  $n=13$ ,  $p < 0.05$ ). Additionally, this study showed that the ROS concentration was significantly

decreased in hearts of nNOS overexpressing mice compared to non-induced animals ( $6.14 \pm 0.685$  vs.  $14.53 \pm 1.7 \mu\text{M}$ ,  $n=8$ ,  $p < 0.01$ ). Application of different inhibitors, Western Blot analysis and activity assays showed that the lower ROS concentration in nNOS overexpressing mice was caused by inhibition of the xanthine oxidoreductase (XOR) activity by the increased abundance of nNOS expression.

In summary, this study demonstrated that the conditional transgenic overexpression of nNOS resulted in myocardial protection after ischemia-reperfusion injury. Besides reduction of myocardial  $\text{Ca}^{2+}$ -overload after reperfusion this might be caused by inhibition of mitochondrial function through nNOS, which reduced myocardial oxygen consumption already under baseline conditions (Burkard N. conditionally accepted by Circ).

**Zusammenfassung:**

Wie früher schon gezeigt, wird der L-Typ  $\text{Ca}^{2+}$ -Kanal durch eine induzierbare, myokardspezifische Überexpression der neuronalen Stickstoffmonoxidsynthase (nNOS) inhibiert. Gleichzeitig bewirkt diese Überexpression eine verminderte kardiale Kontraktilität<sup>1</sup> (Burkard N. et al. (2007). *Circ Res* 100, 32-44). nNOS interagiert mit vielen verschiedenen Kompartimenten und Kanälen innerhalb der Zelle. In dieser Arbeit wurde gezeigt, dass eine nNOS Überexpression nach Ischämie-Reperfusion kardioprotektiv wirkt. Dieses wird durch eine Inhibition der Mitochondrienfunktion und durch eine Verminderung der reaktiven Sauerstoffspezies (ROS) ermöglicht.

In einer früheren Arbeit wurde der Effekt der induzierbaren und myokardspezifischen Überexpression von nNOS unter physiologischen Bedingungen am transgenen Tiermodell untersucht. Diese Arbeit beschäftigt sich nun mit der Überexpression von nNOS unter pathophysiologischen (Ischämie-Reperfusion) Bedingungen. Ein Ischämie-Reperfusionsschaden bewirkt bei Wildtyp-Mäusen, sowie bei transgener nNOS Überexpression eine Anreicherung von nNOS in den Mitochondrien. Elektronenmikroskopische Aufnahmen von Mausmyokard haben gezeigt, dass bei Überexpression nNOS zusätzlich in den Mitochondrien lokalisiert ist. Diese Translokation von nNOS in die Mitochondrien ist abhängig von HSP90. Ischämie-Reperfusionsexperimente an isolierten Mäuseherzen zeigten einen kardioprotektiven Effekt der nNOS Überexpression (30min post ischemia, LVDP  $27.0 \pm 2.5$  mmHg vs.  $45.2 \pm 1.9$  mmHg,  $n=12$ ,  $p<0.05$ ). Dieser positive Effekt konnte bei der Bestimmung der Infarktgröße bestätigt werden. nNOS überexprimierende Mäuse hatten eine kleinere Infarktgröße nach Ischämie-Reperfusion ( $36.6 \pm 8.4$  relative % vs.  $61.1 \pm 2.9$  relative %,  $n=8$ ,  $p<0.05$ ). Die Überexpression von nNOS bewirkte ebenfalls einen signifikanten Anstieg des mitochondrialen Nitrit-Niveaus, begleitet von einer Verminderung der Cytochrom C Oxidase Aktivität ( $72.0 \pm 8.9$  units/ml in nNOS overexpressing mice vs.  $113.2 \pm 17.1$  units/ml in non-induced mice,  $n=12$ ,  $p<0.01$ ), was zu einer Hemmung der Mitochondrienfunktion führt. Dementsprechend war der Sauerstoffverbrauch (gemessen an isolierten Herzmuskelstreifen) schon unter basalen Bedingungen bei

nNOS Überexpression vermindert ( $0.016 \pm 0.0015$  vs.  $0.024 \pm 0.006 \text{ ml}[\text{O}_2] \times \text{mm}^{-3} \times \text{min}^{-1}$ ,  $n=13$ ,  $p<0.05$ ). Außerdem war die ROS Konzentration in Herzen von nNOS überexprimierenden Mäusen signifikant vermindert ( $6.14 \pm 0.685$  vs.  $14.53 \pm 1.7 \mu\text{M}$ ,  $n=8$ ,  $p<0.01$ ). Die Zugabe von verschiedenen Inhibitoren, Western Blot- und Aktivitätsuntersuchungen zeigten schließlich, dass diese niedrigere ROS Konzentration durch eine verminderte Xanthin Oxidoreduktase Aktivität hervorgerufen wurde.

Zusammenfassend hat diese Arbeit gezeigt, dass eine induzierbare und myokardspezifische Überexpression von nNOS unter pathophysiologischen Bedingungen (Ischämie-Reperfusion) kardioprotektiv wirkt. Zusätzlich zu der Verminderung des myokardialen  $\text{Ca}^{2+}$ -Überschusses nach Reperfusion könnte dieser protektive Effekt durch eine Hemmung der Mitochondrienfunktion bedingt sein, schließlich wird der Sauerstoffverbrauch schon unter basalen Bedingungen reduziert (Burkard N. unter Vorbehalt akzeptiert durch Circ).

## 1. Introduction:

### 1.1. Nitric oxide:

Nitric oxide (NO) is an ubiquitous intra- and intercellular signaling molecule generated by a family of NO synthases (NOSs), which catalyses the conversion of the amino acid L-arginine to L-citrulline in a reaction that requires O<sub>2</sub> and cofactors. NO is a member of the labile radical entities known as reactive oxygen species (ROS) and contains 1 nitrogen atom covalently bound to an oxygen atom with 1 unpaired electron. It is particularly reactive with oxygen and haem-iron containing groups, which reduce NO to more stable nitrate compounds<sup>2</sup>. For this reason, the bioavailability of NO in certain tissues<sup>3</sup> is extremely low and the biological actions are restricted temporally and spatially close to its site of synthesis. NO is also lipid-soluble, making it highly membrane permeant<sup>4</sup>. Therefore, many of its well-described actions involve its diffusion between cells to act as a paracrine-signaling molecule. This makes quantifying NO with the respecting functional correlation to its signaling a difficult task. The term NO “bioavailability” is often used to quantify the functional potential for endogenously synthesised NO in any tissue at any time. These contradictory properties of NO may be appropriate to its functional roles within the heart, where discrete NO-producing microdomains are flanked by myoglobin-rich, NO-scavenging ones, thus making its biological action more site-specific. After synthesis, NO has a number of different fates.

NO was shown to signal through at least two distinct pathways: cGMP-dependent and cGMP-independent<sup>5</sup>. The cGMP-dependent effects of NO result from the NO-induced activation of guanylate cyclase, leading to increased cGMP levels, which modulate the activity of protein kinase G (PKG), as well as cGMP-regulated phosphodiesterases (PDE; cGMP-stimulated: PDE2; cGMP-inhibited: PDE3). cGMP-independent effects occur mainly via S-nitrosylation, an important protein modification related to cell signaling<sup>6</sup>. NO can also directly activate adenylate cyclase, thus increasing cAMP levels and myocardial contractility<sup>7</sup>. Additionally, NO may couple to other reactive oxygen and nitrogen species, leading to formation of



related compounds, such as peroxynitrite (ONNO<sup>-</sup>). These related species may also influence cardiac contractility, and in some cases produce markedly differing effects from those observed with NO alone. Therefore, it is not surprising that paradoxical results have been reported in the literature, as both positive and negative effects of NO and related compounds have been observed. Recent studies are resolving these contradictions by determining that the contractile effects of NO are greatly influenced by NOS isoform localisation<sup>8,9</sup>, and the activation of distinct cGMP-dependent and cGMP-independent signaling pathways which target individual excitation-contraction coupling (ECC) proteins in the cardiac myocyte. Additional studies have determined that these contractile effects are further confounded by such factors as gender<sup>10</sup>, site of production<sup>11,12</sup>, species produced<sup>13,14,15</sup>, concentration<sup>13,16</sup>, and cardiac myocyte contractile state<sup>13,14</sup>. These factors are relevant to the contractile effects of NO and related congeners during both, health and disease, and are sensitive to cellular redox state.

However, recent studies are beginning to resolve these apparent controversies, and although conflicting reports regarding NO signaling exist, these results indicate that NO does indeed play a key role regarding myocardial function, and my study will make a contribution to this large field.

## 1.2. Nitric oxide synthases (NOS):

In mammals, NO is synthesised enzymatically from L-arginine through the actions of the nitric oxide synthases (NOSs). The three known NOS isoforms are all dimeric, bi-domain enzymes that contain iron protoporphyrin IX, flavin adenine dinucleotide (FAD), flavin mononucleotide (FMN), and tetrahydrobiopterin (BH<sub>4</sub>) as bound prosthetic groups.

### 1.2.1. Structure and catalysed reaction of NOS:

The three distinct genes for human neuronal (nNOS), inducible (iNOS) and endothelial NOS (eNOS) isoforms exist, with a single copy of each in the haploid genome<sup>17,18,19,20,21,22,23</sup>. The NOS genes have a similar genomic structure, suggesting a common ancestral NOS gene. NOSs exhibit a bidomain structure in which a N-terminal oxygenase domain containing binding site for haem, BH<sub>4</sub> and L-arginine is linked via a calmodulin (CaM)-recognition site to a C-terminal reductase domain that contains binding sites for FAD, FMN and nicotinamideadeninedinucleotidphosphate (NADPH) (figure 1).

**Figure 1: Domain structure of human nNOS, eNOS and iNOS:**

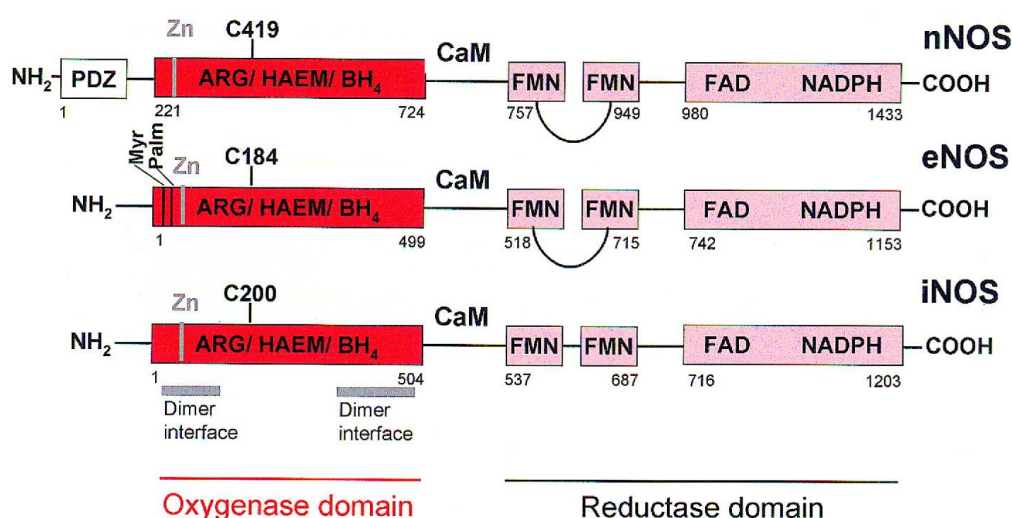


**Figure 1 legend: Domain structure of human nNOS, eNOS and iNOS**

Oxygenase, reductase and PDZ domains are denoted by solid boxes, the amino acid residue number at the start/end of each domain is shown. The cysteine residue which ligates the haem and CaM-binding site is indicated for each isoform. Myristoylation (Myr) and palmitoylation (Palm) sites on eNOS and the location of the zinc-ligating cysteines (in grey) are shown. The autoinhibitory loop within the FMN regions of nNOS and eNOS are also shown, grey bars indicate the dimer interface within the oxygenase domain (adapted from Alderton W.K., 2001).

Biosynthesis of NO involves a two step oxidation of L-arginine to L-citrulline, with concomitant production of NO (figure 2).

**Figure 2: Two step synthesis of NO:**

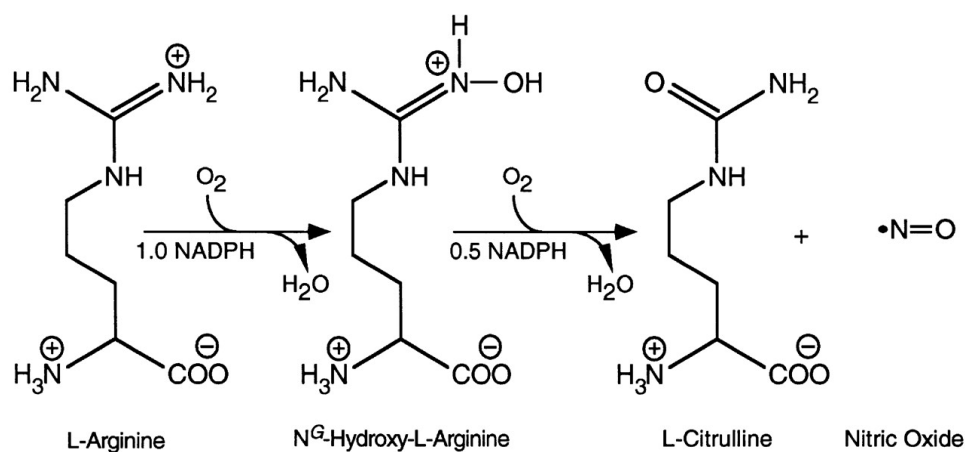


**Figure 2 legend: Two step synthesis of NO**

The two reactions of NO synthesis as catalysed by NOS. The NADPH and oxygen requirements for each reaction are shown (adapted from Andrew P.J., 1999).

The reaction consumes 1.5mol NADPH and 2mol of oxygen per mol of L-citrulline formed. The proposed mechanisms involve an initial hydroxylation of L-arginine, leading to the formation of N<sup>G</sup>-hydroxy-L-arginine, which can also act as a substrate for NOS. This is followed by oxidation of the intermediate, using a single electron from NADPH<sup>24</sup>, to form L-citrulline and NO. Although this scheme represents the assumed reaction catalysed by NOS, the enzyme is also capable of catalysing the production of additional products, notably superoxide anion (O<sub>2</sub><sup>-</sup>).

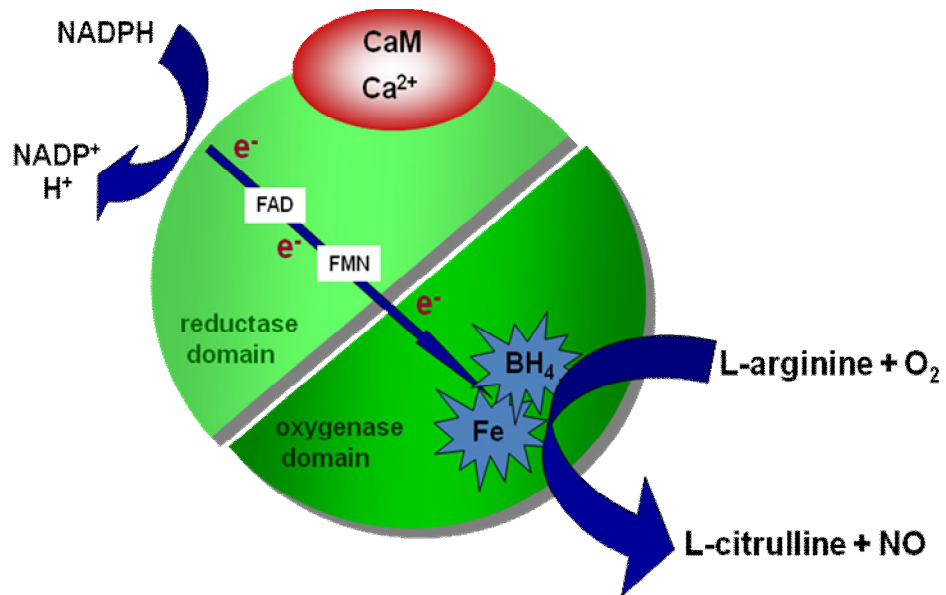
### 1.2.2. The reductase and oxygenase domains:

These two domains perform catalytically distinct functions. While the isolated reductase domain is able to transfer electrons from NADPH to cytochrome c via the flavins FAD and FMN, the oxygenase domain dimer can convert the reaction of the

intermediate N<sup>G</sup>-hydroxy-L-arginine to NO and L-citrulline<sup>25,26,27</sup>. The reductase domain itself is highly homologous to enzymes such as the NADPH:cytochrome P450 reductase and its dependence on the CaM-binding domain for efficient electron transfer is unique<sup>28</sup>. The cofactor binding sites have been well-defined as a result of their close homology with related reductases as well as evidence obtained from mutagenesis studies<sup>29,30,31</sup>. In contrast, the binding sites for L-arginine, haem, and BH<sub>4</sub> in the oxygenase domain are less well characterised. Two residues important for L-arginine binding have been identified in this region: E371 and D376 in iNOS<sup>32</sup>, and the analogous E361 in eNOS<sup>33</sup>. Several other acidic residues which affect L-arginine and BH<sub>4</sub> binding, were also identified within this region<sup>33</sup>. The crystal structure of a dimeric iNOS oxygenase truncation mutant (residues 66-498) revealed a structure which is unusual for haem-binding proteins in that it contains a large amount of β-sheets<sup>34</sup>. The authors describe the structure in analogy with a baseball glove, with the haem cradled between the proximal “thumb” and the distal “palm”. BH<sub>4</sub> binds on the proximal side, while L-arginine is located on the distal side. Another notable feature of the oxygenase domain dimer is the presence of a zinc atom which is tetrahedrally coordinated to two pairs of cysteine (Cys) residues. The metal may be important in determining the spectroscopic specificity of the BH<sub>4</sub> binding site.

The reductase and oxygenase domains of NOS are therefore distinct catalytic units, which together provide the complete machinery required for NO production.

The intact NOS function is a mix of both, monooxygenase and reductase reaction. In all NOS reactions, electrons are sequentially shuttled within the reductase domain from NADPH to FAD and finally to FMN. Calmodulin is believed to function in facilitating the flow of electrons from the reductase domain to the monooxygenase domain as well as from FAD to FMN<sup>35</sup>. Because electrons appear to flow from the reductase domain to another NOS monomer, enzyme dimerisation is required for full enzyme activity<sup>36</sup> (figure 3).

**Figure 3: Electron transfer in NOS reaction:****Figure 3 legend: Electron transfer in NOS reaction**

Electrons ( $e^-$ ) are donated by NADPH to the reductase domain of the enzyme and proceed to the oxygenase domain via FAD and FMN redox carriers. There they interact with the haem iron and tetrahydrobiopterin ( $BH_4$ ) at the active site to catalyse the reaction of oxygen with L-arginine, generating L-citrulline and NO as products. Electron flow through the reductase domain requires the presence of bound  $Ca^{2+}$ /Calmodulin (CaM) (modified from Alderton W.K., 2001).

### 1.3. NOS isoforms:

Three NOS isoforms have been identified: nNOS, iNOS and eNOS.

The three isoforms are products of distinct genes but share approximately 50-60% sequence identity. Although these isoforms share similar overall enzymatic and chemical properties, distinctive catalytic and regulatory properties are characteristic for each of the different isoforms.

The chromosomal location of the nNOS, eNOS and iNOS genes has been determined by Southern blotting analysis of a panel of human-rodent hybrid cell lines, using isoenzyme-specific cDNA probes. The nNOS gene appears to be an intron-containing gene of at least 20kb, and is unequivocally localised at a single position

on the human chromosome 12<sup>37,38</sup>. The eNOS gene maps to chromosome 7<sup>39</sup>. In contrast to nNOS and eNOS, iNOS cDNA probes identify several positive hybridisation signals, located on either side of the centromere of chromosome 17<sup>39</sup>. It is not clear whether these codes for alternative forms of iNOS or whether some are intronless pseudogenes. The NO synthase genes therefore represent a dispersed gene family on three different chromosomes.

eNOS and nNOS are constitutively expressed and activated by an increase of intracellular calcium levels. The expression of iNOS is induced by inflammatory stimuli and its activation is calcium independent. iNOS can be expressed ubiquitously and generates high levels of NO. Once iNOS is expressed, it is continuously active (unlike the constitutive NOS isoforms, which are more tightly regulated). Differential expression and regulation of this family of NOS genes and their products is the key for achieving the diverse actions of NO. The most fundamental level of NOS regulation is reflected in the tissue-specific expression of the different isoforms. nNOS is widely expressed in neurons of the central and peripheral nervous system, but is also found in skeletal muscle, the adventitial layer of some blood vessels, pulmonary epithelium, the gastrointestinal system, and the genitourinary system. iNOS was first recognised in activated macrophages, but has since been identified in numerous activated cell types including monocytes, neutrophils, eosinophils, hepatocytes, vascular smooth muscle, myocytes, osteoblasts, fibroblasts, epithelium, and endothelium. eNOS is expressed in vascular endothelium as well as blood platelets and cardiac myocytes. As originally identified, eNOS and nNOS were believed to be only constitutively expressed in their characteristic tissue, whereas expression of iNOS was inducible upon immunoactivation, for example, in response to LPS, interferon  $\gamma$ , TNF- $\alpha$ , and IL-1. However, nNOS is known to be upregulated in diverse tissue models, including cutaneous wound repair and ischemic preconditioning<sup>40,41</sup>. Similarly, eNOS transcription can be actively modulated in endothelial cells, for example, in response to laminar stress, regulated in part by the transcriptional factor KLF2<sup>42,43</sup>. The rho/rho kinase pathway is another mediator of eNOS transcription, and it may function in a variety of cardiovascular physiologic and

pathophysiologic states<sup>44</sup>. rho represents a family of small GTPases anchored to membranes by geranylgeranyl anchors. rho regulates the rho kinase, which helps to modulate and reorganise the actin cytoskeleton by inhibiting myosin light-chain phosphatase<sup>45</sup>. The rho-mediated effects on the actin cytoskeleton have been connected to modulating gene expression of a number of proteins, including eNOS. Thus, all three NOS isoforms exhibit inducible and constitutive patterns of expression in different tissue environments.

#### 1.4. nNOS:

The human nNOS gene maps to the q14-qter region of chromosome 12<sup>37</sup>, with homologous genes on chromosome 5 of the mouse genome<sup>46</sup> and chromosome 12 in the rat<sup>47</sup>. The locus of the human nNOS gene is scattered over 200 kb and the mRNA transcript found in neuronal tissue is encoded by 29 exons (1434 AA, 160 kDa). Analyses of intron-exon splice junctions predicted that the open reading frame is encoded by 28 exons, with translation initiation and termination in exon 2 and exon 29. Genotypic analyses have demonstrated multiple alleles, mainly resulting from transcription using alternative promoters. These are also subjects to posttranscriptional modifications including cassette exon deletion or insertion to give the well-described splice variants nNOS $\alpha$  (155kDa), nNOS $\beta$  (136kDa), nNOS $\gamma$  (125kDa) and nNOS-2 (105kDa). Although numerous other variants have been found, nNOS $\alpha$  is the most commonly expressed variant in striated muscle and neuronal tissue. Mature skeletal muscle<sup>48</sup>, human and rat penis and urethra<sup>49</sup> express the nNOS $\mu$  variant (164 kDa) following exon insertion between the calmodulin and flavin-binding domains. nNOS $\beta$  and nNOS $\gamma$  are derived from transcripts following deletion of exon 2, which encodes the postsynaptic density protein 95/discs-large/zona occludens-1 (PDZ) binding domain, which precludes this variant from associating with synaptic membranes<sup>50</sup>. Furthermore, of all these splice variants, additional variation in size exists owing to different numbers of CA/TG

dinucleotide repeats in the 5' flanking region<sup>18</sup>. It is thought that variation of this kind allows for differences in basal promoter activity<sup>51</sup> (figure 4).

**Figure 4: Genomic organisation of the human nNOS:**

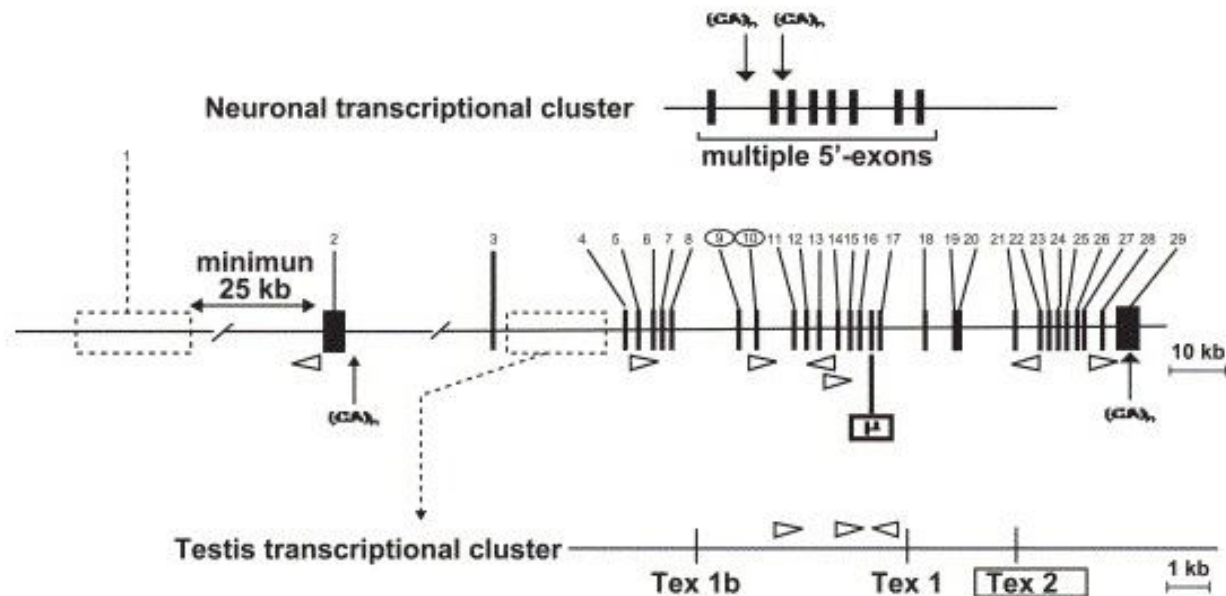


**Figure 4 legend: Genomic organisation of the human nNOS**

The nucleotide sequence corresponding to the major neuronal mRNA transcript is encoded by 29 exons. Many exons are of relatively small size, ranging from 59 to 266 bp. Two described transcriptional clusters (neuronal and testis specific) are shown above and below the genomic map. Due to the presence of multiple promoters and transcription start sites, different first exons (5' exons) can be used. All first exons of the neuronal cluster seem to splice to the common exon 2; therefore, one unique translation product corresponding to the full-length protein is likely to be assembled. Transcription from the testis-specific cluster, located between exon 3 and exon 4, gives rise to mRNA transcripts encoding for NH<sub>2</sub>-truncated enzymes. Possible cassette exon deletions of exon 10 or exon 9 and 10 are circled. Reported cassette exon insertions in the full-length nNOS are boxed: Tex 2 from the testis transcriptional cluster and the nNOS<sub>μ</sub> insert located between exon 16 and 17 of the human nNOS. Locations for the respective elements are indicated; the human gene contains three sets of dinucleotide CA repeats and one (CG)<sub>n</sub> island. Members of the Alu repetitive sequences, indicated by triangles, are also found scattered at several locations along the human nNOS gene (adapted from Danson E.J., 2005).



### 1.5. Myocardial ischemia-reperfusion injury:

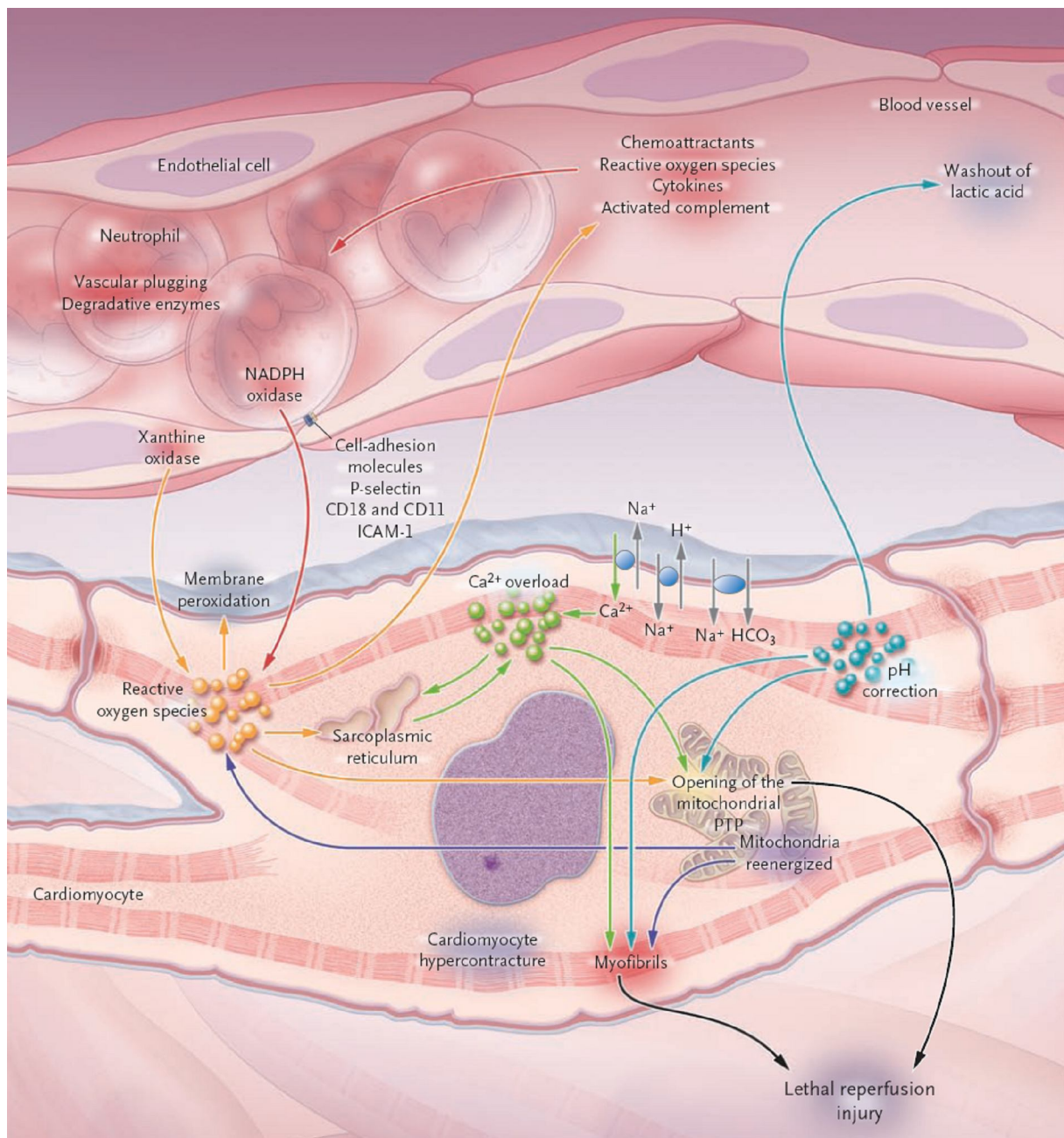
Coronary heart disease is the leading cause of death worldwide and 3.8 million men and 3.4 million women die of the disease each year. After an acute myocardial infarction (MI), an early successful myocardial reperfusion with the use of thrombolytic therapy or primary percutaneous coronary intervention (PCI) is the most effective strategy for reducing infarct size and improving clinical outcome. The process of restoring blood flow to the ischemic myocardium, however, can induce injury. This phenomenon, termed myocardial reperfusion injury, can paradoxically reduce the beneficial effects of myocardial reperfusion.

Myocardial reperfusion injury was first postulated in 1960 by Jennings et al.<sup>52</sup> in their description of the histologic features of reperfused ischemic canine myocardium. They reported cell swelling, contracture of myofibrils, disruption of the sarcolemma, and the appearance of intramitochondrial calcium phosphate particles. The injury to the heart during myocardial reperfusion causes four types of cardiac dysfunction. The first type is myocardial stunning, a term denoting the “mechanical dysfunction that persists after reperfusion despite the absence of irreversible damage and despite restoration of normal or near-normal coronary flow”<sup>53</sup>. The myocardium usually recovers from this reversible form of injury after several days or weeks. The second type of cardiac dysfunction, the no-flow phenomenon, was originally defined as the “inability to reperfuse a previously ischemic region”<sup>54</sup>. It refers to the impedance of microvascular blood flow encountered during opening of the infarct-related coronary artery<sup>55</sup>. The third type of cardiac dysfunction, reperfusion arrhythmias, is potentially harmful, but effective treatments are available<sup>56</sup>. The last type is lethal reperfusion injury. There are several comprehensive reviews of myocardial stunning<sup>57</sup>, the no-flow phenomenon<sup>55</sup>, and reperfusion arrhythmias<sup>56</sup>.

The concept of lethal reperfusion injury as an independent mediator of cardiomyocyte death, distinct from ischemic injury has been extremely debated. Some researchers have suggested that reperfusion only exacerbates the cellular injury that was sustained during the ischemic period<sup>58</sup>. The uncertainty relates to the inability to

accurately assess the progress of necrosis during the transition from myocardial ischemia to reperfusion *in situ*<sup>59</sup>. As a result, the most convincing means of showing the existence of lethal reperfusion injury as a distinct mediator of cardiomyocyte death is to show that the size of myocardial infarction can be reduced by an intervention used at the beginning of myocardial reperfusion<sup>59,60</sup>.

Experimental studies have established that the reperfusion of ischemic myocardium generates oxidative stress, which itself can mediate myocardial injury<sup>61</sup>. Oxidative stress during myocardial reperfusion also reduces the bioavailability of the intracellular signaling molecule NO, thereby removing its cardioprotective effects. These effects include the inhibition of neutrophil accumulation, inactivation of superoxide radicals, and improvement of coronary blood flow<sup>62</sup> (figure 5). NO reperfusion therapy to increase NO levels can reduce the size of myocardial infarction in animals<sup>63</sup>.

**Figure 5: Major mediators of lethal reperfusion injury:****Figure 5 legend: Major mediators of lethal reperfusion injury**

During myocardial reperfusion, the acute ischemic myocardium is subjected to several abrupt biochemical and metabolic changes, which compound the changes generated during the period of myocardial ischemia. These changes include mitochondrial re-energisation (purple), the generation of ROS (orange), intracellular Ca<sup>2+</sup>-overload (green), the rapid

restoration of physiologic pH (blue), and inflammation (red). All of these changes interact with each other (adapted from Yellon D.M., 2007).

The biochemical and metabolic changes during myocardial reperfusion mediate cardiomyocyte death through the opening of the mitochondrial permeability transition pore (PTP) and the induction of cardiomyocyte hypercontracture. During myocardial reperfusion, ROS are generated by XOR (mainly from endothelial cells) and the re-energised electron transport chain in the cardiomyocyte mitochondria. Several hours later, a further source of ROS is the NADPH oxidase (mainly from neutrophils). ROS mediate myocardial injury by inducing mitochondrial PTP opening, acting as neutrophil chemoattractants, mediating dysfunction of the sarcoplasmic reticulum and contributing to intracellular  $\text{Ca}^{2+}$ -overload, damaging the cell membrane by lipid peroxidation, inducing enzyme denaturation, and causing direct oxidative damage to DNA. During myocardial reperfusion, the already  $\text{Ca}^{2+}$ -overloaded cardiomyocyte is subjected to a further influx of  $\text{Ca}^{2+}$  through a damaged sarcolemmal membrane, ROS mediated dysfunction of the sarcoplasmic reticulum, and reverse function of the  $\text{Na}^+$ - $\text{Ca}^{2+}$  exchanger. The generation of ATP by the re-energised electron transport chain in the setting of intracellular  $\text{Ca}^{2+}$ -overload induces cardiomyocyte death via hypercontraction a process that is facilitated by the rapid restoration of physiologic pH during myocardial reperfusion. Furthermore, the restoration of the mitochondrial membrane potential drives the entry of  $\text{Ca}^{2+}$  into the mitochondria which, in conjunction with the loss of the inhibitory effect of the acidic pH on the mitochondrial PTP and the generation of ROS, act together to mediate the opening of the mitochondrial PTP. This opening induces cardiomyocyte death by uncoupling oxidative phosphorylation and inducing mitochondrial swelling. During myocardial reperfusion, the rapid washout of lactic acid together with the function of  $\text{Na}^+$ - $\text{H}^+$  and  $\text{Na}^+$ - $\text{HCO}_3^-$  transporters mediate the rapid restoration of physiologic pH, facilitating mitochondrial PTP opening and cardiomyocyte hypercontracture. Several hours after the onset of myocardial reperfusion, neutrophils accumulate in the infarcted myocardial tissue in response to the release of chemoattractants (ROS, cytokines,

and the activated complement). The up-regulated cell-adhesion molecules P-selectin, CD18 and CD11, and intracellular adhesion molecule 1 (ICAM 1) then facilitate the migration of neutrophils into the tissue, where they mediate cardiomyocyte death by causing vascular plugging, releasing degradative enzymes, and generating ROS.

## 1.6. Mitochondria:

### 1.6.1. *Mitochondria and ROS:*

Mitochondria are the main source for ATP used by eukaryotic cells in the course of cellular function. One consequence of mitochondrial function is the production of ROS during physiological and pathophysiological states. This process has been extensively studied because ROS have a major role in mediating functional alterations of cell physiology in inflammation, ischemia, aging and other conditions<sup>64,65,66</sup>. There is also an emerging field of studies of ROS control in cellular functions<sup>67</sup>.

ROS refer to a group of oxygen containing compounds with the ability to react with reducible compounds: They comprise superoxide ( $O_2^- \bullet$ ), hydrogen peroxide ( $H_2O_2$ ), and the highly reactive hydroxyl radical ( $\bullet OH$ ), although minor amounts of single oxygen can also be formed by cells.

The initial product of the electron transport chain (ETC) is  $O_2^- \bullet$ , which is quickly transformed into  $H_2O_2$  by the enzyme superoxide dismutase (SOD).  $H_2O_2$  can be reduced to water by catalase or glutathione peroxidase or can be converted into  $\bullet OH$  in presence of reduced transition metals (reduced copper or iron).

The main source of  $O_2^- \bullet$  are the respiratory complexes I and III which are located at the inner mitochondrial membrane<sup>65,68,69</sup>. These complexes generate a small amount of  $O_2^- \bullet$  as a side product of electron transport during oxidative phosphorylation.  $O_2^- \bullet$  is released into the matrix in the case of complex I and to both, the matrix and the intermembranous space by complex III. Complex III forms  $O_2^- \bullet$  during cycling of the

electron acceptor ubiquinone, which can donate electrons to molecular oxygen in both, the internal and external face of the inner mitochondrial membrane.

The relative importance of these sites in  $O_2^- \bullet$  mitochondrial output depends on tissue and mitochondria respiratory status. For example, in fully respiring mitochondria from heart muscle (characterised by high electron flow, fast ATP synthesis, partial depolarisation, and a decreased NADH-to-NAD<sup>+</sup> ratio), complex III seems to be dominant, and the generation of  $O_2^- \bullet$  is proportional to the electron flow rate<sup>70</sup>. In this situation oxygen, reduced substrates, and downstream electron acceptors are needed. Therefore, inhibition of electron flow into the ubiquinone cycle of complex III (by inhibition of complex I with rotenone, blockade of the cycle with myxothiazol, or inhibition of downstream electron acceptor cytochrome c reduces  $O_2^- \bullet$  generation, whereas antimycin enhances it by building up the partially reduced form of ubiquinone (figure 6)).

Complex I is the main source of  $O_2^- \bullet$ , when electron transport rate and ATP synthesis are low and substrates are highly reduced (high NADH-to-NAD<sup>+</sup> ratio). The redox potential of complex I seems to be even higher than the NADH/NAD<sup>+</sup> couple, which renders it a thermodynamically unstable center prone to electron leakage to oxygen<sup>71</sup>. In this center,  $O_2^- \bullet$  production is increased in any situation leading to reduction of ETC components (for example, by application of rotenone, which blocks complex I distal to the  $O_2^- \bullet$  production point, or inhibition of electron flow at the level of cytochrome c.

Superoxide anions in the mitochondrial matrix are quickly dismutated by manganese-containing SOD, whereas those in the intermembranous space are converted by Zn- or Cu-SOD<sup>69</sup>. If the  $O_2^- \bullet$  concentration in the matrix is high enough, part of the anion escapes to the intermembranous space and cytosol via anion channels<sup>72</sup>.

The mechanisms described above are supported by experimental results from isolated mitochondria studies. Results from mitochondria in intact living cells support a main role of complex III as ROS source in several systems. This is based on the

fact that rotenone or myxothiazol can impair ROS production in active cells<sup>72,73,74,75</sup>. Cellular stimulation leads to fast increase of reduced substrates derived from the Krebs cycle (NADH and FADH<sub>2</sub>) in the mitochondrial matrix, which has been related to cytosolic calcium concentration ([Ca<sup>2+</sup>]<sub>i</sub>) increases within mitochondria<sup>76,77,78,79</sup>. At the same time this situation will favour increased electron flow and the rate of ATP demand (used for Ca<sup>2+</sup> homeostasis, contraction, exocytosis, etc.), which would facilitate ROS production at complex III<sup>80</sup>. Several systems have been reported to increase ROS generation in response to a variety of stimuli<sup>74,81,82,83,84,85,86,87,88</sup>.

**Figure 6: Main mechanism for mitochondrial ROS generation:**

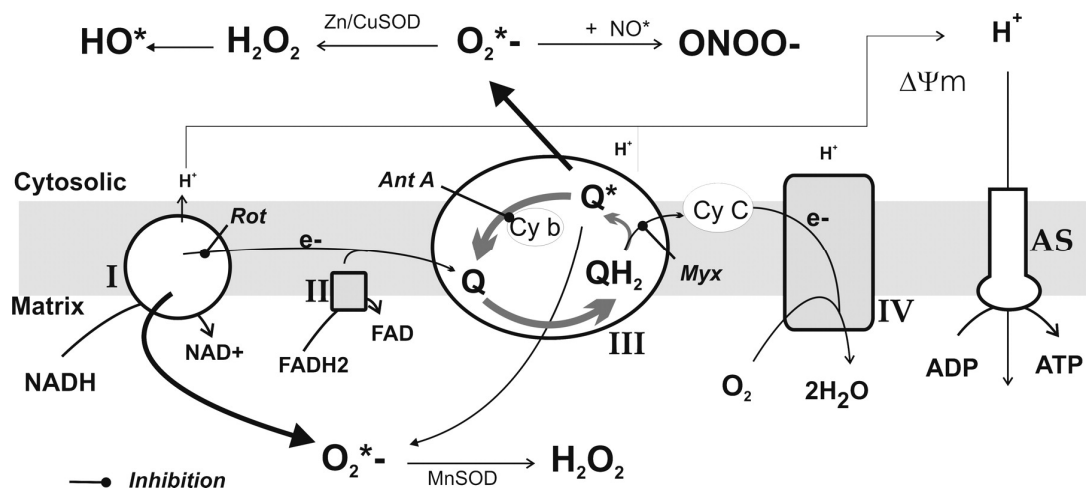


**Figure 6 legend: Main mechanism for mitochondrial ROS generation**

Main mechanism for mitochondrial reactive oxygen species (ROS) generation. Reduced substrates synthesised in metabolic pathways supply electrons (e<sup>-</sup>) to complex I and II of the electron transport chain. The main centers for superoxide (O<sub>2</sub><sup>-</sup>) formation are complex I and III, although small amounts can be formed at complex II and IV (omitted for clarity). The electron carrier of complex III, ubiquinone (Q), is reduced to ubiquinol (QH<sub>2</sub>), which transfers an electron to cytochrome c (Cy C) through an iron protein (not shown) inhibited by myxothiazol (Myx). The resulting semiubiquinone (Q\*) is oxidised back to ubiquinone by cytochrome b (Cy b), and can also transfer electrons to oxygen to form O<sub>2</sub><sup>-</sup>. Myxothiazol reduces O<sub>2</sub><sup>-</sup> production because it blocks Q\* formation, whereas antimycin A (Ant A) enhances it by increasing Q\* levels. Rotenone (Rot) inhibits electron flow distal to O<sub>2</sub><sup>-</sup> generation, enhancing its production. The main routes for O<sub>2</sub><sup>-</sup> transformation are represented. SOD, superoxide dismutase; H<sub>2</sub>O<sub>2</sub>, hydrogen peroxide; ONOO<sup>-</sup>, peroxynitrite; NO<sup>\*</sup>, nitric oxide; m: mitochondrial potential; AS, ATP synthase. Only the inner mitochondrial membrane is represented (adapted from Camello-Alvarez, 2006).

### 1.6.2 Mitochondria and NO:

Mitochondrial respiration and its regulation by NO is important in the heart for several reasons. Firstly, mitochondria generate almost all the ATP required for muscle contraction in the heart, so that inhibition of mitochondrial respiration results in an inhibition of contractility. Secondly, inhibition of mitochondrial respiration stimulates mitochondrial production of ROS which regulates signal transduction pathways within the heart. Thirdly, inhibition of mitochondrial respiration can cause necrosis or apoptosis within the heart.

NO interacts with the mitochondrial respiratory chain by different means: (A) NO itself causes rapid, selective, potent, but reversible inhibition of cytochrome oxidase, and (B) reactive nitrogen species (RNS, which include ONOO<sup>-</sup>(peroxynitrite), NO<sub>2</sub>, N<sub>2</sub>O<sub>3</sub> and S-nitrosothiols) cause slow, non-selective, weak, but irreversible (or slowly reversible) inhibition of many mitochondrial components. NO causes rapid and reversible inhibition of cytochrome c oxidase at nanomolar levels of NO<sup>89,90</sup>, so that NO is potentially a physiological regulator of respiration. NO reversibly inhibits cytochrome oxidase apparently by two different means involving NO binding to two different components of the oxygen binding site, which in both cases blocks oxygen binding. The oxygen-binding site consists of two metals, the iron of haem a<sub>3</sub> and the copper of the Cu<sub>B</sub> centre. Oxygen is bound between them (and is rapidly reduced by them) when both metals are reduced (a<sub>3</sub><sup>2+</sup> and Cu<sup>+</sup>). NO can either (1) bind to reduced cytochrome a<sub>3</sub> to give cytochrome a<sub>3</sub><sup>2+</sup>-NO, or (2) NO can bind and reduce oxidised Cu<sub>B</sub><sup>2+</sup> to give Cu<sub>B</sub><sup>+</sup>-NO<sup>+</sup>, and the NO<sup>+</sup> can rapidly hydrate to give nitrite (NO<sub>2</sub><sup>-</sup>)<sup>91,92,93</sup>. Both forms of inhibition are rapid and reversible, due to debinding of NO in (1) and debinding of nitrite in (2). The first form of inhibition is competitive with oxygen and reversible by light whereas the second is not, and these characteristics may be used to distinguish between them<sup>91</sup>. It seems that at least *in vitro* both forms of inhibition may occur simultaneously, but the first form is favoured at high levels of cytochrome reduction and low oxygen, whereas the second form is favoured by the opposite conditions<sup>91,93</sup>.



---

NO and RNS can also stimulate ROS and RNS production by mitochondria, which may be important signals in the heart, mediating for example ischemic preconditioning<sup>94</sup>. At high levels, NO can directly react with oxygen in the mitochondrial bilayer to give NO<sub>2</sub> and N<sub>2</sub>O<sub>3</sub><sup>95</sup>. At moderate levels NO can acutely increase O<sub>2</sub><sup>-</sup> and H<sub>2</sub>O<sub>2</sub> production by inhibiting mitochondrial respiration, while at higher levels it inhibits H<sub>2</sub>O<sub>2</sub> production by scavenging the precursor superoxide, resulting in peroxynitrite production<sup>96,97,98</sup>. NO may also apparently react with ubiquinol (QH<sub>2</sub>) to produce NO<sup>-</sup> (which may react with O<sub>2</sub> to produce ONOO<sup>-</sup>) and ubisemiquinone (QH<sup>•</sup>) (part of which may react with O<sub>2</sub> to produce O<sub>2</sub><sup>-</sup>)<sup>99</sup>. S-nitrosothiol-inactivation of complex I can also reversibly increase ROS production from complex I several fold<sup>100,101</sup>. NO and RNS inhibition of respiration may result in local peroxynitrite production (due to local superoxide production) causing irreversible inhibition of respiration and further oxidant production — a vicious cycle that might contribute to cell death<sup>98,102</sup>. In addition to stimulating H<sub>2</sub>O<sub>2</sub> production, NO or RNS can also inhibit catalase, deplete cellular glutathione and inhibit glutathione peroxidase, thus increasing H<sub>2</sub>O<sub>2</sub> levels in cells<sup>96,98,103</sup>.

*In vitro*, peroxynitrite and S-nitrosothiols can cause direct permeabilisation of mitochondrial membranes, and this effect is inhibited by cyclosporin A, indicating involvement of the mitochondrial permeability transition pore (MPT) in the permeabilisation event<sup>104,105,106</sup>. Opening of MPT pore has two important implications: (1) MPT causes mitochondrial depolarisation and subsequent inhibition of ATP synthesis which may lead to cellular ATP depletion and necrotic cell death; and (2) opening of MPT pore can cause the release of several proteins from mitochondria, including cytochrome c, which may lead to activation of caspases and apoptosis. NO itself may promote MPT by inhibiting respiration and thus lowering the membrane potential which favours MPT<sup>107</sup>. However, in the absence of a membrane potential, mitochondria cannot take up calcium to trigger MPT, and this may be the dominant effect of NO<sup>108</sup>. NO may affect MPT indirectly through (a) activation of soluble guanylate cyclase leading to activation of PKG which may phosphorylate some, yet unidentified components of MPT resulting in lower probability of MPT opening<sup>109,110</sup>,

(b) modulation of cellular calcium homeostasis<sup>111</sup>, or (c) stimulation of mitochondrial ROS production.

1.7. Reduced nicotinamide adenine dinucleotide phosphate (NADPH) oxidase and xanthine oxidoreductase (XOR):

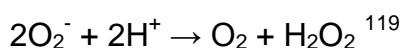
The NADPH oxidase and the XOR are the major sources of ROS.

1.7.1. *NADPH oxidase:*

NADPH oxidase is an enzyme that catalyses the production of superoxide ( $O_2^-$ ) from oxygen and NADPH, according to the following reaction<sup>112</sup>:



This enzyme, which makes very large amounts of superoxide, is found in professional phagocytes (neutrophils<sup>113</sup>, eosinophils, monocytes and macrophages<sup>114</sup>) at certain stages of their development. There is also a small group of superoxide-producing enzymes each known as a 'nox'<sup>115,116</sup>, which are more widespread (found in endothelium, kidney and spleen<sup>116</sup>) and make superoxide in small amounts, apparently for purposes of signaling. The function of NADPH oxidase in professional phagocytes, however, is to provide agents that kill organisms that are in contact with the phagocytes. These organisms can be ingested, in the case of neutrophils, monocytes and macrophages, and applied, in the case of eosinophils, which kill metazoans such as worms<sup>117</sup>. The oxidising agents generated by NADPH oxidase include  $H_2O_2$ , which is produced by the dismutation of superoxide<sup>118</sup>:



Other oxidising agents generated by NADPH oxidase include HOCl, which is generated by the  $\text{H}_2\text{O}_2$ -mediated oxidation of  $\text{Cl}^-$ , a reaction catalysed by myeloperoxidase (HOBr<sup>120</sup> or HOSCN<sup>121</sup> in the case of eosinophils, which have a unique peroxidase),  $\text{O}_2$ <sup>122,123</sup>, which is derived by the reaction of HOCl and  $\text{H}_2\text{O}_2$ , ozone<sup>124,125,126</sup>, whose origin is mysterious at present, and  $\text{OH}\bullet$ , which is postulated to arise from the oxidation of reduced metals ( $\text{Fe}^{2+}$  or  $\text{Cu}^+$ ) by  $\text{H}_2\text{O}_2$ <sup>127</sup>. However, free reduced metals are very scarce in biological systems, although  $\text{Fe}^{2+}$  can be released from iron–sulfur proteins by  $\text{O}_2^-$ <sup>128,129,130</sup>. A more probable source of  $\text{OH}\bullet$  is the reaction between ozone and  $\text{H}_2\text{O}_2$ .

**Figure 7: Structure of the neutrophil NADPH oxidase:**

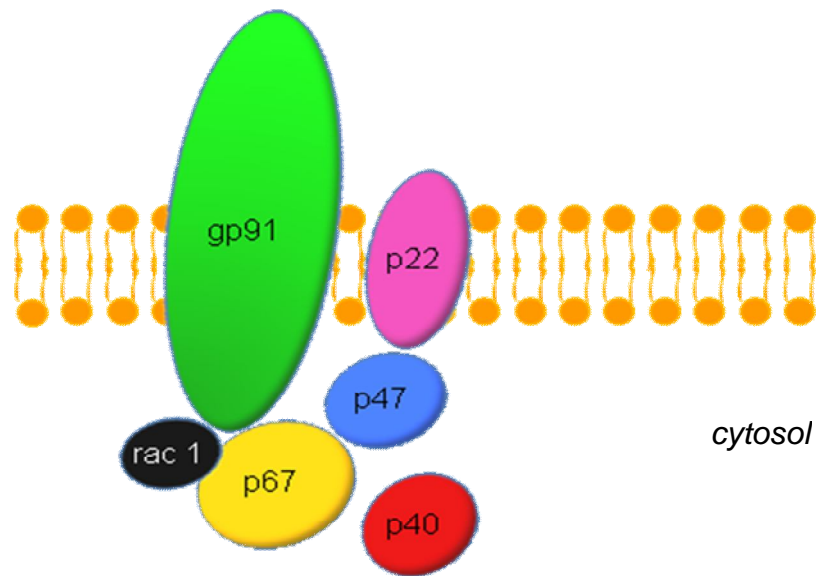


**Figure 7 legend: Structure of the neutrophil NADPH oxidase**

Functional structure of the neutrophil NADPH oxidase. gp91<sup>PHOX</sup> and p22<sup>PHOX</sup> are membrane bound components of the NADPH oxidase, and p47<sup>PHOX</sup> and p67<sup>PHOX</sup> are cytosolic components that interact with these 2 proteins to modulate its activity. The low molecular weight G protein rac also serves a regulatory function.

---

The structure of NADPH oxidase is quite complex (figure 7), consisting of two membrane-bound elements (gp91<sup>PHOX</sup> and p22<sup>PHOX</sup>), three cytosolic components (p67<sup>PHOX</sup>, p47<sup>PHOX</sup> and p40<sup>PHOX</sup>), and a low-molecular-weight G protein (either rac 2 or rac 1)<sup>119</sup>. The racs are kept inactive by binding to a guanine nucleotide dissociation inhibitor, which prevents the exchange of guanine nucleotides from the rac proteins<sup>131</sup>. Activation of NADPH oxidase is associated with, and probably caused by, the migration of the cytosolic components to the cell membrane so that the complete oxidase can be assembled.

The essential element of NADPH oxidase is gp91<sup>PHOX</sup>, to which the electron carrying components of the oxidase are bound. These include flavin adenine dinucleotide<sup>132</sup>, which, according to bioinformatics, associates about halfway down the cytosolic tail of the component, and a pair of haemes that are located in the membrane-associated portion of the component<sup>133</sup>. The two haems, whose redox potentials are very low, are both hexacoordinate (i.e. all six coordination positions on the haem iron are occupied)<sup>134,135</sup>, which raises the question whether they could participate in electron transfer to oxygen in the oxidase, particularly as flavins are remarkably efficient at one-electron reductions of oxygen. Nevertheless, it is generally believed that both the haems and the flavin are involved in electron transfer by NADPH oxidase.

p67<sup>PHOX</sup> is generally thought of as an 'accessory protein', whose exact function is unclear, although it is required for the activity of the oxidase. It contains two Src homology 3 (SH3) domains, one in the middle of the protein and one near the carboxyl terminus. Although originally thought to be an accessory protein with a mysterious function, p67<sup>PHOX</sup> is now known to be inactivated by NADPH dialdehyde with kinetics similar to the kinetics shown by NADPH in the catalytic reaction of NADPH oxidase<sup>136,137,138</sup>. Furthermore, p67<sup>PHOX</sup> catalyses the transfer of electrons from NADPH to electron acceptor dyes (although not to oxygen)<sup>139</sup>. These findings suggest that p67<sup>PHOX</sup> might be involved in the transfer of electrons directly from NADPH to oxygen to form superoxide.

---

**p47<sup>PHOX</sup>** is the protein that carries the cytosolic proteins to the membrane proteins to assemble the active oxidase. It is not absolutely required, because at sufficiently high concentrations of p67<sup>PHOX</sup>, superoxide production takes place in the absence of p47<sup>PHOX</sup><sup>140</sup>. It is essential in the neutrophils, however, because patients whose neutrophils are deficient in p47<sup>PHOX</sup> have chronic granulomatous disease, a disease in which neutrophils are unable to produce superoxide. Chronic granulomatous disease also occurs in patients with deficiencies in p67<sup>PHOX</sup> and deficiencies in the two membrane components of the oxidase: gp91<sup>PHOX</sup> and p22<sup>PHOX</sup>.

It has subsequently been established that smooth muscle cells and fibroblasts account for the majority of O<sub>2</sub><sup>-</sup> produced in the normal vessel wall<sup>141,142,143,144</sup>. Currently, attention is focused on NADPH oxidases as critical determinants of the redox state of blood vessels and the myocardium.

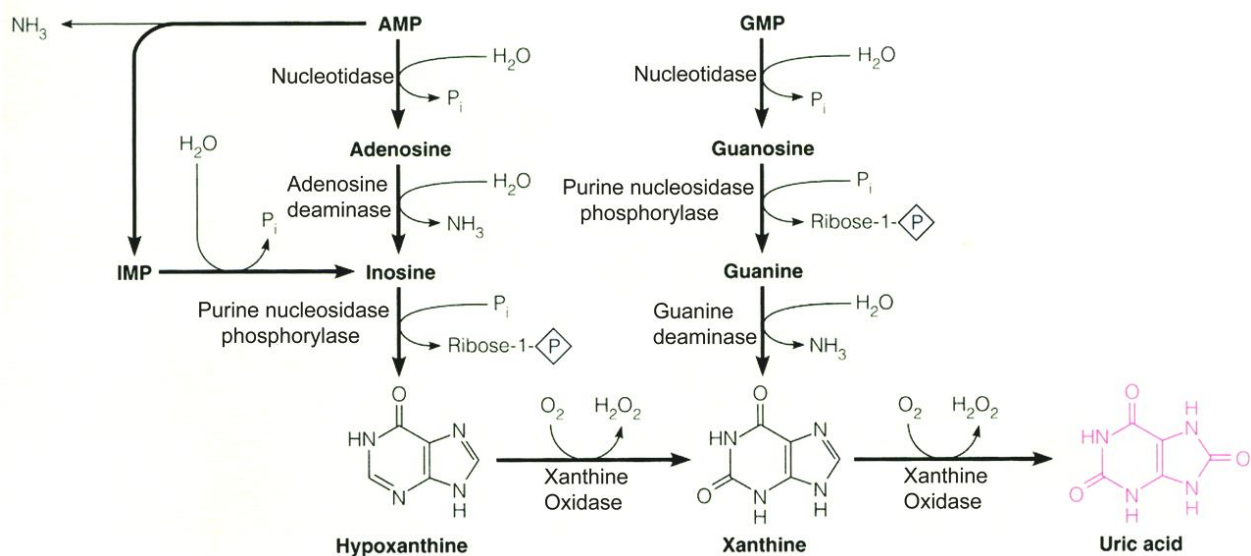
Regulation of NADPH oxidase activity in cardiovascular cells occurs in at least two levels. First, activation of the oxidase can be mediated by intracellular second messengers, including calcium<sup>145</sup>. Secondly, oxidase activity can also be modulated by upregulation of the component mRNAs. For example, tumor necrosis factor  $\alpha$  (TNF  $\alpha$ ) increases NADPH oxidase activity in vascular smooth muscle cells (VSMC) over 24 hours, an event that depends on increased transcription of p22<sup>PHOX</sup><sup>146</sup>. p22<sup>PHOX</sup> mRNA and O<sub>2</sub><sup>-</sup> production are upregulated in the aortas of rats made hypertensive by angiotensin II infusion<sup>147</sup>, and angiotensin II increases the expression of p67<sup>PHOX</sup> in adventitial fibroblasts<sup>148</sup>.

### 1.7.2. XOR:

XOR first identified a century ago in milk<sup>149</sup>, is a highly conserved member of the molybdoenzyme family, which also includes aldehyde oxidase (AO) and sulphite oxidase (SO)<sup>150</sup>. XOR has two interconvertible forms, xanthine dehydrogenase (XDH) and xanthine oxidase (XO)<sup>151</sup>. They differ in that XO only reduces oxygen, whereas XDH can reduce either oxygen or NAD<sup>+</sup> but has greater affinity for the latter<sup>152</sup>. Both forms catalyse the conversion of hypoxanthine to xanthine and xanthine to uric acid

(UA)<sup>153</sup>, the terminal two reactions of the purine degradation pathway (figure 8). XOR cofactors include (a) molybdopterin (Mo–Co) (b) two iron–sulphur centers (Fe<sub>2</sub>–S<sub>2</sub>), and (c) flavin adenine dinucleotide (FAD)<sup>153</sup>. Interest in XOR has grown over the past two decades because of its ability to generate ROS, its suspected role in reperfusion injury, and most recently its pathophysiological role in congestive heart failure.

**Figure 8: The purine degradation pathway (adapted from Berry C., 2004):**



The gene encoding human XOR is >60 kb, comprises 36 exons<sup>154</sup>, and is located on the short arm of chromosome 2<sup>155,156</sup>. The mRNA transcript contains an open reading frame of 3999 bp encoding 1333 amino acids<sup>157,158</sup>. The amino acid sequence is 91% homologous with rat and mouse XOR<sup>158</sup>, with binding sites for XOR cofactors well conserved amongst human, chicken, rat and mouse XOR<sup>155</sup>. The Mo–Co binding site is the most conserved region of XOR with 94% homology between human, rat and mouse amino acid sequences<sup>158</sup>.

The gene encoding the related enzyme AO exhibits striking similarity to XOR. The intron–exon organisation is almost identical between XOR and AO genes<sup>159</sup>, and their amino acid sequences are 50% homologous as determined from bovine cDNA<sup>160</sup> (figure 9). Their similarities in primary structure extend to their tertiary structures, for they share the same cofactors and redox center distribution, as well as many of the same substrates<sup>159</sup>. The genes encoding AO and XOR are closely spaced on chromosome 2<sup>159</sup>, suggesting they arose from an ancestral gene via tandem duplication. The functional role of AO remains unknown but is likely to be different from XOR as it lacks dehydrogenase activity<sup>161</sup>.

**Figure 9: Gene structure of XOR, AO and SO:**

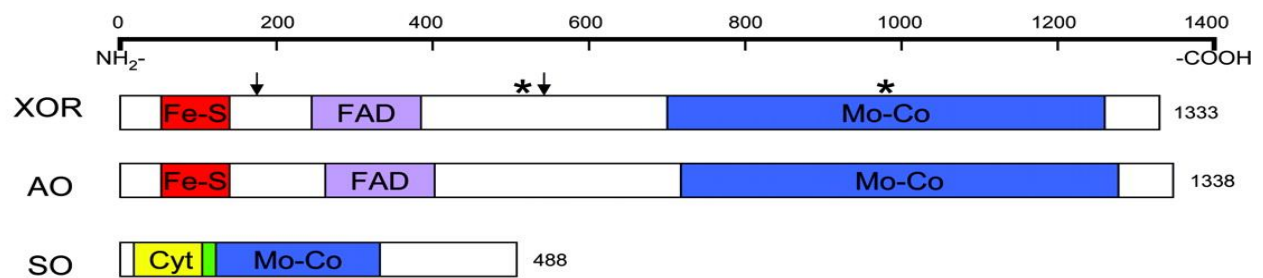
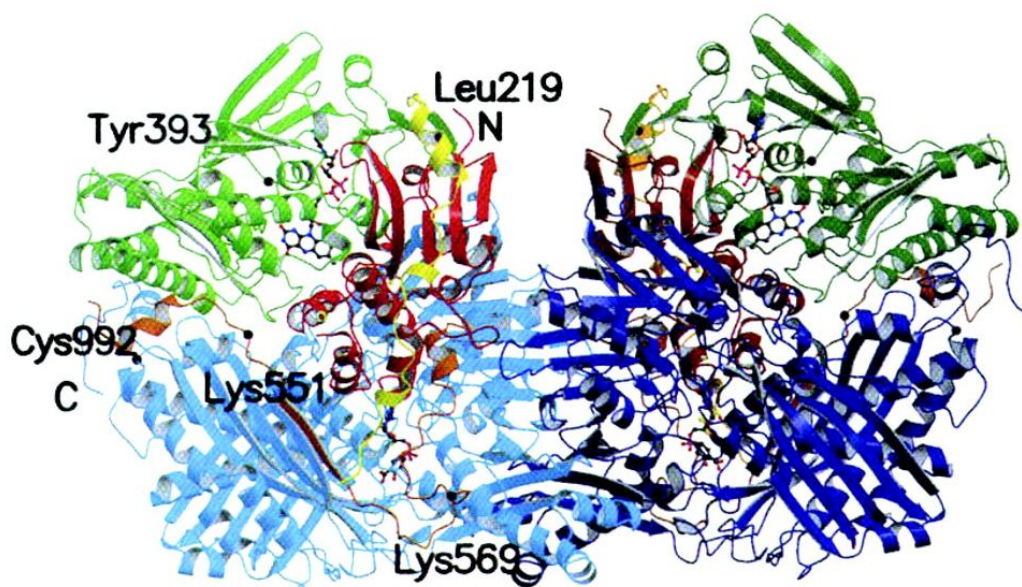


**Figure 9 legend: Gene structure of XOR, AO and SO**

Secondary structure of molybdoenzymes XOR, AO and SO. Arrows indicate trypsin sites. Stars indicate cysteine residues modified in reversible XOR conversion (adapted from Berry C.E., 2004).

**Figure 10: Crystal structure of bovine XOR homodimer (adapted from Berry C.E., 2004):**



The XOR enzyme is a homodimer composed of catalytically independent subunits with an approximate molecular mass of 150 kDa each<sup>162</sup>. The interface between the subunits leads to the overall complex having a butterfly shape. Each subunit is organised into three domains associated with a specific cofactor. The N-terminal domain (amino acids 1–165) is composed of two subdomains, each with one Fe<sub>2</sub>–S<sub>2</sub> center coordinated to four cysteine residues. A linker peptide connects it to the intermediate domain (amino acids 226–531), which holds a deep binding pocket for FAD that positions the flavin ring in close proximity to a Fe<sub>2</sub>–S<sub>2</sub> center. Another linker peptide joins the FAD domain with the C-terminal domain (amino acids 590–1332), which is the largest domain and the location of Mo–Co binding<sup>163</sup>.

The crystal structure of aldehyde oxidoreductase (figure 10), a molybdoenzyme from the organism *Desulfovibrio gigas*, demonstrates penta-coordination of the molybdenum ion with one oxo ligand, one water molecule, one sulphido group, and two dithiolene sulphur atoms from molybdopterin<sup>164,165</sup>. In XOR, the sulphido group is necessary for maintaining enzyme activity, as the desulpho-form is unable to react with substrate<sup>150</sup>. Similarities between the crystal structures of aldehyde oxidoreductase and bovine XOR suggest the coordination of the molybdenum ion in aldehyde oxidoreductase may apply to XOR as well<sup>163,164,165</sup>.

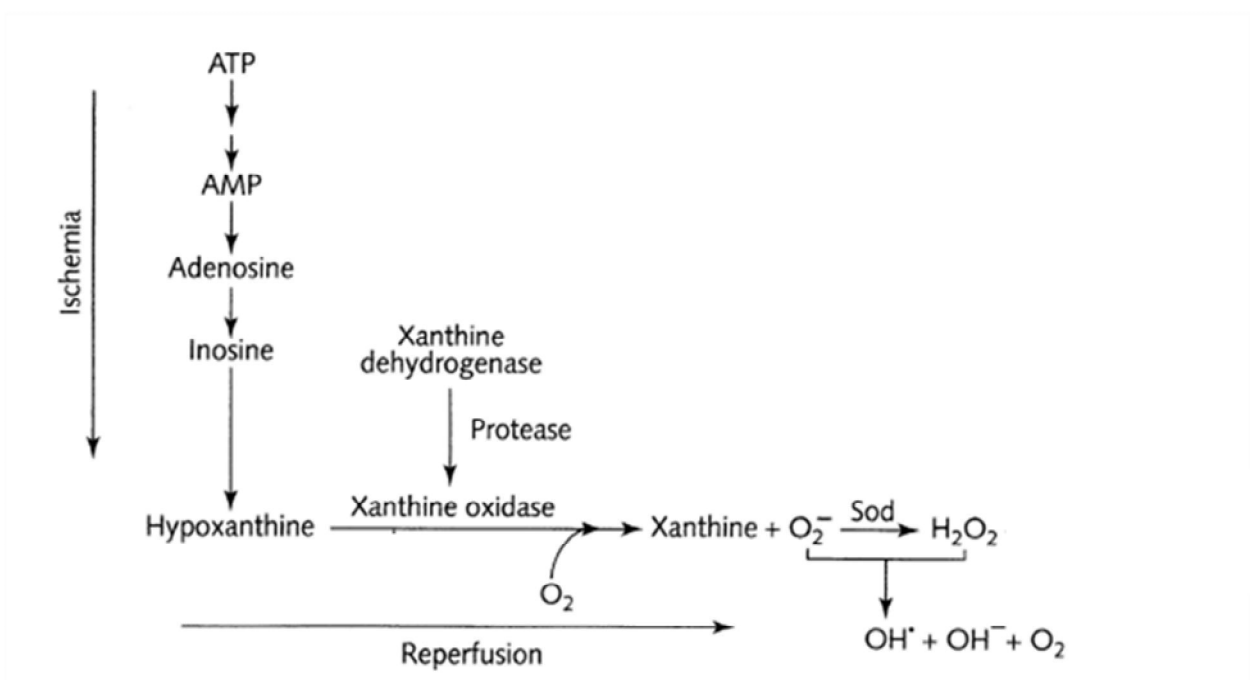
For many decades, the sole purpose of XOR was presumed to be purine catabolism, but growing evidence suggests a much broader biological role for this enzyme. For example, XOR has antimicrobial properties, as it inhibits the growth of bacteria *in vitro* in an NO-dependent manner<sup>166</sup>. There is also evidence that XOR plays an antimicrobial role *in vivo*, for infants who receive breast milk rich in XOR are less likely to develop gastroenteritis than those who are fed formula<sup>167</sup>. Furthermore, in mice with chronic granulomatous disease, allopurinol (XOR inhibitor) decreases clearance of pathogens and reduces killing efficiency *in vivo*, suggesting XOR may contribute to host defense against oxidant-sensitive organisms<sup>168</sup>. Although XOR clearly participates in antimicrobial defense, patients with xanthinuria are not immunocompromised, indicating the role of XOR in host defense is non-essential<sup>169</sup>.



Uric acid (UA) production by XOR may itself have broader biological consequences beyond purine degradation, for it possesses antioxidant properties<sup>170</sup>. Importantly, humans have higher UA concentrations compared to other mammals, as urate oxidase is inactivated in primates<sup>171</sup>. Previous studies hypothesised that this provided a survival advantage for humans because hyperuricaemia maintains blood pressure in the face of low dietary salt<sup>172</sup>. Furthermore, others have speculated that UA contributes to increased life span in humans by providing protection against oxidative stress-provoked ageing and cancer<sup>173</sup>.

XOR-generated ROS are implicated in both tissue structural damage and cell signaling interference. Classically, ROS can cause lipid peroxidation, resulting in disruption of membrane architecture and lysosomal enzyme release<sup>174</sup>, and DNA and amino acid oxidation, causing genetic mutations and enzyme dysfunction or proteolysis<sup>175</sup>. In regard to XOR, oxidative injury is often achieved via the byproducts of  $O_2^-$  and  $H_2O_2$  generation.

Granger and colleagues<sup>176,177,178</sup> focused attention on XOR by proposing a key role for the enzyme in the pathogenesis of ischemia-reperfusion injury (figure 11).

**Figure 11: Mechanism of generation of ROS in ischemia-reperfusion injury:****Figure 11 legend: Mechanism of generation of ROS in ischemia-reperfusion injury**

In the course of ischemia, transmembrane ion gradients are dissipated, allowing elevated cytosolic concentrations of calcium. This, in turn, activates a protease that irreversibly converts Xanthine dehydrogenase (XDH) into xanthine oxidase (XO). Currently, cellular ATP is catabolised to hypoxanthine, which accumulates. On reperfusion, readmitted oxygen, hypoxanthine, and XO combine to generate superoxide ( $O_2^-$ ) and hydrogen peroxide ( $H_2O_2$ ). These reactive oxygen species can interact to yield a range of cytotoxic agents, including hydroxyl radicals (modified from Granger D.N., 1986).

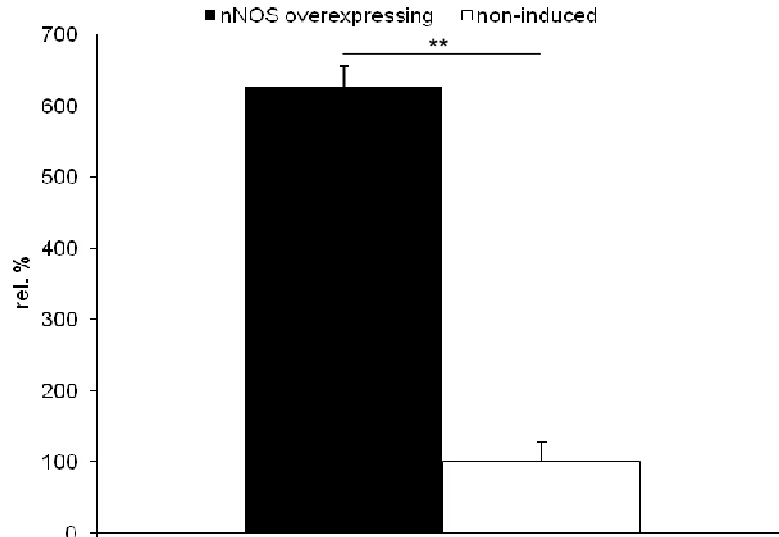
### 1.8. Conditional nNOS overexpression impairs myocardial contractility:

I previously investigated my transgenic mouse model allowing conditional, myocardial specific nNOS overexpression<sup>1</sup>. The hypothesis was that the close proximity of nNOS and certain effector molecules like L-type  $Ca^{2+}$ -channel has an impact on myocardial contractility.

Western Blot analysis of transgenic nNOS overexpression showed a 6-fold increase in nNOS protein expression compared with non-induced littermates (figure 12).

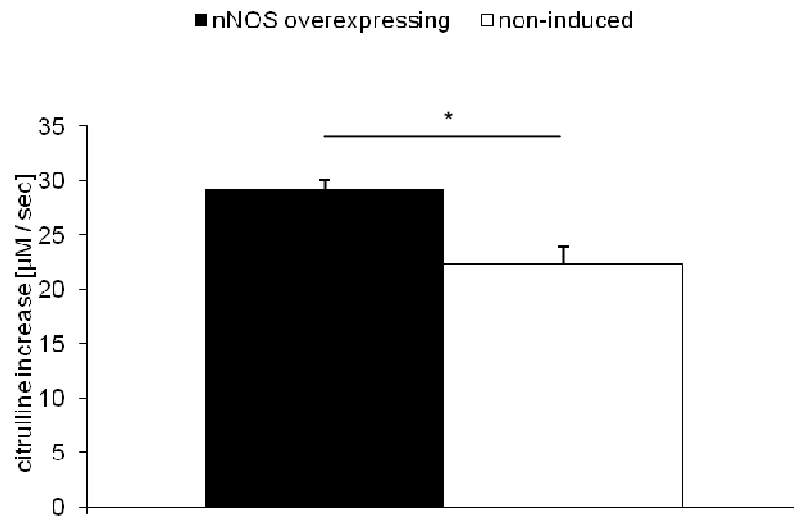
Measuring total NOS activity by conversion of [<sup>3</sup>H]-L-arginine to [<sup>3</sup>H]-L-citrulline showed a 30% increase in nNOS overexpressing mice (figure 13). After two weeks of induction, nNOS overexpressing mice showed a reduced myocardial contractility. *In vivo* examinations of the nNOS overexpressing mice revealed decrease of  $+dp/dt_{max}$  compared with non-induced mice (figure 14). Likewise, ejection fraction (LVEF) was significantly reduced (figure 14). Interestingly, coimmunoprecipitation experiments indicated interaction of nNOS with SERCA2a and additionally with L-type  $Ca^{2+}$ -channel in nNOS overexpressing mice (figure 15). Accordingly, in isolated adult cardiac myocytes,  $I_{Ca,L}$  density was significantly decreased in nNOS overexpressing cells (figure 16). Intracellular  $Ca^{2+}$ -transients and fractional shortening in cardiomyocytes were also clearly impaired in nNOS overexpressing animals versus non-induced littermates (figure 17, 18).

**Figure 12: nNOS protein expression:**



**Figure 12 legend: nNOS protein expression**

Total myocardial nNOS protein expression was increased more than 6-fold in the nNOS overexpressing mice (627±13% vs. 100±7%, n=19, p<0.01). Statistical evaluation of Western Blot was done by a densitometric analysis with the Scan Pac software (Biometra).

**Figure 13: NOS activity:****Figure 13 legend: NOS activity**

Whole heart homogenates from nNOS overexpressing mice showed a 30% increase in total NOS activity compared to non-induced animals ( $22 \pm 1.5$  vs.  $29 \pm 1 \mu\text{M}/\text{sec}$ ,  $n=18$ ,  $p<0.05$ ).

**Figure 14: Hemodynamics:**

	non-induced	nNOS overexpressing	dobutamine	
			non-induced	nNOS overexpressing
HR [bpm]	525±51	546±38	616±50†	640±54†
LVEF [%]	65±3	42±4*	72±7†	46±4*
+dp/dt <sub>max</sub> [mmHg/sec]	8,701±372	7,295±502*	11,710±1116†	7,948±465*
-dp/dt <sub>min</sub> [mmHg/sec]	7,291±391	7,527±610	7,305±836	7,809±748
(dp/dt <sub>max</sub> )/IP [sec <sup>-1</sup> ]	184±6	161±7*	228±11†	191±10
τ [ms]	9.7±1.3	9.2±0.8	10.3±0.9	9.2±0.4
LVEDP	5.5±0.4	7.4±0.7*	5.0±0.5	8.0±1.0*

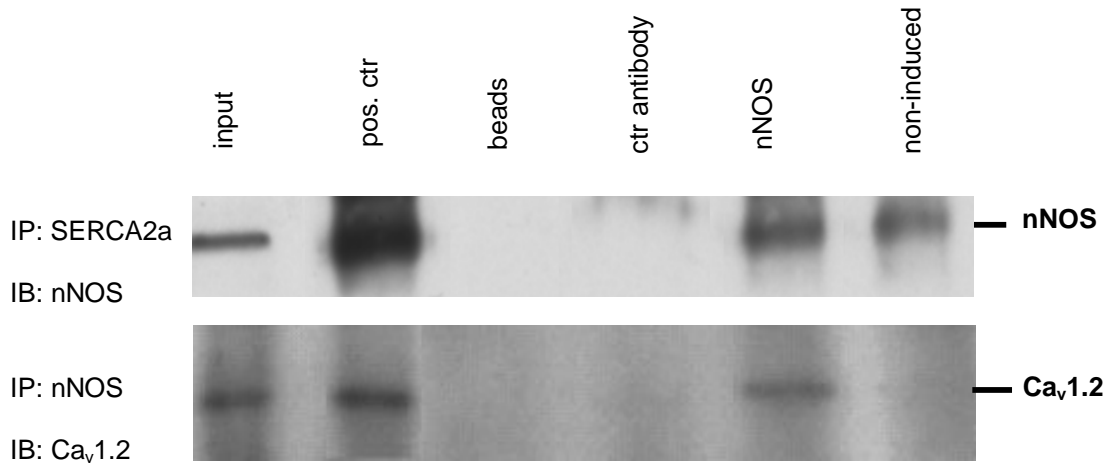
**Figure 14 legend: Hemodynamics**

\*= p<0.05 for comparisons between non-induced and nNOS overexpressing mice

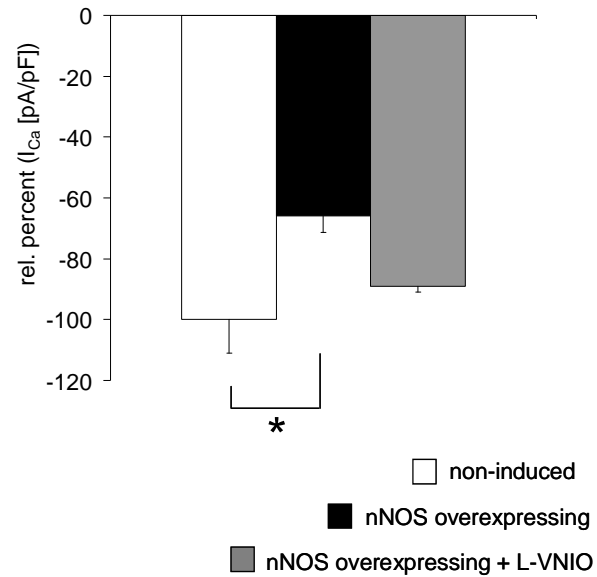
†= p<0.05 for comparison between basal values and during dobutamine infusion

Dobutamin infusion was at a rate of 16ng/g/min

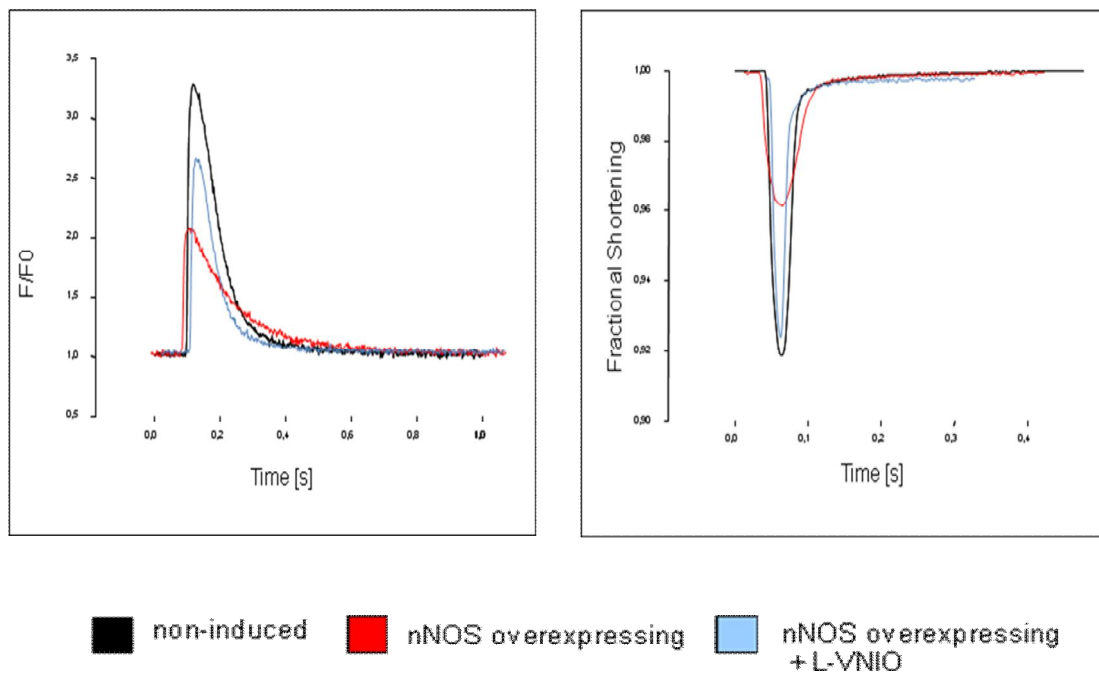
Under basal conditions, non-induced mice showed a higher left ventricular inotropy than their nNOS overexpressing littermates, as evaluated by LVEF, +dp/dt<sub>max</sub> and (dp/dt<sub>max</sub>)/IP. The LV response to β-adrenergic stimulation with dobutamine was also significantly blunted in nNOS overexpressing mice. LV relaxation did not differ under basal conditions and during dobutamine infusion between nNOS overexpressing mice and non-induced animals as shown by unchanged values for -dp/dt<sub>max</sub> and T.

**Figure 15: Coimmunoprecipitation experiments:****Figure 15 legend: Coimmunoprecipitation experiments**

Left ventricular lysates were immunoprecipitated (IP) with anti-SERCA2a monoclonal antibody and immunoblotted (IB) for nNOS. On the lower panel lysates were immunoprecipitated with anti-nNOS monoclonal antibody and immunoblotted with Ca<sub>v</sub> 1.2 polyclonal antibody. Association between nNOS and SERCA2a is demonstrated both in non-induced and nNOS overexpressing mice, whereas an association between nNOS and the L-type Ca<sup>2+</sup>-channel was demonstrated only in the nNOS overexpressing mice. As a positive control mouse brain was used.

**Figure 16: Calcium current density:****Figure 16 legend: Calcium current density**

Calcium current density was significantly reduced in nNOS overexpressing adult cardiac myocytes ( $100 \pm 0.5$  vs.  $67.8 \pm 0.5$  rel. %  $I_{Ca,L}$  [pA/pF]),  $n=12$ ,  $p<0.05$ ). Application of the specific nNOS inhibitor L-VNIO ( $100 \mu\text{M}$ ) rescued the nNOS phenotype.

**Figure 17: Intracellular calcium transients:****Figure 17 legend: Intracellular calcium transients**

Representative records of tracings from  $[Ca^{2+}]_i$  transients at 1Hz in fluo-3-loaded myocytes (left panel) in isolated adult cardiac myocytes non-induced, nNOS overexpressing and nNOS overexpressing cardiac myocytes treated with L-VNIO (100 $\mu$ M). Right panel shows representative myocyte shortening (fractional shortening).

$[Ca^{2+}]_i$  transients were significantly decreased in nNOS overexpressing myocytes compared with non-induced controls when stimulated with 1Hz ( $3.0 \pm 0.4$  F/F<sub>0</sub> vs.  $2.2 \pm 0.2$  F/F<sub>0</sub>, n=13, p<0.05). Application of the nNOS specific inhibitor L-VNIO to the nNOS overexpressing myocytes rescued the nNOS phenotype in part ( $2.7 \pm 0.2$  F/F<sub>0</sub>, n=17, p=n.s. for comparison with non-induced animals).



Figure 18: Fractional shortening:

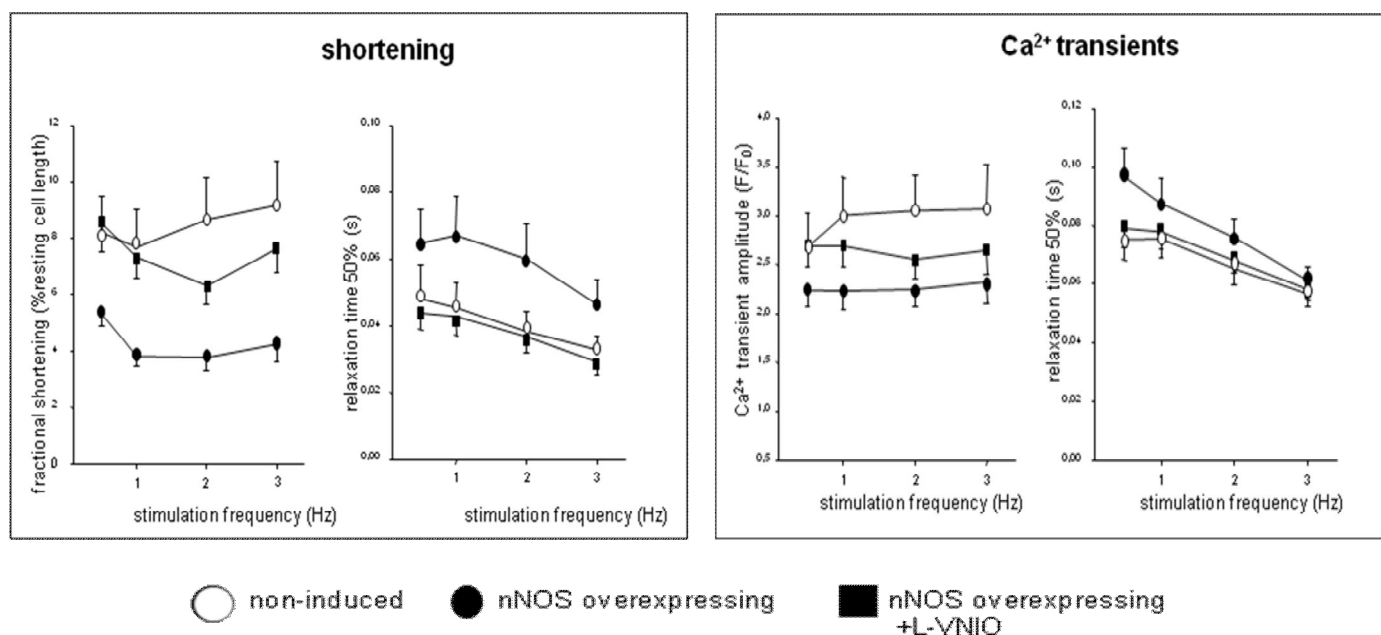


Figure 18 legend: Fractional shortening

[Ca<sup>2+</sup>]<sub>i</sub> transients amplitudes (right panel) and fractional shortening (in % of resting cell length, left panel) in isolated myocytes from non-induced animals, nNOS overexpressing mice and nNOS overexpressing mice were treated with L-VNIO (100μM). Stimulation frequency was from 0.5 to 3Hz.

Fractional shortening of isolated cardiac myocytes was significantly impaired in nNOS overexpressing cells (7.7±1.3 vs. 3.8±0.5% at 1Hz, n=13, p<0.05). Again L-VNIO improved contractility in nNOS overexpressing cardiac myocytes (7.3±0.8% at 1Hz, n=17, p=n.s. for comparison with nNOS overexpressing mice).

Relaxation time (50%) in the experiments for myocyte shortening was significantly prolonged in nNOS overexpressing myocytes (0.067±12 vs. 0.045±7s at 1Hz, n=13, p<0.05) and was accelerated in nNOS overexpressing myocytes treated with L-VNIO (0.043±6s at 1Hz, n=17, p=n.s. for comparison with nNOS overexpressing mice). Similarly, nNOS overexpression prolonged Ca<sup>2+</sup> decay (50%) (0.088±9 vs. 0.076±7s at 1Hz, n=13, p<0.05) with an acceleration caused by L-VNIO (0.078±6s at 1Hz, n=17, p=n.s. for comparison with nNOS overexpressing mice).

In this previous study I demonstrated that conditional transgenic overexpression of nNOS results in an inhibition of myocardial contractility as well as in an impairment of the contractile response to adrenergic stimulation.

The conditional nNOS mouse model resembles a heart failure model with additional localisation of the overexpressed nNOS at the surface membrane. I found an inhibitory effect of abundant nNOS on  $I_{Ca,L}$  density and  $Ca^{2+}$ -transients amplitudes. The attenuation of  $I_{Ca,L}$  in nNOS overexpressing mice may contribute to the decreased contractile performance I observed. A reduction of the  $Ca^{2+}$ -influx through the L-type  $Ca^{2+}$ -channel impairs the trigger effect on the  $Ca^{2+}$ -induced  $Ca^{2+}$ -release resulting in a reduction of myocardial contractility.

In the present study, I investigated the role of conditional nNOS overexpression during ischemia-reperfusion injury.

### 1.9. Aim of the study:

Several studies of recent years investigated nNOS effects exerted on the cardiomyocytes with special emphasis on the intracellular localisation of nNOS. However, the results from pharmacological inhibition and genetic deletion or from conditional overexpression of nNOS brought diverging results. Interestingly, despite the fact that current studies demonstrated discrepant findings in terms of myocardial contractility and  $\text{Ca}^{2+}$  homeostasis, it seems consistent that nNOS is upregulated and acts cardioprotective in different models of heart disease<sup>179,180,181</sup>. However, the mechanism underlying this protection is unknown. In this context, different targets of nNOS relevant for  $\text{Ca}^{2+}$  cycling, e.g. ryanodine receptor 2 (RyR2)<sup>182</sup>, L-type  $\text{Ca}^{2+}$ -channel<sup>1</sup>, SERCA2a<sup>183</sup> and phospholamban (PLN)<sup>184</sup> were identified in the past. Additionally, cardioprotective implications have also been ascribed to effects on the XOR, one of the major sources of  $\text{O}_2^-$  production in the heart. It has been shown that XOR targeted inhibition maintains the balance between the production of reactive nitrogen species (RNS) and reactive oxygen species (ROS)<sup>181,185,186</sup> in cardiac tissues. nNOS is also found in the mitochondria<sup>187,188</sup> and inhibits the mitochondrial respiratory chain resulting in an inhibition of ATP production and increased oxidant production. NO reversibly binds to the oxygen binding site of the cytochrome c oxidase, reacting either with the oxidized copper to give inhibitory nitrite, or with the reduced haem, resulting in a reversible inhibition in competition with oxygen<sup>189</sup>. However, it was also suggested that NO derived from nNOS does not directly contribute to the inhibition of mitochondrial respiration but rather represents an antioxidant system by inhibiting XOR activity<sup>190</sup>.

Further, S-nitrosylation of protein targets (e.g. L-type  $\text{Ca}^{2+}$  channel) was suggested to be one major mechanism to protect cardiac cells against ischemia-reperfusion injury, although until now there is no direct evidence for a role of nNOS in this setting<sup>10,191</sup>. The aim of this study is to elucidate the impact of the abundance of nNOS on cardiomyocyte function, and to assess the direct and subcellular effects of conditional overexpression of nNOS in ischemia-reperfusion injury. The hypothesis of this study is that nNOS acts cardioprotective via a decrease in superoxide formation and differential effects on mitochondrial respiration.

## 2. Materials:

### 2.1. Equipment:

autoclave	Sanoclav	KL-12-3
centrifuge	Sigma	2K15, Sigma 2-15
centrifuge	Hettich	Mikro 12-24
centrifuge	Beckmann	GPKR Centrifuge
centrifuge	Eppendorf	
centrifuge	Heraeus	Biofuge pico
centrifuge	Beckmann	Optima TL Ultrazentrifuge
ELISA reader	Tecan	Tecan Spectra
fluorescence microscope	Zeiss	Axiovert 135
fluorescence microscopoe	Keyence	Biozera BZ-8000K
freezer (-20°C)	Liebherr	Economy
freezer (-20°C)	Bosch	economic
freezer (-80°C)	National Lab	Profi Star
refrigerator	Liebherr	glass line, Premium, comfort
gel dryer	Biotec Fischer	Phero Temp 60
heating block	Eppendorf	ThermoStat plus
heating block	Liebisch	
homogenizer	IKA Labortechnik	Eurostar digital
homogenizer	Janke/Kunkel	Ultra Turrax T25
incubator	Heraeus	Function line
incubator	Forma Scientific	Steri-Cult 200
light table	Uni Würzburg	
luminometer	Berthold Industries	Lumat LB9501
magnetic stirrer	IKA Labortechnik	RH basic2, Ikamag RET, Ikamag RCT
magnetic stirrer	Hartenstein	Hotplate Stirrer L81
microwave	Daewoo	KOR-6305BL
microscope	Leitz	Labovert
oven	MWG Biotech	Mini Oven
PCR machine	Eppendorf	Mastercycler
PCR machine	Perkin Elmer	DNA Thermocycler
photometer	Eppendorf	Bio-Photometer
power supply	Biometra	P25, PP4000
power supply	Hofer	SX250
scale	Sartorius	BP61
scale	Kern	
sealing machine	Severin	Folio
shaker	Heidolph	Duomax 1030
shaker	Hartenstein	L40
shaker	Braun Biotech	Certomat R
spectrometer	Perkin Elmer	LS 50 B
supersonic bath	Julabo	USR05
turner	Heidolph	REAX 2

UV light	BioRad	Mini-Transluminator
vacuum pump	KNF	
vortexer	Heidolph	REAX 1 D R
vortexer	Scientific Industries	Vortex-Genie2
water bath	Haake	Thermo C10
water bath	Inlabo	SW20C

## 2.2. Consumable materials:

### 2.2.1. *Common consumable materials:*

The common consumable material, e.g. tubes and pipette tips, was obtained from the University of Würzburg (Medical Department I; „Zentrallager“), A. Hartenstein Gesellschaft für Labor- und Medizintechnik mbH (Würzburg, Germany) or Weckert Labor-, Röntgen- und Medizintechnik (Kitzingen, Germany).

### 2.2.2. *Chemicals:*

All chemicals were received from the University of Würzburg (Medical Department I, central pharmacy), Merck (Darmstadt, Germany), Roth (Karlsruhe, Germany) or Sigma (München, Germany), A. Hartenstein Gesellschaft für Labor- und Medizintechnik mbH (Würzburg, Germany)

### 2.2.3. *Enzymes:*

The used enzymes were obtained from Fermentas (St. Leon-Rot, Germany)

**Xba I** (Cat. No. ER0681)

**Sfi I** (Cat. No. ER1821)

### 2.3. Working Kits:

Name	Company	Cat. No.
Tet-Off and Tet-On Gene Expression Systems	<b>Clontech</b> , Heidelberg, Germany	# 630921
Taq PCR Core Kit	<b>Qiagen</b> , Hilden, Germany	# 201223
ECL™ Western Blotting Detection	<b>GE Healthcare</b> , Munich, Germany	# RPN2106
Immunoprecipitation Starter Pack	<b>GE Healthcare</b> , Munich, Germany	# 17-6002-35
LIPOFECTAMINE PLUS™ Reagent	<b>Invitrogen</b> , Karlsruhe, Germany	#10964-013
Nitric Oxide Colorimetric Assay Kit	<b>Biomol</b> , Hamburg, Germany	# BML-AK136-0001
Cytochrome C Oxidase Assay Kit	<b>Sigma</b> , Munich, Germany	# CYTOCOX1
Qproteome Mitochondria Isolation Kit	<b>Qiagen</b> , Hilden, Germany	# 37612
TAC-Peroxy Assay Kit	<b>Axxora</b> , Lörrach, Germany	# TAC-Peroxy
Amplex® Red Xanthine Oxidase Assay Kit	<b>Molecular Probes</b> , Karlsruhe, Germany	# A22182

### 2.4. Solutions and buffers:

#### 2.4.1. DNA Electrophoresis:

50x TAE Buffer (Tris-Acetate-EDTA):

component (MW [g/mol])	stock	weight/volume / l	final concentration
Tris [121.14]		242.0g	<b>2.0mM</b>
Acetic acid [60.05]		57.1ml	<b>1.0mM</b>
EDTA [292.25]	0.5M pH 8.0	100.0ml	<b>0.05mM</b>
dH <sub>2</sub> O		ad 1000ml	

6x Loading Dye:

component	final concentration
Bromphenol blue	<b>0.25%</b>
Xylene cyanol	<b>0.25%</b>
Glycerol	<b>30.0 – 60.0%</b>

## 2.4.2. Western blotting:

RIPA (RadiolImmunoPrecipitation Assay) Buffer:

component (MW [g/mol])	stock	volume/weight / 100ml	final concentration
NaCl [58.44]	1.0M	15.0ml	<b>150.0mM</b>
Tris [121.14]	1.0M	5.0ml	<b>50.0mM</b>
PMSF	100.0mM	1.0ml	<b>1.0mM</b>
IGEPAL CA-630		1.0ml	<b>1.0%</b>
Sodium deoxycholate (DOC)	10.0%	5.0ml	<b>0.5%</b>
Sodium dodecyl sulfate (SDS)	10.0%	1.0ml	<b>0.1%</b>
dH <sub>2</sub> O		ad 100.0ml	

Low Salt Buffer:

component (MW [g/mol])	stock	volume/weight / 100 ml	final concentration
Tris [121.14]	1.0M	5.0ml	<b>50.0mM</b>
PMSF	100.0mM	1.0ml	<b>1.0mM</b>
IGEPAL CA-630		1.0ml	<b>1.0%</b>
dH <sub>2</sub> O		ad 100.0ml	

1.5M Tris pH 8.8:

component (MW [g/mol])	weight / 100 ml	final concentration
Tris [121.14]	18.15g	<b>1.5M</b>
dH <sub>2</sub> O (check pH 8.8)	ad 100.0ml	

0.5M Tris pH 6.8:

component (MW [g/mol])	weight / 100 ml	final concentration
Tris [121.14]	6.0g	<b>0.5M</b>
dH <sub>2</sub> O (check pH 6.8)	ad 100.0ml	

10% SDS (Sodium dodecyl sulfate):

component (MW [g/mol])	weight / 100 ml	final concentration
Sodium dodecyl sulfate (SDS)	10.0g	<b>10.0%</b>
dH <sub>2</sub> O (check pH 8.0)	ad 100.0ml	

5x PBS pH 7.4:

component (MW [g/mol])	weight / 5 l	final concentration (5x)	final concentration (1x)
NaCl [58.44]	20.0g	342.0mM	<b>68.4mM</b>
NaH <sub>2</sub> PO <sub>4</sub> *H <sub>2</sub> O [137.99]	11.73g	85.0mM	<b>17.0mM</b>
Na <sub>2</sub> HPO <sub>4</sub> [141.96]	41.17g	290.0mM	<b>58.0mM</b>
dH <sub>2</sub> O (check pH 7.4)	ad 5000ml		

## 5x Electrophoresis Buffer pH 8.3:

component (MW [g/mol])	weight / 5 l	final concentration (5x)	final concentration (1x)
Tris [121.14]	75.0g	0.62M	<b>124.0mM</b>
Glycin [75.07]	360.0g	4.8M	<b>960.0mM</b>
SDS	25.0g	0.5%	<b>0.1%</b>
dH <sub>2</sub> O (check pH 8.3)	ad 5000ml		

## Transfer Buffer pH 8.3:

component	stock	volume / 1 l	final concentration
5x Electrophoresis buffer	5x	200.0ml	<b>1x</b>
Methanol		200.0ml	<b>20.0%</b>
dH <sub>2</sub> O		ad 1000ml	

## Washing solution:

component	stock	volume / 1 l	final concentration
5x PBS pH 7.4	5x	200.0ml	<b>1x</b>
Tween20		0.5ml	<b>0.05%</b>
dH <sub>2</sub> O		ad 1000ml	

## Blocking solution:

component	stock	volume / 1l	final concentration
5x PBS pH 7.4	5x	20.0ml	<b>1x</b>
nonfat dried milk powder		5.0g	<b>5.0%</b>
dH <sub>2</sub> O		ad 100.0ml	

## SDS Gels:

## Separating Gels:

component	5 %	7,5 %	10 %	12 %	15 %
dH <sub>2</sub> O	11.39ml	9.69ml	8.02ml	6.69ml	4.69ml
1.5M Tris pH 8,8	5.0ml	5.0ml	5.0ml	5.0ml	5.0ml
10% SDS	0.2ml	0.2ml	0.2ml	0.2ml	0.2ml
Acrylamide/Bis (30% - Stock)	3.3ml	5.0ml	6.67ml	8.0ml	10.0ml
10% APS	0.1ml	0.1ml	0.1ml	0.1ml	0.1ml
TEMED	0.01ml	0.01ml	0.01ml	0.01ml	0.01ml

## Stacking Gel (5 %):

component	2 Gels
dH <sub>2</sub> O	5.65ml
0.5M Tris pH 6.8	2.5ml
10% SDS	0.1ml
Acrylamide/Bis (30 % - Stock)	1.7ml
10% APS	0.05ml
TEMED	0.01ml



### 2.4.3. Electron microscopy:

Phosphate buffered saline (PBS) pH 7.4:

component	final concentration
NaCl	137mM
KCl	2.7mM
Na <sub>2</sub> HPO <sub>4</sub> x 2H <sub>2</sub> O	8.1mM
KH <sub>2</sub> PO <sub>4</sub>	1.5mM

ascending alcohol bank:

component	time	temperature [°C]
30% ethanol	2 x 15min	4°C
50% ethanol	2 x 30min	-20°C
70% ethanol with 0.2% uranylacetate	2 x 30min	-20°C
90% ethanol with 0.2% uranylacetate	2 x 30min	-20°C
100% ethanol	2 x 60min	-20°C
100% ethanol/LR-White 1:1	over night	4°C
LR-White	1h	4°C
LR-White	3-4h	4°C
LR-White	over night	4°C
LR-White	3-4h	room temperature

### 2.4.4. Immunofluorescence staining of isolated adult cardiac myocytes:

Cardioplegic solution pH 7.4:

component	final concentration
HEPES	24mM
NaHCO <sub>3</sub>	3.8mM
Dextrose	151.3mM
Mannitol	34.4mM
Heparin	140u/mg
KCl	20mM

## Wittenberg Isolation Medium/Insuline pH7.4 (WIM):

component	final concentration
KCl	53.6mM
NaCl	1.16M
NaH <sub>2</sub> PO <sub>4</sub> x H <sub>2</sub> O	10.1mM
Dextrose	50.5mM
Phenol red	0.3mM
MgCl <sub>2</sub> x 6H <sub>2</sub> O	1M
NaHCO <sub>3</sub>	1M
HEPES	1M
KH <sub>2</sub> PO <sub>4</sub>	1M
NaOH	5M
L-Glutamine	200mM
Minimum Essential Medium (MEM) Vitamin Solution (100x)	
MEM Amino Acid Solution (50x)	
BDM	10mM
Taurine	5mM
Insuline	1mg/ml

## Solution A:

component
50ml WIM
250µl 1M MgCl <sub>2</sub> x 6H <sub>2</sub> O

## Solution B:

component
50ml WIM
40mg Collagenase Typ 2
50µl 10mM CaCl <sub>2</sub> x 2H <sub>2</sub> O
250µl 1M MgCl <sub>2</sub> x 6H <sub>2</sub> O

## Solution C:

component
50ml WIM
250mg 3.8M BSA
750µl 10mM CaCl <sub>2</sub> x 2H <sub>2</sub> O
250µl 1M MgCl <sub>2</sub> x 6H <sub>2</sub> O

Solution D:

component
50ml solution C
150µl 10mM CaCl <sub>2</sub> x 2H <sub>2</sub> O

Solution E:

component
15ml solution C
562µl 10mM CaCl <sub>2</sub> x 2H <sub>2</sub> O

0.4M phosphate buffer:

component	final concentration
NaH <sub>2</sub> PO <sub>4</sub> x H <sub>2</sub> O	76mM
Na <sub>2</sub> HPO <sub>4</sub> x 7H <sub>2</sub> O	320mM

4% paraformaldehyde:

component	final concentration
phosphate buffer	0.4M
paraformaldehyde	0.33M

0.1M TB:

component	final concentration
Trizma hydrochloride	84mM
Trizma Base	16mM

0.1M TBS:

component	final concentration
Trizma hydrochloride	84mM
Trizma Base	16Mm
NaCl	150mM

---

### 2.4.5. Mitochondria isolation:

buffer A pH 7.4:

component	final concentration
Mannitol	225mM
Sucrose	75mM
EGTA	0.1mM
fatty acid free BSA	1mg/ml
HEPES	10mM

buffer B pH 7.4:

component	final concentration
Mannitol	225mM
Sucrose	75mM
EGTA	0.1mM
HEPES	10mM

buffer C pH 7.4:

component	final concentration
Sucrose	395mM
EGTA	0.1mM
HEPES	10mM

buffer D pH 7.4:

component	final concentration
Sucrose	1.28M
EGTA	0.4mM
HEPES	40mM

### 2.4.6. Isolation of neonatal rat cardiomyocytes:

Calcium- and Bicarbonate-Free Hanks` with HEPES (CBFHH):

component	final concentration
NaCl	137mM
KCl	5.36mM
MgSO <sub>4</sub> x 7H <sub>2</sub> O	0.81mM
Dextrose	5.5mM
KH <sub>2</sub> PO <sub>4</sub>	0.44mM
Na <sub>2</sub> HPO <sub>4</sub>	0.34mM
HEPES	20.06mM
Penicillin G	50.0U/ml
Streptomycin	50µg/ml

Trypsine & DNase (T&D): CBFHH containing 10mg/ml DNase and 1.5mg/ml  
Trypsine

MEM/5: MEM HBS with NEAA containing

component	final concentration
BrdU	0.1mM
Penicillin G	50µg/ml
Streptomycin	50µg/ml
Vitamin B12	2µg/ml
L-Glutamine	2.0mM
NaHCO <sub>3</sub>	4.2mM
FCS	5%

2.4.7. O<sub>2</sub>-consumption:

cardioplegic solution (modified Krebs-Henseleit-buffer) 4°C:

component	final concentration
NaCl	116.1mM
KCl	5.0mM
MgCl <sub>2</sub> x 6H <sub>2</sub> O	1.2mM
Na <sub>2</sub> O <sub>4</sub>	1.2mM
NaH <sub>2</sub> PO <sub>4</sub> x H <sub>2</sub> O	2.0mM
NaHCO <sub>3</sub>	18.0mM
Glucose	11.2mM
CaCl <sub>2</sub>	0.25mM
BDM	29.7mM

gassed with 95% O<sub>2</sub>, 5% CO<sub>2</sub>

assay solution (modified Krebs-Henseleit-buffer) 37°C:

component	final concentration
NaCl	116.1mM
KCl	5.0mM
MgCl <sub>2</sub> x 6H <sub>2</sub> O	1.2mM
Na <sub>2</sub> O <sub>4</sub>	1.2mM
NaH <sub>2</sub> PO <sub>4</sub> x H <sub>2</sub> O	2.0mM
NaHCO <sub>3</sub>	18.0mM
Glucose	11.2mM
CaCl <sub>2</sub>	2.25mM

gassed with 95% O<sub>2</sub>, 5% CO<sub>2</sub>

### 2.4.8. NADPH oxidase activity:

Krebs-Henseleit buffer (KHS):

component	final concentration
NaCl	118.0mM
KCl	4.7mM
MgSO <sub>4</sub> x 7H <sub>2</sub> O	1.2mM
CaCl <sub>2</sub>	1.75mM
EDTANa <sub>2</sub>	0.5mM
Glucose	11.0mM

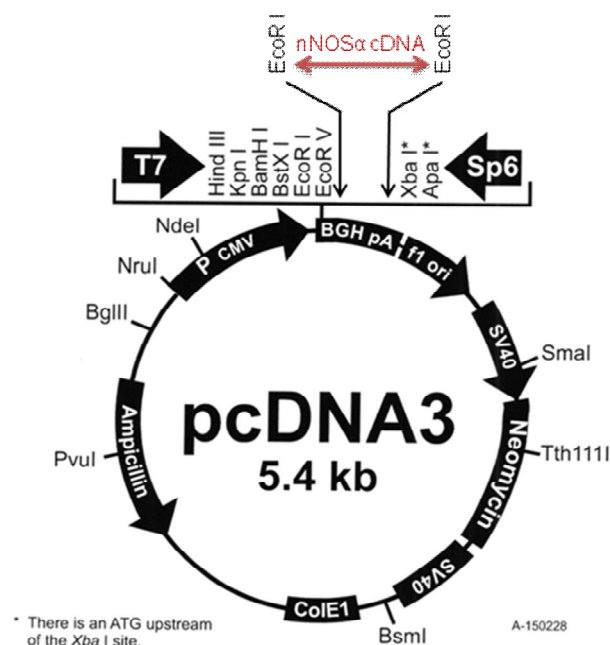
dilution in a.d. and gassed until CO<sub>2</sub>-saturation

component	final concentration
KH <sub>2</sub> PO <sub>4</sub>	1.2mM
NaHCO <sub>3</sub>	25.0mM
2,3-butandion monoxim (BDM)	30.0mM

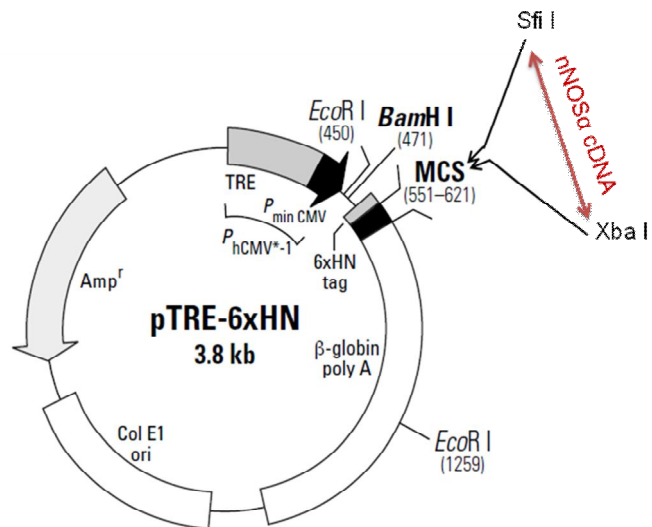
were added after CO<sub>2</sub>-saturation

### 2.5. Vectors:

nNOS $\alpha$  cDNA (provided by David Bredt, USA):



pTRE-6xHN Vector (clontech, Heidelberg, Germany, Cat. No. 61009):



## 2.6. Oligonucleotides:

All ordered from Eurofins MWG operon (Ebersberg, Germany):

Tet-Off-reverse: 5`-GTC AGT CGA GTG CAC AGT TT-3`

Tet-Off-forward: 5`-CAA ATG TTG CTT GTC TGG TG-3`

nNOS-reverse: 5`-GAG ATG ATC ACG GGA GGC-3`

nNOS-forward: 5`-CGC CTG GAG ACG CCA TCC-3`

internal control forward: 5`-CAA ATG TTG CTT GTC TGG TG-3`

internal control reverse: 5`-GTC AGT CGA GTG CAC AGT TT-3`



2.7. Antibodies:

antibody	company	Cat. No.
mouse monoclonal anti-nNOS antibody	<b>BD Transduction Laboratories</b> , Heidelberg, Germany	# 610309
goat anti-mouse IgG antibody conjugated with 12nm or 6nm gold particles	<b>PLANO GmbH</b> , Wetzlar, Germany	# 15750
horseradish peroxidase (HRP)-conjugated anti-mouse IgG	<b>GE Healthcare</b> , Munich, Germany	# NA9310V
rabbit polyclonal anti-prohibitin antibody	<b>abcam</b> , Cambridge, UK	# ab28172
horseradish peroxidase (HRP)-conjugated anti-rabbit IgG	<b>GE Healthcare</b> , Munich, Germany	# NA9340V
mouse monoclonal anti-rac 1 antibody	<b>BD Transduction Laboratories</b> , Heidelberg, Germany	# 610651
mouse monoclonal anti-p47 <sup>PHOX</sup> antibody	<b>BD Transduction Laboratories</b> , Heidelberg, Germany	# 610355
mouse monoclonal anti-p67 <sup>PHOX</sup> antibody	<b>BD Transduction Laboratories</b> , Heidelberg, Germany	# 610913
mouse monoclonal anti-GAPDH antibody	<b>Chemicon</b> , Schwalbach, Germany	# MAB374
rabbit polyclonal anti-xanthine oxidase antibody	<b>abcam</b> , Cambridge, UK	# ab6194
rabbit polyclonal anti-6xHN antibody	<b>BD Biosciences</b> , Heidelberg, Germany	# 8940-1
mouse monoclonal anti-cytochrome c antibody	<b>MitoSciences</b> , Oregon, USA	# MSA06
rabbit polyconal anti-nNOS antibody	<b>Invitrogen</b> , Karlsruhe, Germany	# 61-7000
rabbit polyclonal anti L-type Ca <sup>2+</sup> -channel	<b>Alomone Laboratories</b> , Jerusalem, Israel	# ACC-013
rabbit polyclonal anti-SERCA2a antibody	<b>Badrilla</b> , Leeds, UK	# A010-20
mouse monoclonal anti-porin antibody	<b>MitoSciences</b> , Oregon, USA	# MSA03
mouse monoclonal anti-eNOS antibody	<b>BD Transduction Laboratories</b> , Heidelberg, Germany	# 610297
mouse monoclonal anti iNOS antibody	<b>BD Transduction Laboratories</b> , Heidelberg, Germany	# 610432
mouse monoclonal anti-HSP90 antibody	<b>abcam</b> , Cambridge, UK	# ab 1429
biotinylated anti-rabbit IgG	<b>Vector Laboratories</b> , Lörrach, Germany	# BA-1000
Avidin D fluorescence antibody	<b>Vector Laboratories</b> , Lörrach, Germany	# A-2001

2.8. Mouse strains:

$\alpha$ -MHC mice: FVB.Cg-Tg(Myh6-tTA)6Smbf/J, Stock number 003170, Jackson Laboratory, USA

nNOS transgenic mice: the nNOS $\alpha$  cDNA (provided by D. Bredt) was cloned into the pTRE-6xHN vector (Clontech, Germany)

double transgenic mice:  $\alpha$ -MHC and nNOS transgenic mice were crossbred

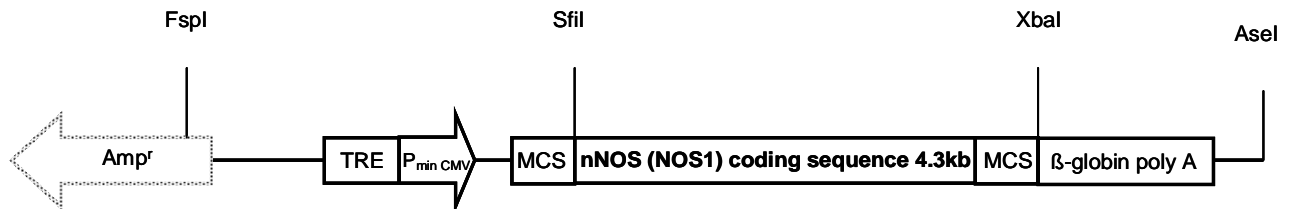
All mice were 8 to 12 weeks old, induction time (for nNOS overexpression) was two weeks

The investigation is conform with the *Guide for the Care and Use of Laboratory Animals* published by the US National Institutes of Health (NIH Publication No. 85-23, revised 1996). The animal research was granted by the "Regierung von Unterfranken" (approval reference number Az. 54-2531.01-37/04).

### 3. Methods:

#### 3.1. Animal model:

To generate transgenic mice the Tet-Off system (clontech, Germany) was used. For this system, two different mouse strains were employed. The first strain encodes the regulatory protein tTA (tetracycline-controlled transactivator) under control of the  $\alpha$ -MHC promoter (FVB.Cg-Tg(Myh6-tTA)6smbf/J, Jackson Laboratory, USA) and guarantees myocardial specificity. The second strain contains the gene of interest (nNOS) under control of the tetracycline-response element (TRE). This strain is responsible for the inducibility of our system and for the expression of our gene of interest (nNOS). To establish this strain, I cloned the nNOS $\alpha$  cDNA (a gift from D. Bredt) into the pTRE-6xHN vector (clontech, Germany). Importantly, this nNOS $\alpha$  isoform contains exon 2, encoding for the nNOS PDZ-domain (PDZ-domains are modular protein interaction domains that bind in a sequence-specific fashion to short C-terminal peptides or internal peptides that fold to a  $\beta$ -finger).



The two different strains were crossbred and the double transgenic offspring were fed with doxycycline (Sigma, Germany) chow (contains 100mg doxycycline per kg chow, Ssniff Spezialdiäten, Soest, Germany).

Figure 19: Scheme of gene regulation in the Tet-Off system: (BD Biosciences, Germany)

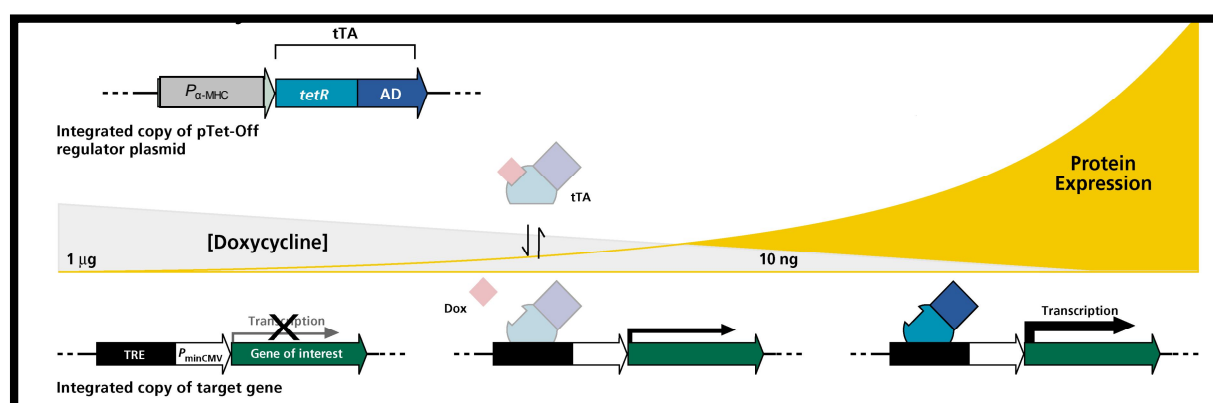


Figure 19 legend: Scheme of gene regulation in the Tet-Off system

The TRE is located upstream of the  $P_{\text{minCMV}}$  (minimal immediate early promoter of cytomegalovirus), which is silent in the presence of doxycycline. Tetracycline-controlled transactivator (tTA) binds the TRE - and thereby activates transcription of the gene of interest (nNOS) - in the *absence* of tetracycline or doxycycline.

Mice were fed with standard mouse chow to induce nNOS overexpression for two weeks. Mice used for experiments were 8 to 12 weeks old.

### 3.2. Genotyping of double transgenic mice:

The genotyping was done by PCR. The following reaction composition was used (*Taq* PCR Core Kit, Qiagen, Germany):

component	volume/reaction	final concentration
10x PCR buffer	5µl	1x
dNTP mix (each 10mM)	1µl	100µM of each
primer A	1µl	0.1µM
primer B	1µl	0.1µM
<i>Taq</i> DNA Polymerase	0.5µl	2.5 units/reaction
distilled water	36.5µl	-
template DNA	5µl	≤1µg/reaction
<b>total volume</b>	<b>50µl</b>	<b>-</b>

For the nNOS- and Tet-Off-PCR fragment the following PCR program was used:

step	temperature	time	note
1	94°C	3min	
2	94°C	20sec	
3	64°C	30sec	-0.5°C per cycle
4	72°C	35sec	Go to step 2, repeat 12 times
5	94°C	20sec	
6	58°C	30sec	
7	72°C	35sec	Go to 5, repeat 25 times
8	72°C	2min	

Three different primer pairs were used to genotype the animals. By using the Tet-Off primer pair (Tet-Off-reverse: 5`-GTC AGT CGA GTG CAC AGT TT-3`; Tet-Off-forward: 5`-CAA ATG TTG CTT GTC TGG TG-3`) (Eurofins MWG operon, Germany) a 450bp fragment within the tTA-region was amplified, whereas the nNOS primer pair (nNOS-reverse: 5`-GAG ATG ATC ACG GGA GGC-3`; nNOS-forward: 5`-CGC CTG GAG ACG CCA TCC-3`) (Eurofins MWG operon, Germany) amplified a 270bp fragment, which contains both, a part of the nNOS sequence and the 6xHN tag. Double transgenic mice are positive in both reactions.

PCR program used as an internal control:

step	temperature	time	note
1	94°C	3min	
2	94°C	1min	
3	68°C	1min	
4	72°C	1min	Go to step 2, repeat 35 times
5	72°C	10min	

The primer pair for the internal control (internal control forward: 5`-CAA ATG TTG CTT GTC TGG TG-3`; internal control reverse: 5`-GTC AGT CGA GTG CAC AGT

TT-3') (Eurofins MWG operon, Germany) amplified a 200bp fragment from the wildtype allele.

### 3.3. Infarct size measurement after ischemia-reperfusion *in vivo*:

Infarct size measurement and ischemia-reperfusion experiments were performed as recently described<sup>192</sup> in cooperation with AG Frantz. After anesthesia (1.5% isoflurane, central pharmacy, Würzburg, Germany) and intubation, mice were ventilated with a volume-cycled rodent respirator. For ischemia-reperfusion studies, ligation of the anterior descending branch of the left coronary artery (LAD) was achieved by tying 6-0 silk suture, 2-3mm from the tip of the left auricle, around the artery. After occlusion for 30min, blood flow was restored by removing the ligature and polyethylene tubing. Proper reperfusion was determined by visual inspection and changes in ventricular function. The chest wall was closed with a continuous 6-0 prolene suture and the skin with 4-0 polyester suture. For infarct size measurement after 24h reperfusion, the animals were again intubated, the suture reoccluded and 5% Evans Blue (Sigma, Germany) injected into the apex of the heart. The heart was removed, washed with NaCl (Merck, Germany) and frozen in Tissue Tek (Hartenstein, Germany) at -20°C. The frozen heart was cut into five parallel transverse slices, which were stained with 2% triphenyl-tetrazolium-choride (TTC) (Sigma, Germany) for 10min at 37°C. After TTC staining, viable myocardium stains red and the infarcted areas appear pale. After fixation in formalin (Sigma, Germany), slices were weighed on a scale, imaged and the area of infarction for each section was determined by computerised planimetry using an image analysis software program (ScionImage imaging software). The size of infarction was determined by the following equations. Weight of infarction = (A1 x Wt1) + (A2 x Wt2) + (A3 x Wt3) + (A4 x Wt4) + (A5 x Wt5), where A is area of infarction in percent by planimetry and Wt is the weight of each section. Percentage of infarcted left ventricle = (weight of infarction/weight of left ventricle) x 100. Area at risk as a percentage of left ventricle = (weight of left ventricle-weight of left ventricle stained blue)/weight of left ventricle.

### 3.4. In vitro ischemia-reperfusion experiments with isolated hearts (Langendorff):

*In vitro* ischemia-reperfusion experiments with isolated hearts were performed as follows: Mice were anesthetised by injecting pentobarbital (central pharmacy, Würzburg, Germany) intraperitoneally. The heart was rapidly excised, the aorta was dissected free and mounted onto a cannula attached to a perfusion apparatus as described previously<sup>193</sup>. Retrograde perfusion of the heart was started in the Langendorff mode at 37°C using a constant coronary perfusion pressure of 100mmHg. Oxygenated Krebs-Henseleit buffer (KHS), gassed with 95% O<sub>2</sub> and 5% CO<sub>2</sub>, was used for perfusion and hearts were immersed in their own perfusate in a water-jacketed reservoir. A water filled balloon was inserted in the left ventricle and fixed by a ligature. The balloon was connected to a Statham P23Db pressure transducer (Gould Statham Instruments) for continuous measurement of left ventricular pressure. Pressure volume curves were obtained to find optimal preload by filling the balloon stepwise. After reaching the maximal developed pressure, the intracardial balloon volume was set to 50% of volume of maximal developed pressure. Hearts were subjected to 20min ischemia followed by reperfusion. The specific nNOS inhibitor S-methyl-L-thiocitrulline acetate salt (SMTC) was administered at a final concentration of 0.125mg/kg.

### 3.5. Electron microscopy with immunogold labeling:

Excised hearts were fixed in 4% paraformaldehyde (PFA) (Sigma, Germany) for 20min, cut into small pieces (< 1mm) and incubated in 4% PFA for an additional hour at 4°C. After fixation, specimen were washed with phosphate buffered saline (PBS) at 4°C, incubated with 50mM NH<sub>4</sub>Cl (central pharmacy, Würzburg, Germany) for 15min and again washed several times in a.d. After dehydration with an ascending alcohol bank, heart pieces were embedded in LR-White (Sigma, Germany), transferred into gelatine-capsules and polymerised at 40°C for at least 3 days. Ultrathinsections were made out of the embedded hearts and immunogold labeling was performed in cooperation with Prof. Krohne. The sections were transferred onto

polyvinylbutyrate-plated nickelgrids. The grids were incubated for 5min in PBS and for 5min in PBS containing 1% BSA (Sigma, Germany) and 0.1% Tween 20 (Sigma, Germany). After incubation for 1h with the first antibody, the grids were washed for 20min with PBS containing 1% BSA and 0.1% Tween 20, and for 20 min with PBS containing 0.1% BSA and 0.1% Tween 20. After washing, grids were incubated for 1h with the secondary antibody (goat anti-mouse IgG antibody conjugated with 12nm or 6nm gold particles 1:10 (PLANO GmbH, Germany)). Subsequently, a series of washing steps was performed (20 min with PBS containing 0.1% BSA and 0.1% Tween 20, 5min with PBS, 2min with 1.25% glutaraldehyde (Sigma, Germany) and 15min with a.d. For contrast staining of the sections the grids were incubated for 5min with 2% uranylacetat (Sigma, Germany) and for 5min with leadcitrate (Sigma, Germany).

For detection of transgenic nNOS as first antibody, a polyclonal anti-6xHN antibody 1:50 (BD Biosciences, Germany) was used followed by a secondary antibody coupled to 12nm gold particles.

When nNOS and cytochrome c oxidase expression were investigated simultaneously, a monoclonal anti-cytochrome c oxidase antibody 1:200 (MitoSciences, USA) was used followed by a second antibody that was coupled to 12nm gold particles and a polyclonal anti-nNOS antibody (Invitrogen, Germany) was used followed by a second antibody that was coupled to 6nm gold particles. This anti-nNOS antibody was reactive for both endogenous and overexpressed nNOS.

### 3.6. Immunofluorescence staining of isolated adult cardiac myocytes:

#### 3.6.1. Preparation of adult cardiac myocytes:

Following CO<sub>2</sub>-induced euthanasia, mouse chest was opened and 10ml of ice cold cardioplegic solution, pH 7.4 was injected in the right ventricle. The excised heart was dropped in a Ø 50mm dish containing icecold Wittenberg Isolation Medium/Insuline and fixed on a canula by using a silk thread. The fixed heart was clamped in the Langendorff apparatus and perfused for about 5 to 10min with solution A. After changing to solution B until flow rate speeds up to ~ double the initial



---

rate, the heart was removed from the Langendorff apparatus and put into a fresh dish. After excising the atria, the ventricles were chopped in small pieces and placed in 10ml of solution C. The ventricle pieces were incubated for 20min at 37°C and mixed several times during the first 10min. The supernatant was collected, 15ml of solution D was added to the pellet and incubation for 20 min was enclosed. The same procedure was repeated with solution E. After draining the cell suspension through a 100µm cell strainer (Becton Dickinson, Germany), the cell suspension was centrifuged at 100-200g for 3min. The supernatant was removed and the pellet was resuspended in 7ml SKG MEM Eagle (Sigma, Germany) with 2.5% Foetal Calf Serum (FCS) (PAA Laboratories GmbH, Austria). Finally the isolated adult cardiomyocytes were plated on laminin-coated slides (BD Biosciences, Germany).

### 3.6.2 Immunostaining of cardiac myocytes:

The isolated cells were plated on laminin-coated slides (BD Biosciences, Germany) and rinsed in 0.1M phosphate buffer (1:4 dilution of 0.4M phosphate buffer). After fixation in 4% paraformaldehyde for 30-45min, the cells were again rinsed in 0.1M phosphate buffer. After a series of washes in 0.1M TB and 0.1M TBS, the cells were incubated for 30min in 2% avidin (Vector Laboratories, Germany) and rinsed again in 0.1M TBS. After incubation in 2% biotin (Vector Laboratories, Germany) for 30min, the cells were rinsed in 0.1M TBS. The polyclonal anti-nNOS antibody 1:50 (Invitrogen, Germany) was added and incubated in 0.1M TBS, 0.075% Triton X, 1% goat serum overnight at 4°C. The next day cells were rinsed in 0.1M TBS and probed with biotinylated anti-rabbit IgG 1:300 (Vector Laboratories, Germany) for at least 1h followed by avidin D fluoresce antibody 1:300 (Vector Laboratories, Germany) for 2 hours. Finally, after a series of washes in 0.1M TBS, the cells were coverslipped with Vectashield (Vector Laboratories, Germany).

Further antibodies were used: anti-cytochrome c 1:100 (MitoSciences, USA).

### 3.7. nNOS protein expression in isolated mitochondria:

Enriched mitochondrial fraction from mouse heart was prepared according to a modified protocol developed by R&D Systems (Wiesbaden, Germany). Mouse hearts were homogenised in RIPA buffer, centrifuged for 30min at 15,000g and the resulting pellet was homogenised in buffer A (5ml/0.5g tissue). The resulting homogenate was centrifuged for 10min at 15,000g (4°C). The pellet was homogenised in 500µl buffer B and centrifuged for 10min at 15,000g (4°C). The pellet was resuspended in 600µl buffer C. Mitochondria were further enriched on a gradient of Percoll (Sigma, Germany) by centrifugation in polyallomer tubes in an ultracentrifuge. All solutions, the centrifuge, and tubes were prechilled to 4°C. 500µl of 60% Percoll (Percoll diluted with buffer D), added to the bottom of the centrifuge tube, was carefully overlaid with 900µl 26% Percoll (Percoll diluted with buffer D). 300µl of the pellet resuspended in buffer C was overlaid on the 26% Percoll. The material was centrifuged for 30min at 40,000g (4°C). After centrifugation, the mitochondria were collected from the interface formed between the 26% and 60% Percoll.

For Western Blot analysis of nNOS protein expression in isolated mitochondria, hearts were rapidly excised, rinsed in PBS and shock frozen in liquid nitrogen. Frozen hearts were homogenised in RIPA-buffer with protease inhibitor cocktail (Roche Diagnostics GmbH, Germany). Samples were homogenised for 1min and centrifuged for 15min at 15,000g and 4°C. Total protein concentration of the supernatant was determined by measuring absorbance at 280nm and 40µg of each sample was separated in 10% SDS-PAGE gels. Proteins were transferred electrophoretically onto nitrocellulose membrane (Hartenstein, Germany), while immersed in transfer buffer. After the transfer, non-specific binding was blocked by incubating membranes in blocking buffer for at least 1h. Protein samples were probed with purified mouse monoclonal anti-nNOS antibody 1:200 (BD Transduction Laboratories, Germany) for at least 1h followed by horseradish peroxidase (HRP)-conjugated anti-mouse IgG 1:5,000 (GE Healthcare, Germany) for 1h. Between antibody incubation periods, a series of washing steps with 0.1% Tween/PBS were performed. Bands were visualised via enhanced chemiluminescence (GE Healthcare, Germany). As a loading control, mitochondria samples were probed with purified

rabbit polyclonal anti-prohibitin antibody 1:200 (abcam, UK) for 1h followed by horseradish peroxidase (HRP)-conjugated anti-rabbit IgG 1:5,000 (GE Healthcare, Germany) for 1h.

Further antibodies were used: polyclonal anti-L-type  $\text{Ca}^{2+}$ -channel antibody 1:500 (Alomone Laboratories, Israel), polyclonal anti-SERCA2a antibody 1:5,000 (Badrilla, UK), monoclonal anti-porin antibody 1:1,000 (MitoSciences, USA), monoclonal anti-cytochrome c antibody 1:1,000 (MitoSciences, USA).

### 3.8. Coimmunoprecipitation experiments:

Frozen hearts were homogenised in RIPA-buffer with protease inhibitor cocktail (Roche Diagnostics GmbH). Samples were steamed for 1min and centrifuged for 15min at 15,000g and 4°C. Total protein concentration of the supernatant was determined by measuring absorbance at 280nm.

The Co-IP experiments were done using the Immunoprecipitation Starter Pack (GE Healthcare, Germany). The amount of 300-600µg protein was used. After an initial pre-clearing step of one hour at 4°C (500µl of whole cell lysate with respectively 25µl protein G / A sepharose beads), antigens were coupled overnight at 4°C to 2.5µg purified antibody (anti-nNOS, anti-iNOS or anti-eNOS (all Transduction Laboratories, Germany)). Protein-antibody complexes were precipitated with a mix of 25µl protein A and protein G sepharose beads for one hour at 4°C. The beads were washed three times with isotonic salt buffer (RIPA-buffer), once with wash-buffer (50mM Tris, pH 8) and suspended in 50µl Laemmli buffer (Laemmli sample buffer containing 2-Mercaptoethanol). After denaturation for 5 minutes at 95°C and a following centrifugation step, the supernatant was analysed by SDS-PAGE. Detection was performed with anti-HSP90 antibody (abcam, UK).

### 3.9. Transfection of neonatal cardiomyocytes and treatment with geldanymycin:

#### 3.9.1. Isolation of neonatal rat cardiomyocytes:

Experiments were performed according to 'Institutional Animal Care and Use Committee' and 'National Institute of Health (NIH)' guide lines. After decapitation the hearts were removed from 1- to 2-day old neonatal wistar rats, cut into small pieces and digested in T&D (Trypsine & DNase) (Sigma, Germany). The heart pieces were transferred into a 50ml Falcon tube and put on a magnetic stirrer at the lowest speed (100-140 rpm) and room temperature (22°C). After five minutes of incubation the supernatant was transferred to a 50 ml falcon tube containing 7.5 ml foetal calf serum (FCS), whereby 12.5 ml T&D was added to the remaining tissue pellet. This step was repeated until the whole tissue was digested. The collected supernatants were pelleted by ten minutes of centrifugation at 700 g and resuspended in MEM/5. After filtering through a metal sieve most of the non-cardiomyocytes were removed by preplating for one hour at 37°C in the CO<sub>2</sub> incubator (0.9 %). After preplating, the supernatant containing approximately 90 % of cardiomyocytes, was saved and cells were counted in a Fuchs-Rosenthal chamber and plated in MEM/5 on 6-well plates at a density of 0.7 million cells/well (low-density culture) (for 100 mm dishes: 5.0 million cells/dish; for chamber slides (2 and 4 wells): 200,000 cells/well). After 24 hours the cells were washed with MEM and incubated for additionally 24 hours in MEM/5. After 48 hours after preparation the treatment of cells was specific for each experiment. Non-myocyte contamination of primary cultures 48 hours after isolation consisted of approximately 5 % of the total cell population. Myocardial cells were morphologically distinguished by a coarse, granular cytoplasm containing small, dense nuclei, whereas non-myocytes were readily distinguished by a phase-lucent cytoplasm.

#### 3.9.2 Transfection and treatment of neonatal cardiomyocytes:

NRCMs (neonatal rat cardiomyocytes) were transfected with Lipofectamine (Invitrogen Life Technologies, Germany) 48 hours after preparation, on 6-well plates

---

at a density of  $1 \times 10^6$  cells per well or on chamber slides at a density of 700,000 cells per well. The transfection was performed as described by the manufacturers with the following plasmid: pTRE-6xHN nNOS $\alpha$  cDNA Vector. After incubation for three hours at 37°C in the CO<sub>2</sub>-incubator (0,9 %) following a medium change to MEM/1, cells were treated with 2 $\mu$ M geldanamycin. All cells were harvested 12hours after stimulation. Mitochondria were isolated and Western Blot analysis was performed. Mitochondria samples were probed with purified mouse monoclonal anti-nNOS antibody 1:200 (BD Transduction Laboratories, Germany). Cytochrome c was used as a loading control.

### 3.10. Nitrite level measurement:

Nitrite levels were determined in isolated mitochondria of nNOS overexpressing and non-induced mice. The measurement was performed with a modified version of the Nitric Oxide Colorimetric Assay Kit from Biomol. The kit involves the colorimetric detection of nitrite as a colored azo dye product of the Griess reaction that absorbs visible light at 540nm. The interaction of NO in a system is measured by the determination of the total nitrate and nitrite concentration in the sample. This kit allows for the total determination of both NO products in the sample by conversion of all the sample nitrate into nitrite, followed by the determination of the total concentration of nitrite in the sample. The transient and volatile nature of NO makes it unsuitable for most convenient detection methods. However, two stable breakdown products, nitrate (NO<sub>3</sub>) and nitrite (NO<sub>2</sub>) can be easily detected by photometric means. For the measurement 0.5 $\mu$ g/ $\mu$ l isolated mitochondria were used.

### 3.11. Cytochrome c oxidase activity:

The measurement of cytochrome c oxidase activity was performed with a modified version of the Cytochrome C Oxidase Assay Kit from Sigma. Instead of DTT, 10mM ascorbate was used to reduce the cytochrome c, followed by removal of the reductant by passage through Sephadex G-25 column. The colorimetric assay in this

kit is based on observation of the decrease in absorbance at 550nm of ferrocytochrome c caused by its oxidation to ferricytochrome c by cytochrome c oxidase. Whole mouse hearts were homogenised in RIPA buffer and mitochondria were isolated as described previously. Protein concentration was measured and a final concentration of 0.4µg/µl was used for the assay. Activity was measured using a kinetic program: 5second delay, 10second interval, 6 readings, room temperature.

### 3.12. Myocardial O<sub>2</sub>-consumption:

O<sub>2</sub>-consumption measurements were performed as described previously<sup>194</sup>. Immediately after the anesthetic was administered to mice, a cardiectomy was performed and the heart was submerged in oxygenated (95% O<sub>2</sub>, 5% CO<sub>2</sub>) cardioplegic solution (modified Krebs-Henseleit-buffer). Muscle stripes were excised from the right ventricle (40 x 0.5 x 0.5mm). The muscle preparations were transferred to a chamber containing oxygenated (95% O<sub>2</sub>, 5% CO<sub>2</sub>) assay solution (modified Krebs-Henseleit-buffer) at 37°C and were fixed between steel clamps and a force transducer (Scientific instruments, Germany). Before measuring O<sub>2</sub>-consumption, the protective solution containing 2,3-butandion monoxim (BDM) (Sigma, Germany) was washed out and the muscle stripe was stimulated with 2Hz, 25% over threshold voltage. After the equilibration period, the muscle was carefully stretched to optimal length (defined as steady-state twitch force under isometric conditions). The oxygen measurement setup (see figure 20) consists of a metal cylinder with a heating unit and a closed plexiglas block containing the muscle chamber. The muscle stripe is suspended between two steel clamps, providing means for fixation and electrical stimulation. One of these clamps is connected to a force transducer. An inlet and outlet are used for perfusion. The Clark-oxygen electrode is located perpendicular to the long axis of the muscle stripe, providing direct access to the perfusate. For the measurement, perfusion with oxygenated assay solution was stopped, and the decrease of oxygen partial pressure at a defined distance from the muscle surface was recorded for 20sec. Muscle stripes were stimulated with 1-5Hz (60-300 beats/min). After a steady state was reached, MVO<sub>2</sub> was recorded. Muscle fibers that showed a significant loss in force development compared with the initial 1-Hz value

were excluded. Analysis of oxygen data ( $\text{ml O}_2 \times \text{mm}^{-3} \times \text{min}^{-1}$ ) was performed using Muscle Research System software from Scientific Instruments. Recording of isometrically developed force, force time integral (FTI), was performed by “twitch” software (Scientific Instruments, Germany). FTI (in  $\text{N} \times \text{s}/\text{min}/\text{mm}^2$ ) is defined as the area between peak systolic force during the stimulation interval. It represents an equivalent of work in isometrically contracting myocardium and is a major determinant of  $\text{MVO}_2$ . For better display the ratio of  $\text{MVO}_2/\text{FTI}$  was given in relative % where  $\text{MVO}_2/\text{FTI}$  at rest was set as 100%.

**Figure 20: Oxygen measurement setup:**

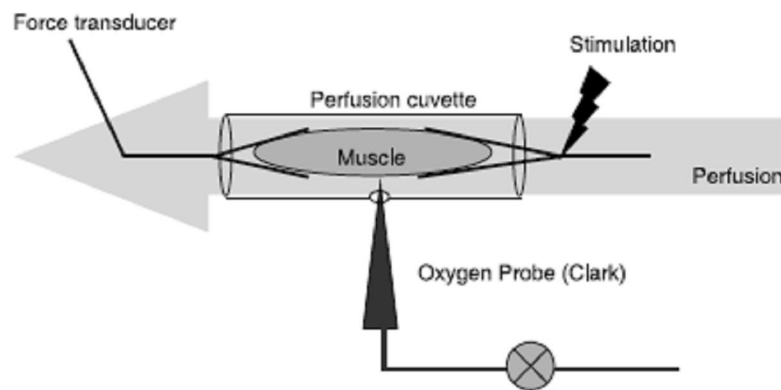


**Figure 20 legend: Oxygen measurement setup**

The muscle fiber is fixed between a force transducer and a servomotor. The muscle was prestretched to optimal length, electrically stimulated and perfused with assay solution ( $37^\circ\text{C}$ ). A Clark-oxygen electrode was placed near the surface of the muscle fiber to measure the oxygen consumption of the working muscle stripe while perfusion was stopped.

### 3.13. $\text{O}_2^-$ production in isolated mitochondria:

$\text{O}_2^-$  production was determined by the oxidation of mito-hydroethidine (Mito-HE/ MitoSOX™ Red; Invitrogen, Germany) to 2-hydroxy-mito-ethidium using HPLC-electrochemical (EC) analysis, as described previously with some modifications<sup>245</sup>. Mitochondria were isolated from the left ventricle using the Qproteome Mitochondria

---

Isolation Kit (Qiagen, Germany). Isolated mitochondria were incubated with Mito-HE (10 $\mu$ mol/l) and the conversion to 2-hydroxy-mito-ethidium monitored by HPLC-EC.

### 3.14. Reactive oxygen free radicals (ROS)-concentration:

For measuring the concentration of reactive oxygen free radicals (ROS), the TAC-Peroxy assay kit (Axxora, Germany) was used. This assay is based on inhibition of luminescence caused by peroxy radicals involved in lipid peroxidation *in vivo*. Biologically relevant peroxy free radicals are generated by thermal decomposition of 2,2'-azobis(2-amidinopropane) (ABAP). The ABAP decomposition products are a pair of C-centered free radicals R• and a nitrogen molecule. The R• free radicals further react with oxygen molecules to form peroxy radicals ROO•, which are similar to those found *in vivo* during lipid peroxidation. These peroxy radicals react with an indicator molecule, luminol (LH<sub>2</sub>), to generate a luminol radical (LH•) which results in emission of blue light centered at ~425nm. When antioxidants are present, such a light production is inhibited until the antioxidants are exhausted. The time of inhibition or the induction time to light production is proportional to the total concentration of antioxidants. The antioxidant concentration is determined by comparing induction time to that of a water-soluble Vitamin E (tocopherol) analog, Trolox.

To determine whether ROS are produced by the NADPH oxidase or the xanthine oxidoreductase, heart samples were incubated with different inhibitors. Apocynin (300 $\mu$ M, 30min incubation at 37°C, Calbiochem, Germany) as an inhibitor for the NADPH oxidase and allopurinol (0.1mM, 1min incubation at room temperature, Sigma, Germany) for the xanthine oxidoreductase.



### 3.15. NADPH oxidase and xanthine oxidoreductase activity:

NADPH oxidase activity was measured by lucigenin-enhanced chemiluminescence. Frozen hearts were homogenised in KHS. Samples were homogenised for 1min and centrifuged for 15min at 15,000g and 4°C. Total protein concentration of the supernatant was determined by measuring absorbance at 280nm. 100µg protein lysate was incubated with 1mM lucigenin (Sigma, Germany), 300µM NADPH (Sigma, Germany) and luminescence was recorded for 20min at 30sec intervals.

The measurement of the xanthine oxidoreductase activity was carried out using the Amplex<sup>®</sup> Red Xanthine Oxidase Assay Kit (Molecular Probes, Germany). In this assay, xanthine oxidoreductase catalyses the oxidation of xanthine to uric acid and superoxide. In the reaction mixture, the superoxide spontaneously degrades to hydrogen peroxide (H<sub>2</sub>O<sub>2</sub>) which, in the presence of HRP, reacts stoichiometrically with Amplex Red reagent to generate the red-fluorescent oxidation product resorufin. Resorufin has an absorbance and fluorescence emission maxima of approximately 571nm and 585nm. As a first step, a xanthine oxidoreductase standard curve with concentrations of 0 to 10mU/ml was assessed. In the assay, the homogenised hearts were used at a final concentration of 5µg/µl. The samples were diluted in a working solution containing Amplex Red reagent solution, HRP solution, xanthine and reaction buffer. This mixture was filled into a 96-microplate, incubated for 30min at 37°C and measured at 560nm (ELISA Reader).

### 3.16. NADPH oxidase and XOR protein expression:

Western Blot analysis was performed to investigate the protein expression of different subunits of the NADPH oxidase (p47<sup>PHOX</sup>, p67<sup>PHOX</sup> and rac 1). Hearts were rapidly excised, rinsed in PBS and shock frozen in liquid nitrogen. Frozen hearts were homogenised in RIPA-buffer containing protease inhibitor cocktail (Roche Diagnostics GmbH, Germany). Samples were homogenised for 1min and centrifuged for 15min at 15,000g and 4°C. Total protein concentration of the supernatant was determined by measuring absorbance at 280nm and 40µg of each sample was separated in 10% SDS-PAGE gels. Proteins were transferred electrophoretically onto

nitrocellulose membrane, while immersed in transfer buffer. After the transfer, non-specific binding was blocked by incubating membranes in blocking buffer for at least 1h. Protein samples were probed with purified mouse monoclonal anti-rac 1 antibody 1:500, purified mouse monoclonal anti-p47<sup>PHOX</sup> antibody 1:500 or purified mouse monoclonal anti-p67<sup>PHOX</sup> antibody (all BD Transduction Laboratories, Germany) for at least 1h followed by HRP-conjugated anti-mouse IgG 1:5,000 (GE Healthcare, Germany) for 1h. Between antibody incubation periods, a series of washing steps with 0.1% Tween/PBS were performed. Bands were visualised via enhanced chemiluminescence (GE Healthcare, Germany). As a loading control, protein samples were probed with purified mouse monoclonal anti-GAPDH antibody 1:8,000 (Chemicon, Germany) for 1h followed by HRP-conjugated anti-mouse IgG 1:5,000 (GE Healthcare, Germany) for 1h.

For Western Blot analysis of XOR protein expression, hearts were rapidly excised, rinsed in PBS and frozen in liquid nitrogen. Frozen hearts were homogenised in RIPA-buffer with protease inhibitor cocktail (Roche Diagnostics GmbH, Germany). Samples were homogenised for 1min and centrifuged for 15min at 15,000g and 4°C. Total protein concentration of the supernatant was determined by measuring absorbance at 280nm and 40µg of each sample was separated on 10% SDS-PAGE gels. Proteins were transferred electrophoretically onto nitrocellulose membrane, while immersed in transfer buffer. After the transfer, non-specific binding was blocked by incubating membranes in blocking buffer for at least 1h. Protein samples were probed with purified rabbit polyclonal to xanthine oxidase antibody 1:1,000 (abcam, UK) for 1h followed by incubation with HRP-conjugated anti-rabbit IgG 1:5,000 (GE Healthcare, Germany) for 1h. Between antibody incubation periods, a series of washing steps with 0.1% Tween/PBS were performed. Bands were visualised via enhanced chemiluminescence (GE Healthcare, Germany). As a loading control, protein samples were probed with purified mouse monoclonal anti-GAPDH antibody 1:8,000 (Chemicon, Germany) for 1h followed by incubation with HRP-conjugated anti-mouse IgG 1:5,000 (GE Healthcare, Germany) for 1h.

### 3.17. Statistics:

All data are presented as mean $\pm$ SEM. Statistical analyses were performed using Student`s *t*-test or the one way ANOVA for repeated measurements where appropriate. Significance was assigned as a value of  $p < 0.05$  (\*) and  $p < 0.01$  (\*\*). No significant differences were denoted by n.s.

---

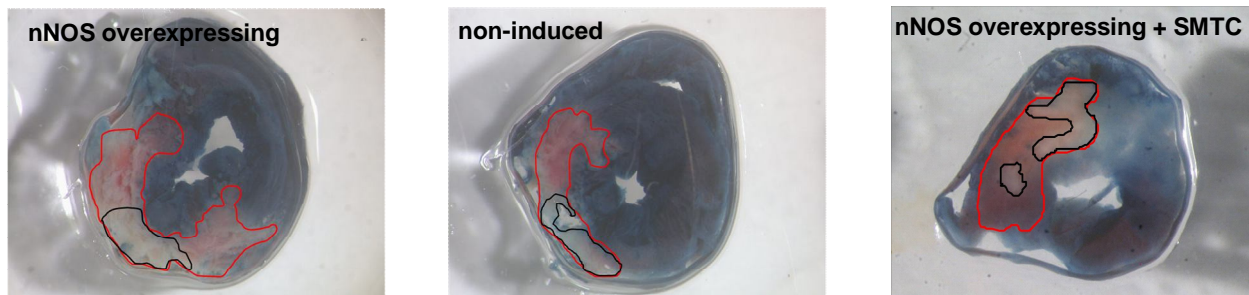
## 4. Results:

All mice used for the experiments were 8 to 12 weeks old. Mice were fed with standard mouse chow to induce nNOS overexpression for two weeks. As a control group non-induced mice were used.

### 4.1. nNOS overexpression reduced infarct size *in vivo* after ischemia-reperfusion injury:

I previously demonstrated that conditional nNOS overexpression decreases myocardial contractility under baseline conditions<sup>1</sup>. In this work I investigated the impact of nNOS overexpression under pathophysiological conditions (ischemia-reperfusion injury). *In vivo* occlusion of the left coronary artery (LAD) was performed for 30min in nNOS overexpressing mice and non-induced littermates. Immediately after the 24h reperfusion period, Evans Blue staining was performed. The infarct size within the area at risk was significantly decreased in nNOS overexpressing mice compared to non-induced animals ( $36.6 \pm 8.4$  vs.  $61.1 \pm 2.9\%$ ,  $n=8$ ,  $p<0.05$ ) (figure 21, 22). Application of SMTC (specific nNOS inhibitor, 0.125mg/kg) inhibited the cardioprotective effect of nNOS ( $59.05 \pm 05\%$ ,  $n=8$ ,  $p<0.05$ ) (figure 21, 22). In contrast, the area at risk referring to the whole heart section was not significantly altered between nNOS overexpressing mice, non-induced littermates and nNOS overexpressing mice treated with SMTC ( $35.1 \pm 6.2$  vs.  $34.1 \pm 3.6\%$  vs.  $25.9 \pm 6.9\%$ ,  $n=8$ , n.s.) (figure 23).

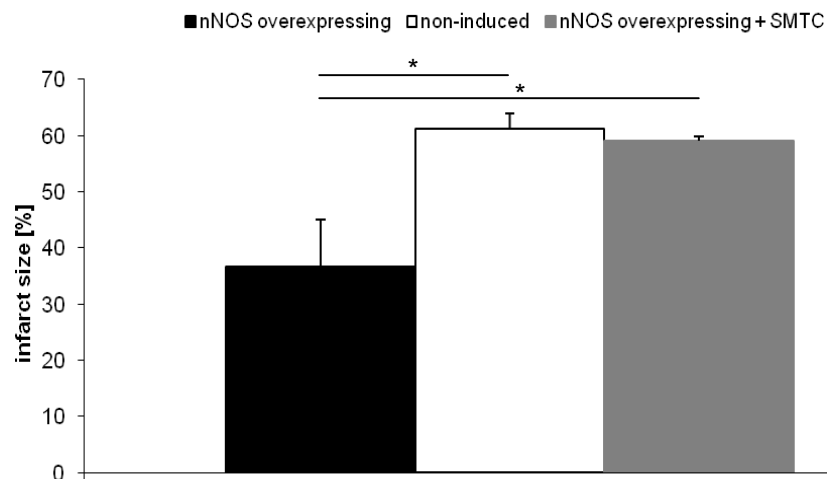
*In vivo* ischemia-reperfusion experiments were performed in cooperation with AG Frantz.

**Figure 21: Representative heart sections:****Figure legend 21: Representative heart sections**

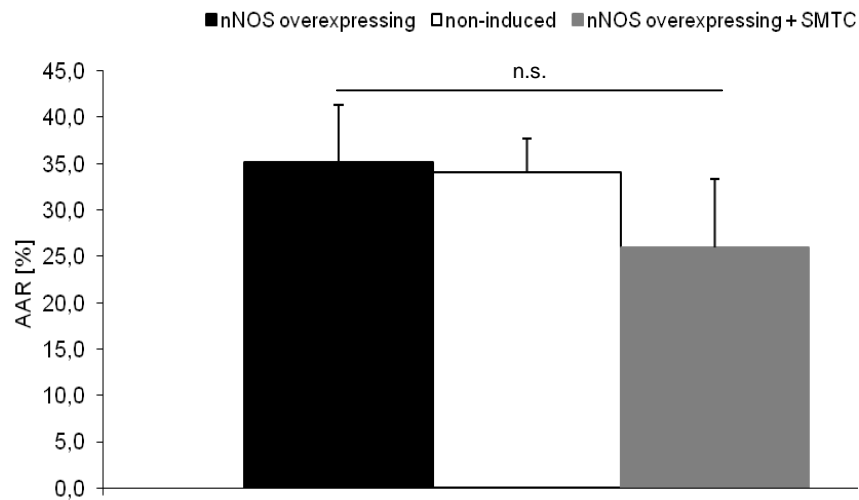
Representative heart sections of nNOS overexpressing mice, non-induced littermates and nNOS overexpressing mice treated with SMTC.

**Red encircled** = area at risk

**Black encircled** = infarcted area

**Figure 22: Infarct area within area at risk (AAR):****Figure legend 22: Infarct area within area at risk (AAR)**

Infarct size within the area at risk was significantly reduced in nNOS overexpressing mice compared to non-induced animals (36.6±8.4 vs. 61.1±2.9%, n=8, p<0.05). Application of SMTC inhibited the cardioprotective effect of nNOS overexpression (59.05±05%, n=8, p<0.05).

**Figure 23: Area at risk (AAR):****Figure legend 23: Area at risk (AAR)**

The area at risk was not significantly changed after ischemia-reperfusion (35.1±6.2% in nNOS overexpressing mice vs. 34.1±3.6% non-induced animals vs. 25.9±6.9% nNOS overexpressing mice treated with SMTC, n=8, n.s.).

SMTC=specific nNOS inhibitor (0.125mg/kg)

#### 4.2. Recovery of left ventricular developed pressure (LVDP) after ischemia-reperfusion injury in isolated hearts (Langendorff):

To assess the functional recovery after *in vitro* ischemia-reperfusion experiments, isolated hearts of nNOS overexpressing and non-induced animals were investigated. LVDP was significantly elevated in hearts of nNOS overexpressing mice (30min post-ischemia, LVDP 27.0±2.5mmHg in non-induced animals vs. 45.2±1.9mmHg in nNOS overexpressing mice, n=12, p<0.05) even though LVDP was significantly higher before ischemia in non-induced mice (90.0±3.0mmHg in hearts of non-induced animals vs. 72.0±2.3mmHg in hearts of nNOS overexpressing mice, n=12, p<0.05)

(figure 24). Application of the specific nNOS inhibitor SMTC (0.125mg/kg) again reversed the positive effects of the transgene nNOS overexpression (30min post-ischemia LVDP  $34.0 \pm 2.0$  mmHg,  $n=12$ ,  $p<0.05$ ). Recovery of ventricular function was improved over the whole reperfusion period in nNOS overexpressing animals.

**Figure 24: Ischemia-reperfusion injury:**

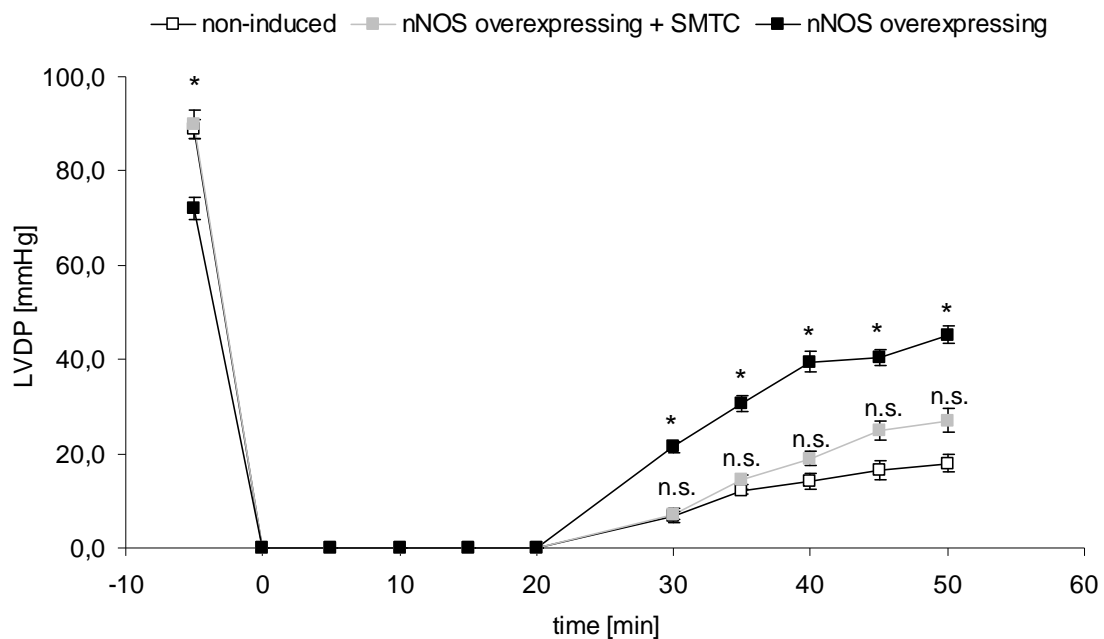


**Figure legend 24: Ischemia-reperfusion injury**

LVDP was significantly increased in isolated hearts of nNOS overexpressing mice compared to non-induced animals (30min post-ischemia, LVDP  $27 \pm 2.5$  mmHg in non-induced animals vs.  $45.2 \pm 1.9$  mmHg in nNOS overexpressing mice,  $n=12$ ,  $p<0.05$ ). Application of the specific nNOS inhibitor SMTC (0.125mg/kg) reversed the positive effects of the transgene nNOS overexpression (30min post-ischemia LVDP  $34.0 \pm 2.0$  mmHg,  $n=12$ ,  $p<0.05$ )

Both *in vivo* and *in vitro* ischemia-reperfusion experiments showed a cardioprotective effect of nNOS overexpression.

#### 4.3. nNOS protein expression in the mitochondria:

To investigate the subcellular distribution of nNOS, immunogold labeling, immunofluorescence staining and Western Blot analysis were performed. Electron microscopy of mouse myocardium from nNOS overexpressing mice showed that nNOS is additionally localised in mitochondria after induction of nNOS expression (figure 25). Immunogold labeling was positive for the 6xHN tag, indicating conditional nNOS overexpression. Immunogold labeling also showed a close proximity of nNOS and cytochrome c oxidase in the mitochondria (figure 26). Immunofluorescence staining of isolated adult cardiac myocytes indicated a colocalisation of nNOS and cytochrome c oxidase (a mitochondrial marker) in nNOS overexpressing mice (figure 27).

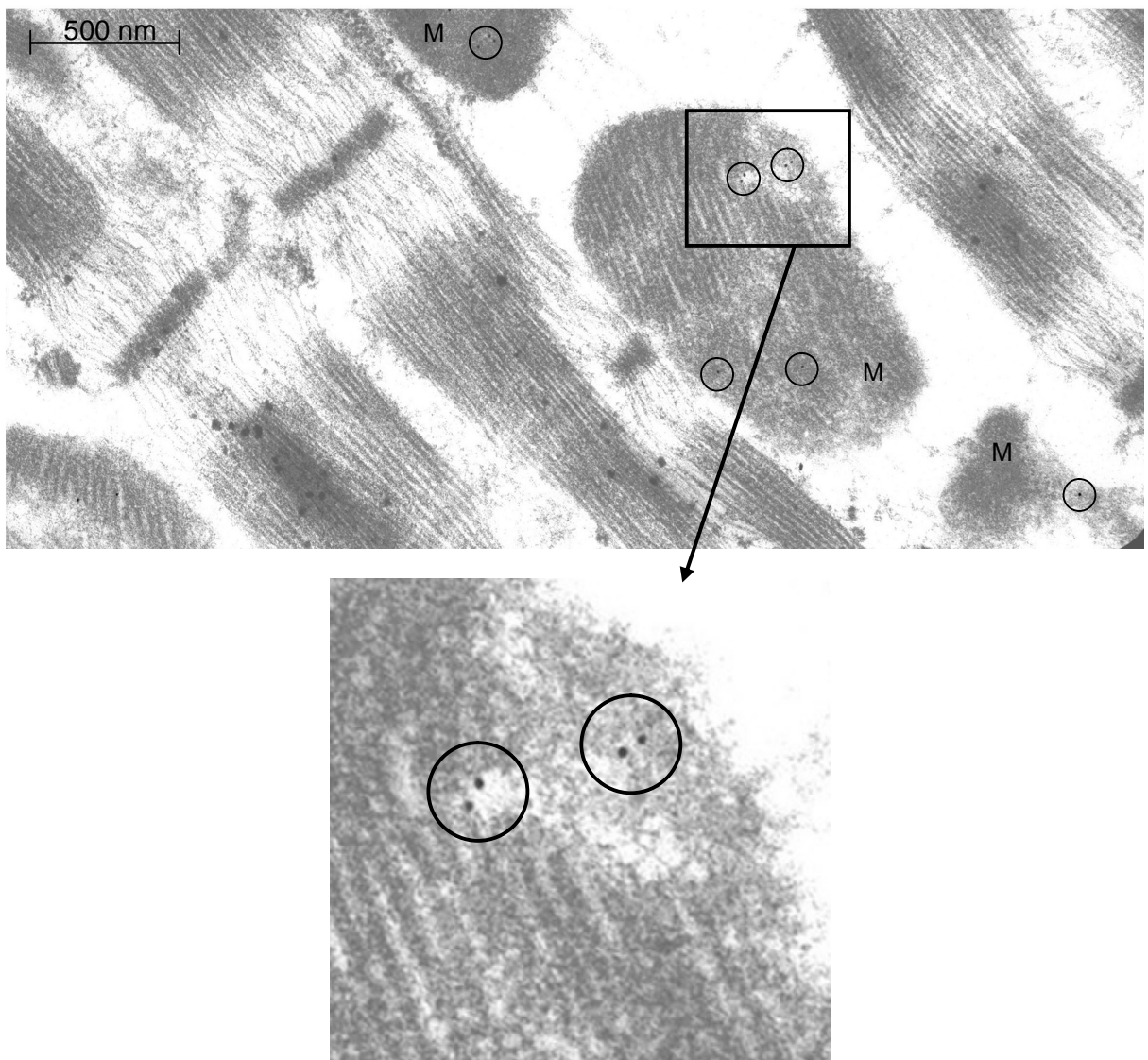
To approve this result, we isolated mitochondria from hearts of nNOS overexpressing mice and non-induced animals. Western Blot analysis showed a significantly increased nNOS protein expression in isolated mitochondria of nNOS overexpressing mice ( $221.2 \pm 10.7 \text{rel.}\%$  vs.  $100 \pm 8.1 \text{rel.}\%$ ,  $n=12$ ,  $p<0.01$ ) (figure 28, 29). To test for contamination of the isolated mitochondria we performed different Western Blot analysis. Figures 30, 31 showed that there is no detectable protein expression of L-type  $\text{Ca}^{2+}$ -channel and SERCA2a neither in non-induced animals nor in nNOS overexpressing mice. Porin protein expression (localised in the outer membrane of mitochondria) and cytochrome c (attached to the inner mitochondrial membrane) were only found in the isolated mitochondria, not in the supernatant (taken during mitochondria preparation) (porin protein expression:  $11.0 \pm 20.0 \text{rel.}\%$  vs.  $226.5 \pm 0.5 \text{rel.}\%$ ,  $n=6$ ,  $p<0.01$ ) (figure 32, 33) (cytochrome c protein expression:  $14.0 \pm 7.0 \text{rel.}\%$  vs.  $84.0 \pm 5.0 \text{rel.}\%$ ,  $n=6$ ,  $p<0.01$ ) (figure 34, 35).

Of note, there is also endogenous nNOS located at the mitochondria in non-induced animals but endogenous nNOS was increased in isolated mitochondria of mouse wildtype hearts after ischemia-reperfusion ( $306.9 \pm 40.5 \text{rel.}\%$  vs.  $100.0 \pm 7.5 \text{rel.}\%$ ,  $n=7$ ,  $p<0.05$ ) (figure 36, 37).

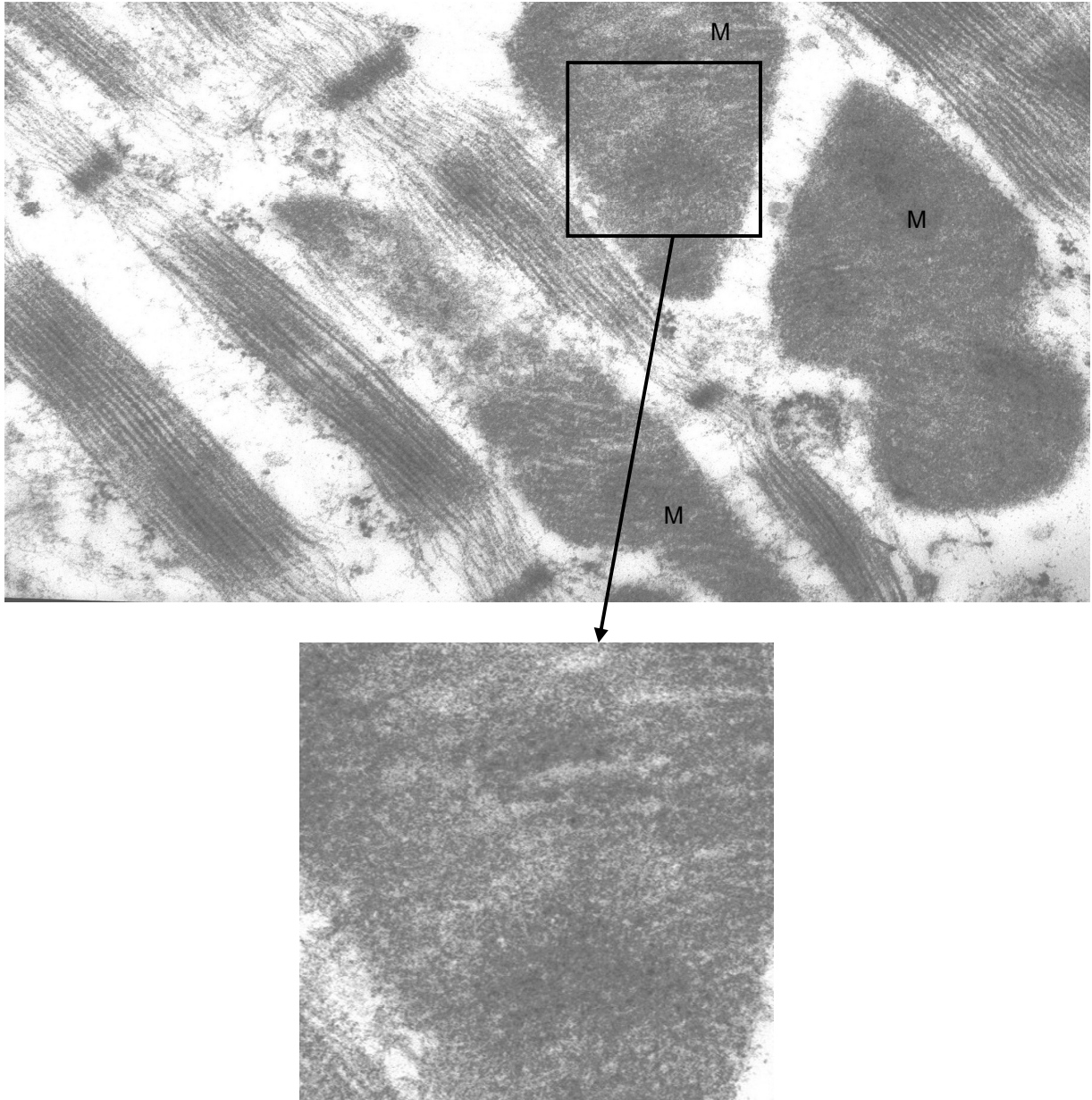


Figure 25: Electron microscopy of mouse myocardium (in cooperation with Prof. Krohne):

nNOS overexpressing



non-induced

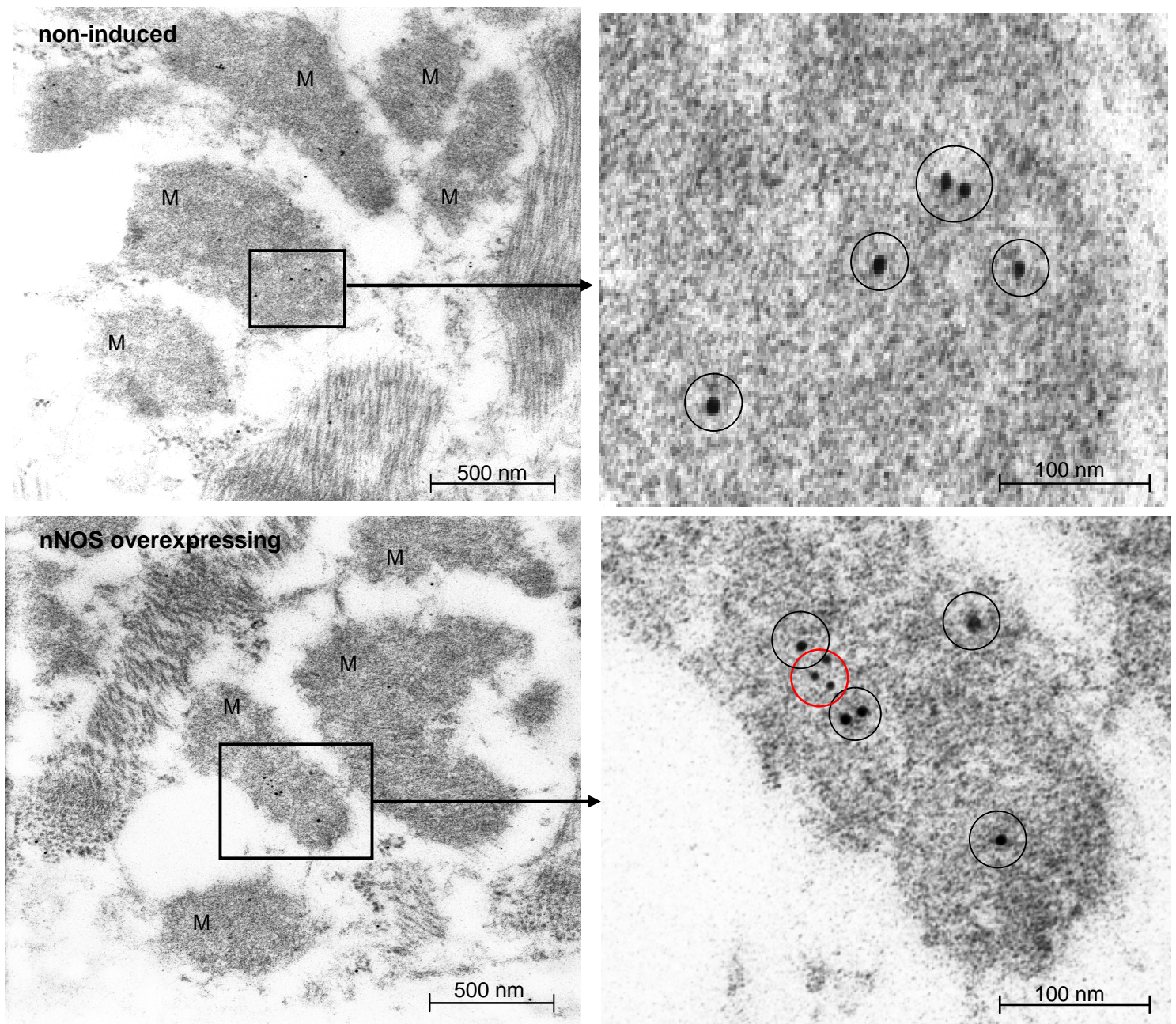


**Figure legend 25: Electron microscopy of mouse myocardium**

Immunogold labeling indicates 6xHN tag of overexpressed nNOS (black circles) and demonstrates nNOS localisation. Overexpressed (transgenic) nNOS is additionally localised in mitochondria in hearts of nNOS overexpressing mice. In contrast, there is no transgenic nNOS localisation in mitochondria of non-induced animals.

**M** = mitochondria

Figure 26: Electron microscopy with two different antibodies:

**Figure 26 legend: Electron microscopy with two different antibodies**

Immunogold labeling of mouse myocardium from non-induced and nNOS overexpressing animals. The polyclonal anti-nNOS antibody was used followed by a second antibody that was coupled to 6nm gold particles; simultaneously the monoclonal anti-cytochrome c oxidase antibody was used followed by a second antibody that was coupled to 12nm gold particles. The anti-nNOS antibody used in this experiment was reactive for both endogenous and overexpressed nNOS. Immunogold labeling of mouse myocardium from non-induced and nNOS overexpressing animals. The polyclonal anti-nNOS antibody was used followed by a second antibody that was coupled to 6nm gold particles; simultaneously the monoclonal anti-cytochrome c oxidase antibody was used followed by a second antibody that was coupled to 12nm gold particles. The anti-nNOS antibody used in this experiment was reactive for both endogenous and overexpressed nNOS.

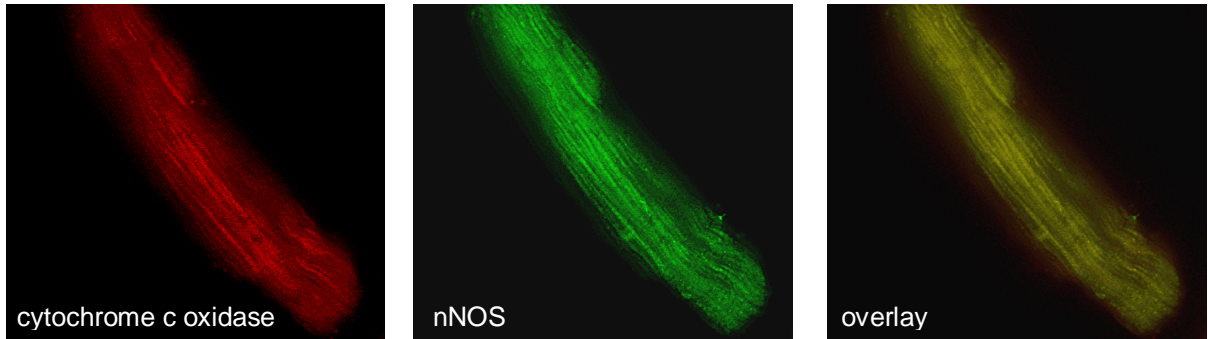
In nNOS overexpressing mice there was a close proximity between cytochrome c oxidase and nNOS.

**Black circles** = cytochrome c oxidase; **red circle** = nNOS

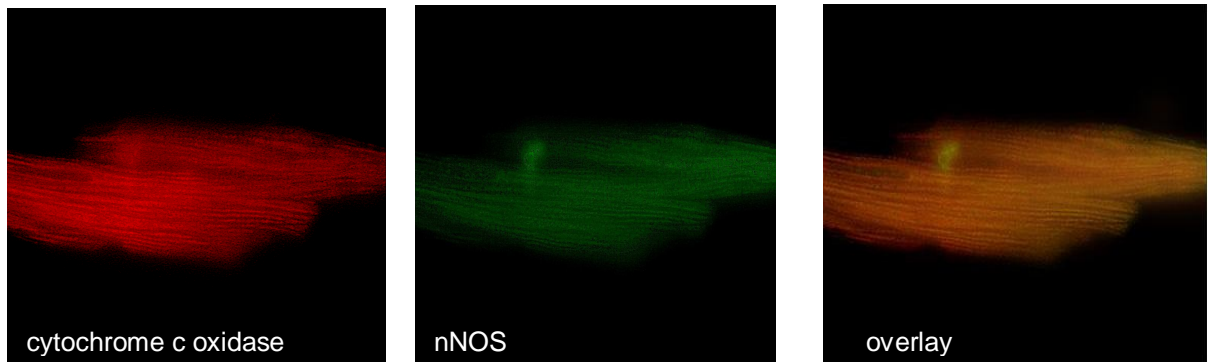
**M** = mitochondria

**Figure 27: Immunofluorescence staining of isolated adult cardiac myocytes:**

isolated adult cardiac myocytes of nNOS overexpressing mice:



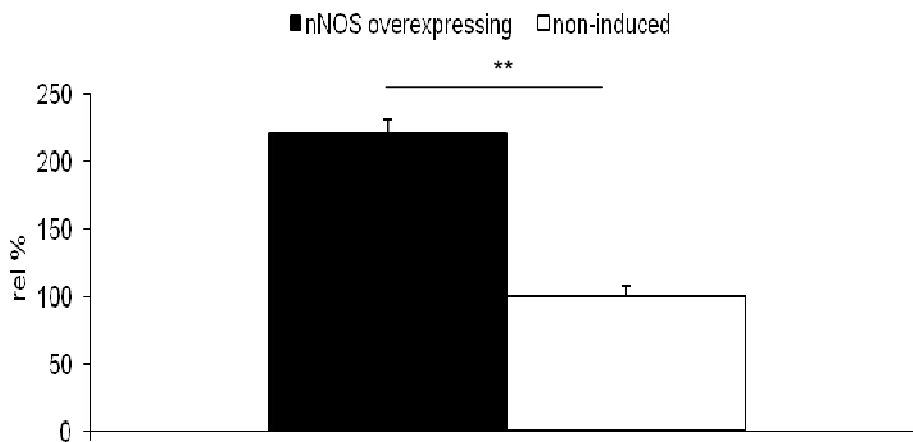
isolated adult cardiac myocytes of non-induced mice:

**Figure legend 27: Immunofluorescence staining of isolated adult cardiac myocytes**

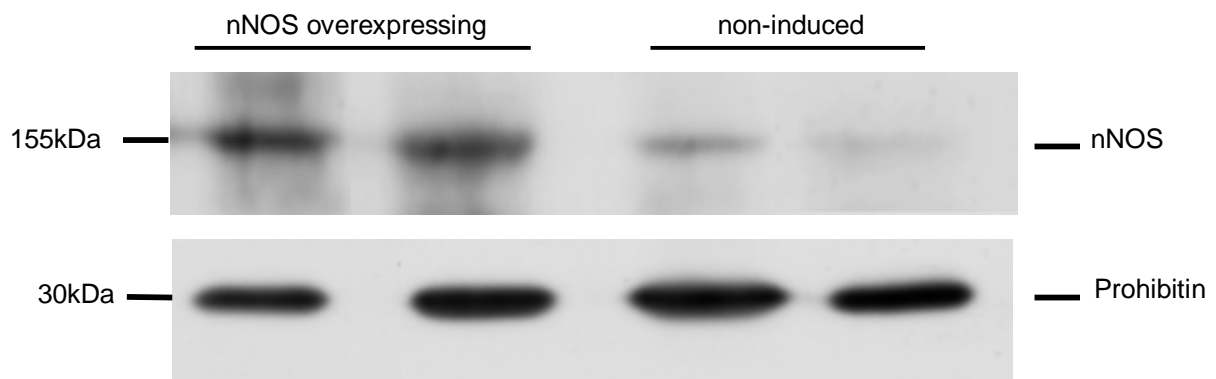
Immunofluorescence staining of isolated adult cardiac myocytes showed a colocalisation of nNOS and cytochrome c oxidase (a mitochondrial marker) in nNOS overexpressing mice.

**red = cytochrome c oxidase**

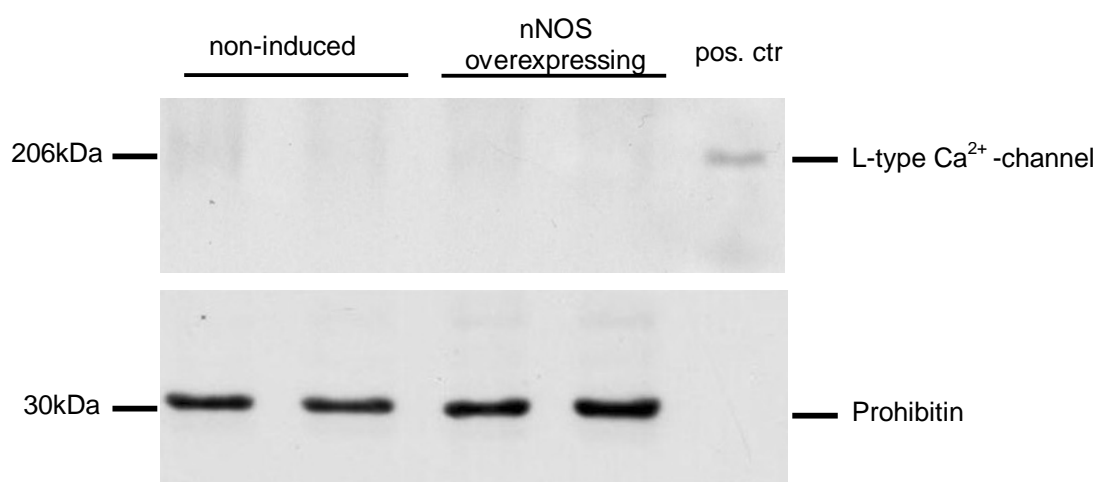
**green = nNOS**

**Figure 28: nNOS protein expression in isolated mitochondria:****Figure 28 legend: nNOS protein expression in isolated mitochondria**

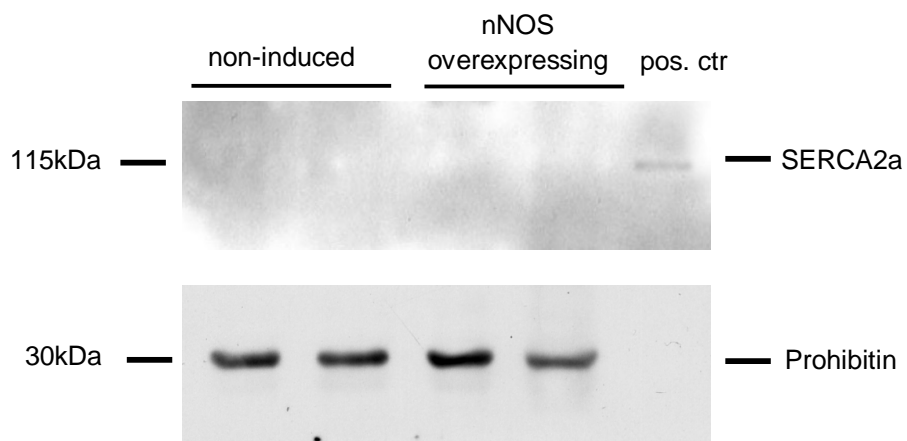
Western Blot analysis of isolated mitochondria showed a significantly increased nNOS protein expression in hearts of nNOS overexpressing mice compared to non-induced animals ( $221.2 \pm 10.7 \text{ rel. \%}$  vs.  $100 \pm 8.1 \text{ rel. \%}$ ,  $n = 12$ ,  $p < 0.01$ ).

**Figure 29: Representative Western Blot of nNOS protein expression in isolated mitochondria:****Figure 29 legend: Representative Western Blot of nNOS protein expression in isolated mitochondria**

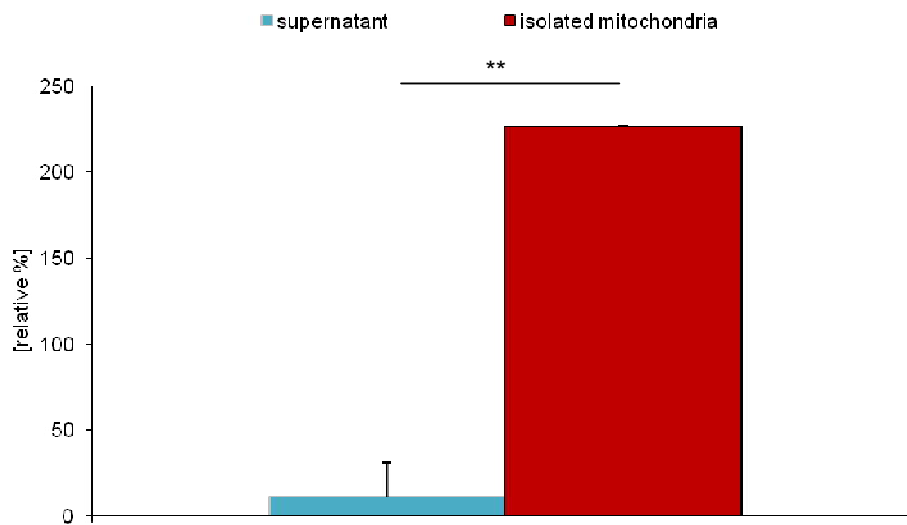
Total nNOS protein expression was significantly increased in isolated mitochondria of nNOS overexpressing mice. Prohibitin (a mitochondrial marker) was used as loading control.

**Figure 30: Protein expression of L-type Ca<sup>2+</sup>-channel:****Figure 30 legend: Protein expression of L-type Ca<sup>2+</sup>-channel**

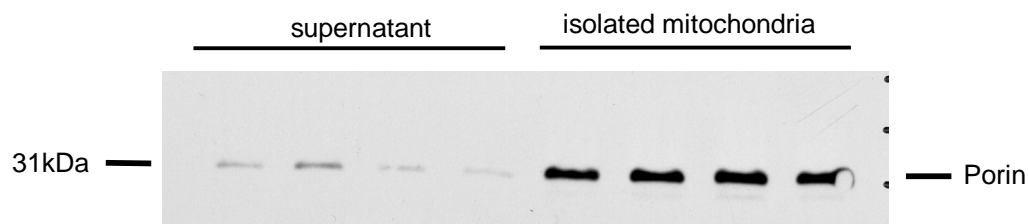
L-type Ca<sup>2+</sup>-channel protein expression was not detectable. Prohibitin (a mitochondrial marker) was used as loading control and rat heart membranes as a positive control.

**Figure 31: Protein expression of SERCA2a:****Figure 31 legend: Protein expression of SERCA2a**

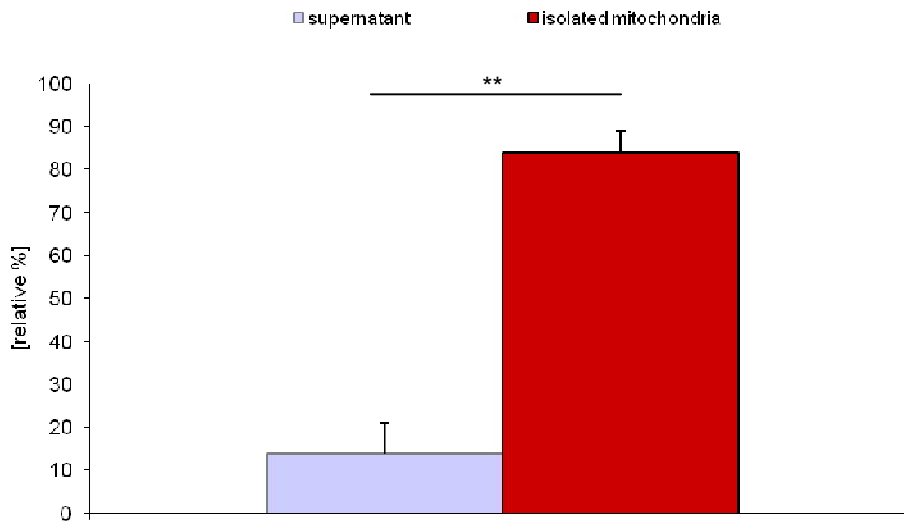
SERCA2a protein expression was not detectable. Prohibitin (a mitochondrial marker) was used as loading control and cardiac SR vesicles as a positive control.

**Figure 32: Porin protein expression:****Figure 32 legend: Porin protein expression**

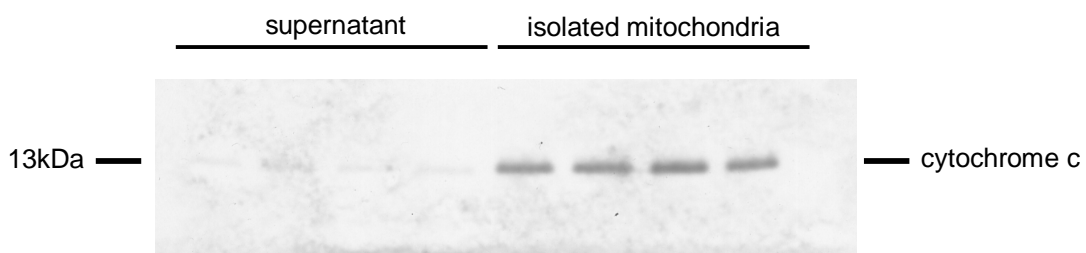
Porin protein expression was only found in isolated mitochondria, not in the supernatant (taken during mitochondria preparation) ( $11 \pm 20$ rel.% vs.  $226.5 \pm 0.5$ rel.%,  $n=6$ ,  $p < 0.01$ ).

**Figure 33: Representative Western Blot of porin protein expression:****Figure 33 legend: Representative Western Blot of porin protein expression**

There was hardly any porin protein expression detectable in the supernatant taken during mitochondria preparation.

**Figure 34: Cytochrome c protein expression:****Figure 34 legend: Cytochrome c protein expression**

Cytochrome c protein expression was only found in isolated mitochondria, not in the supernatant (taken during mitochondria preparation) ( $14.0 \pm 7.0 \text{rel.}\%$  vs.  $84.0 \pm 5.0 \text{rel}\%$ ,  $n=6$ ,  $p<0.01$ ).

**Figure 35: Representative Western Blot of cytochrome c oxidase activity:****Figure 35 legend: Representative Western Blot of cytochrome c oxidase activity**

There was hardly any cytochrome c protein expression detectable in the supernatant taken during mitochondria preparation.



**Figure 36: nNOS protein expression in isolated mitochondria in WT mice after ischemia reperfusion:**

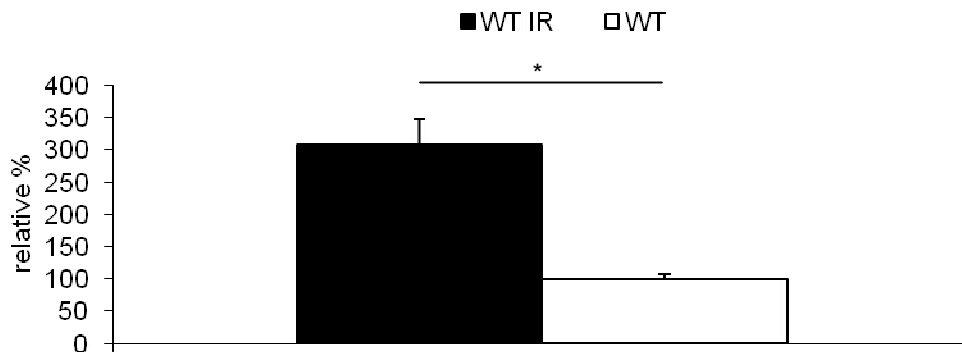


**Figure 36 legend: nNOS protein expression in isolated mitochondria in WT mice after ischemia reperfusion**

Western Blot analysis of isolated mitochondria of mouse wildtype hearts (WT) showed an increased nNOS protein expression after ischemia-reperfusion (WT IR) ( $306.9 \pm 40.5 \text{rel.}\%$  vs.  $100.0 \pm 7.5 \text{rel.}\%$ ,  $n=7$ ,  $p<0.05$ ).

**Figure 37: Representative Western Blot of nNOS protein expression in isolated mitochondria in WT mice after ischemia reperfusion:**

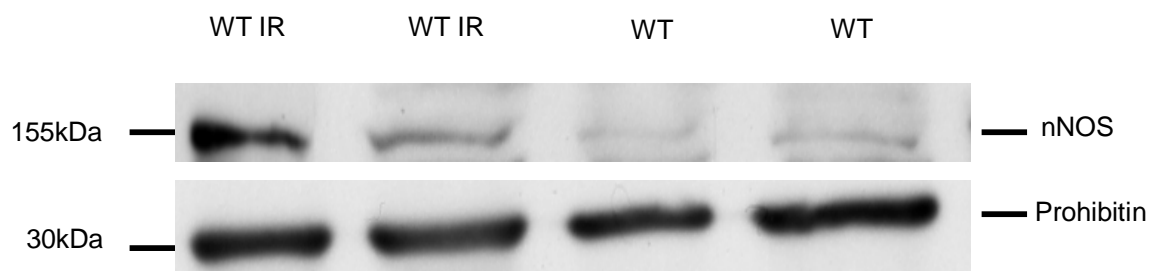


**Figure 37 legend: Representative Western Blot of nNOS protein expression in isolated mitochondria in WT mice after ischemia reperfusion**

nNOS protein expression was increased in isolated mitochondria in wildtype hearts after ischemia-reperfusion.

Prohibitin (a mitochondrial marker) was used as a loading control.

#### 4.4. Translocation of nNOS to mitochondria:

To analyse the transport mechanism of nNOS into the mitochondria we performed coimmunoprecipitation experiments. Coimmunoprecipitation analysis showed an interaction between nNOS and HSP90 in both non-induced and nNOS overexpressing mice (figure 38). Notably, immunoreactivity in the nNOS overexpressing mice was stronger than in the non-induced animals. There was no interaction between iNOS and HSP90 (figure 39), whereas the interaction between eNOS and HSP90 again was detectable in both nNOS overexpressing and non-induced mice (figure 40).

To further assess the mechanism of nNOS translocation, neonatal rat cardiomyocytes were transfected with nNOS and treated with geldanamycin (a specific inhibitor of HSP90 activity). Western Blot analysis of isolated mitochondria showed a significant suppression of nNOS protein expression in geldanamycin-treated cardiomyocytes ( $17.0 \pm 3.9\text{rel.}\%$  vs.  $100.0\% \pm 6.1\text{rel.}\%$ ,  $n=11$ ,  $p<0.01$ ) (figure 41, 42).

Obviously, nNOS is shuttled into the mitochondria via interaction with HSP90 which could be sufficiently inhibited by geldanamycin.

**Figure 38: Coimmunoprecipitation of nNOS and HSP90:**

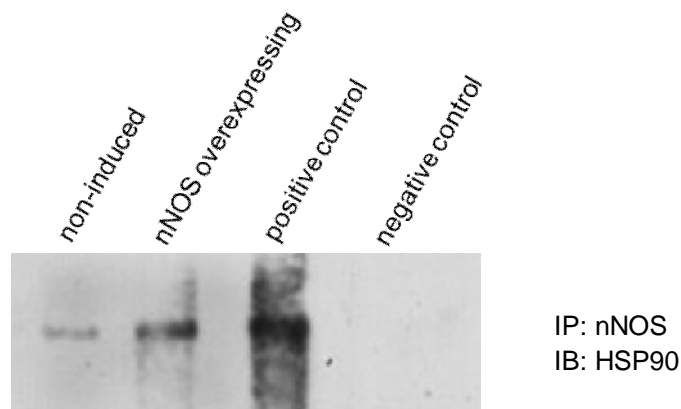


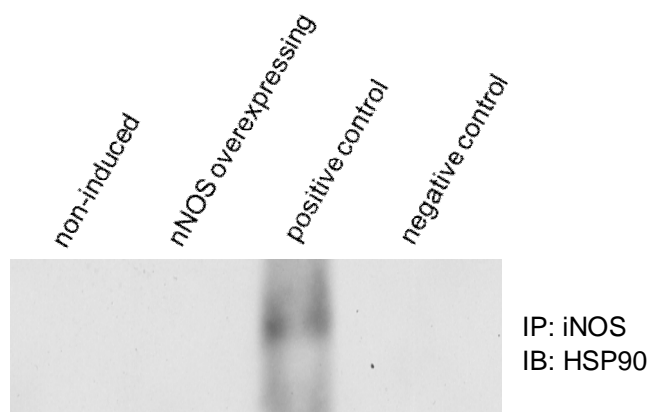
**Figure 38 legend: Coimmunoprecipitation of nNOS and HSP90**

Whole heart lysates were immunoprecipitated (IP) with anti-nNOS antibody and immunoblotted (IB) for HSP90.

Association between nNOS and HSP90 was demonstrated in both non-induced and nNOS overexpressing mice.

As a positive control HeLa cell lysate was used.

As a negative control IP was performed with an irrelevant antibody (anti-HA antibody).

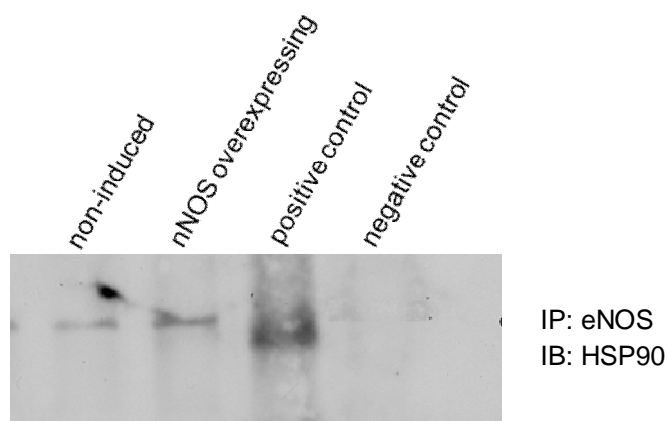
**Figure 39: Coimmunoprecipitation of iNOS and HSP90:****Figure 39 legend: Coimmunoprecipitation of iNOS and HSP90**

Whole heart lysates were immunoprecipitated (IP) with anti-iNOS antibody and immunoblotted (IB) for HSP90.

There was no interaction between iNOS and HSP90.

As a positive control HeLa cell lysate was used.

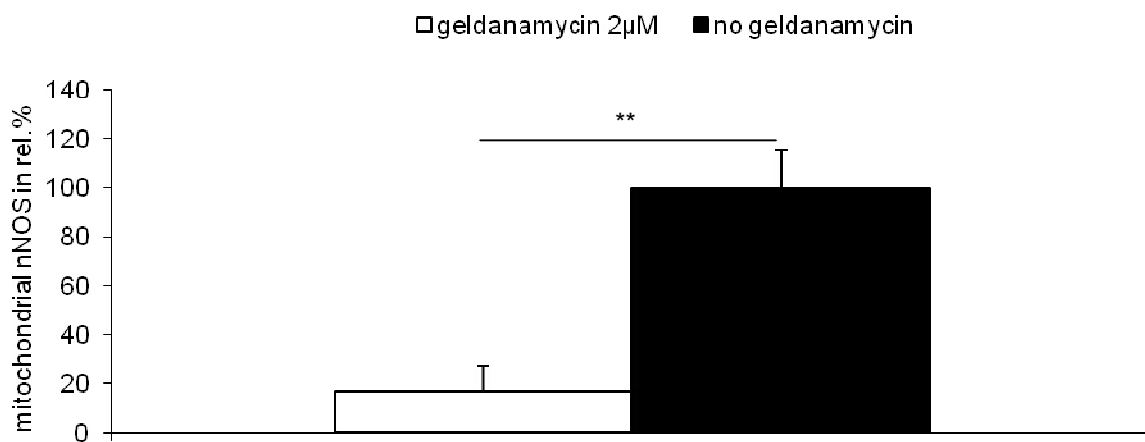
As a negative control IP was performed with an irrelevant antibody (anti-HA antibody).

**Figure 40: Coimmunoprecipitation of eNOS and HSP90:****Figure 40 legend: Coimmunoprecipitation of eNOS and HSP90**

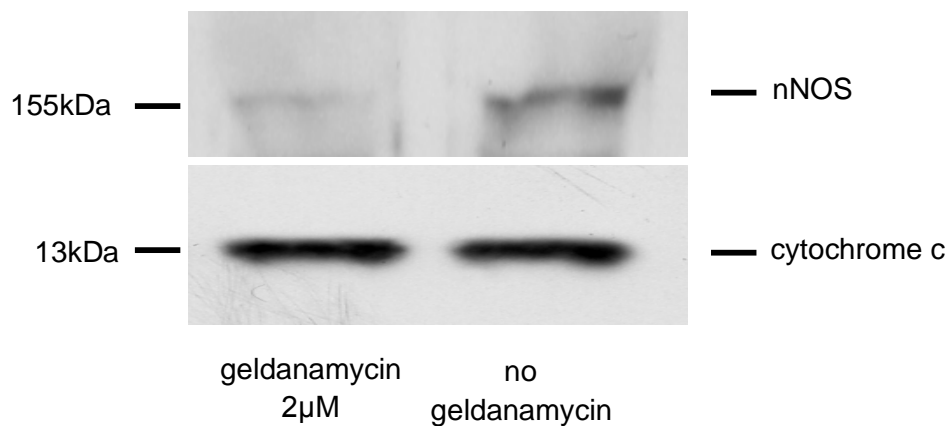
Whole heart lysates were immunoprecipitated (IP) with anti-eNOS antibody and immunoblotted (IB) for HSP90. Association between eNOS and HSP90 was demonstrated in both non-induced and nNOS overexpressing mice.

As a positive control HeLa cell lysate was used.

As a negative control IP was performed with an irrelevant antibody (anti-HA antibody).

**Figure 41: HSP90 dependency of mitochondrial nNOS translocation:****Figure 41 legend: HSP90 dependency of mitochondrial nNOS translocation**

Neonatale cardiomyocytes were transfected with nNOS and treated with geldanamycin (2µM, inhibitor of HSP90). Western Blot analysis of isolated mitochondria showed a significant suppression of nNOS protein expression in geldanamycin-treated cardiomyocytes (17.0±3.9rel.% vs. 100.0%±6.1rel.%, n=11, p<0.01).

**Figure 42: Representative Western Blot of HSP90 dependency of mitochondrial nNOS translocation:****Figure 42 legend: Representative Western Blot of HSP90 dependency of mitochondrial nNOS translocation**

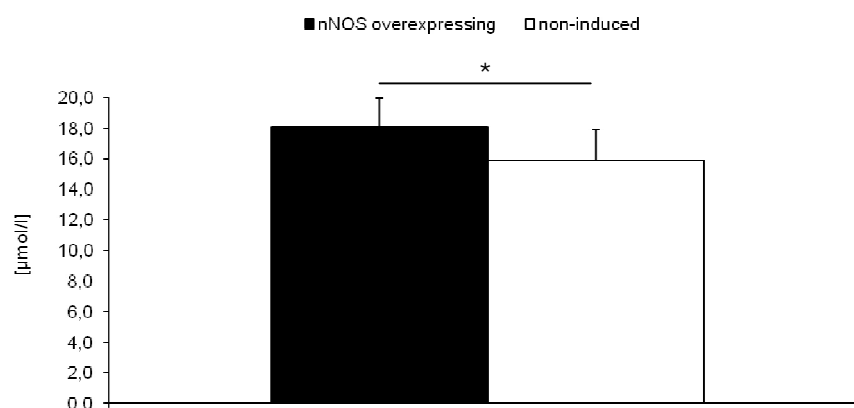
nNOS protein expression was decreased in isolated mitochondria treated with geldanamycin. Cytochrome c was used as a loading control.

#### 4.5. nNOS impairs cytochrome c oxidase activity and nitrite level:

To analyse the role of nNOS in mitochondria, we investigated cytochrome c oxidase activity. It was previously shown that endogenous nitric oxide (NO) reversibly inhibits oxygen consumption and ATP synthesis by competitive inhibition of cytochrome c oxidase<sup>189</sup>. In our study, we demonstrated that nitrite levels were significantly increased in isolated mitochondria of nNOS overexpressing mice compared to non-induced littermates ( $18.1 \pm 3.6 \mu\text{mol/l}$  vs.  $11.0 \pm 2.0 \mu\text{mol/l}$ ,  $n=10$ ,  $p<0.05$ ) (figure 43).

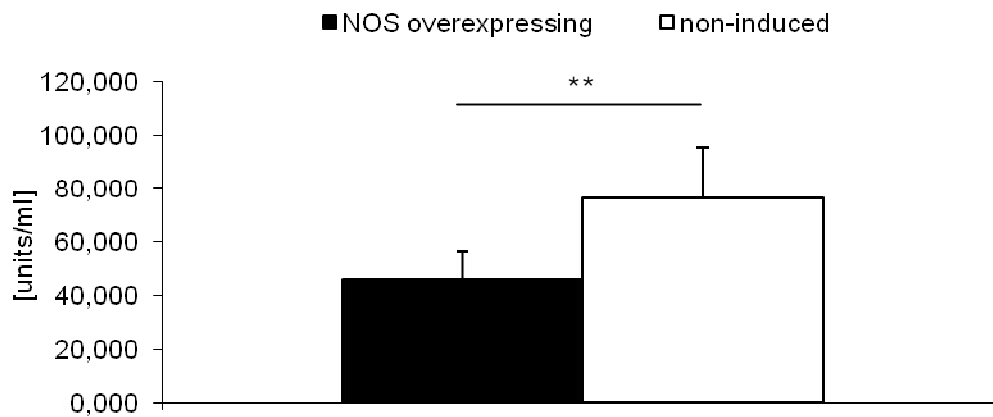
Simultaneously, nNOS overexpression significantly suppressed cytochrome c oxidase activity ( $72.0 \pm 8.9 \text{ units/ml}$  in nNOS overexpressing mice vs.  $113.2 \pm 17.1 \text{ units/ml}$  in non-induced mice,  $n=12$ ,  $p<0.01$ ) (figure 44). To investigate whether cytochrome c oxidase activity was inhibited by NO binding to cysteine or to the haem we added either DTT (which destroyed S-nitrosothiols) or haemoglobin (which scavenged NO of the haem in cytochrome c oxidase) (figure 45, 46). From these experiments we concluded that inhibition of cytochrome c oxidase activity is inhibited by NO-binding to a cysteine thiol of cytochrome c oxidase (rather than binding to the haem).

**Figure 43: Nitrite-level of isolated mitochondria:**

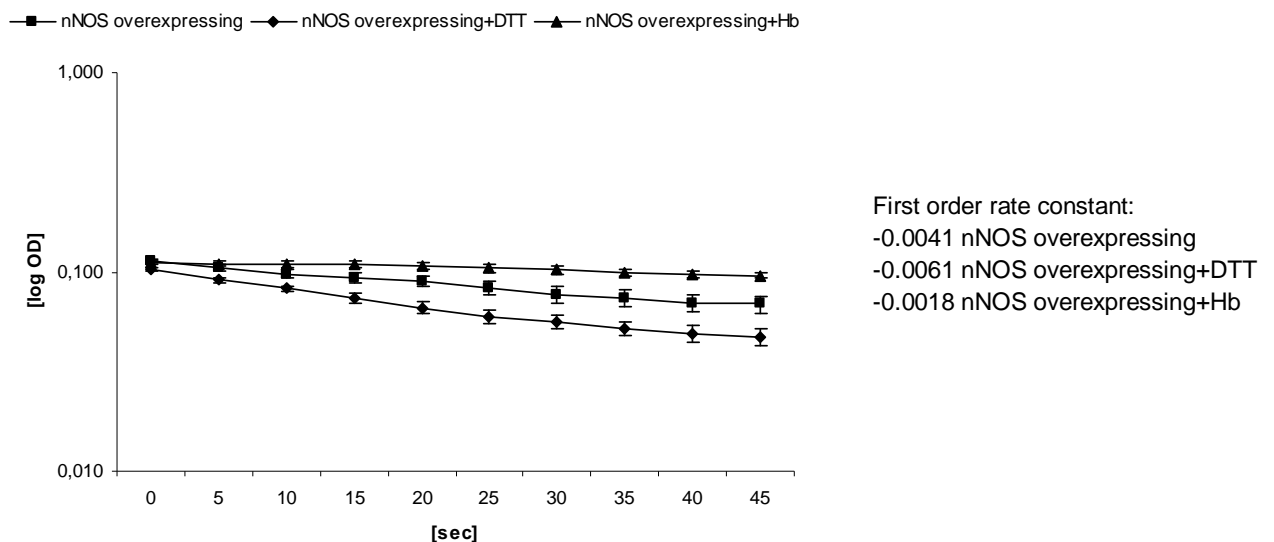


**Figure 43 legend: Nitrite-level of isolated mitochondria**

Nitrite level of isolated mitochondria was significantly increased in nNOS overexpressing mice compared to non-induced animals ( $18.1 \pm 3.6 \mu\text{mol/l}$  vs.  $11.0 \pm 2.0 \mu\text{mol/l}$ ,  $n=10$ ,  $p<0.05$ ).

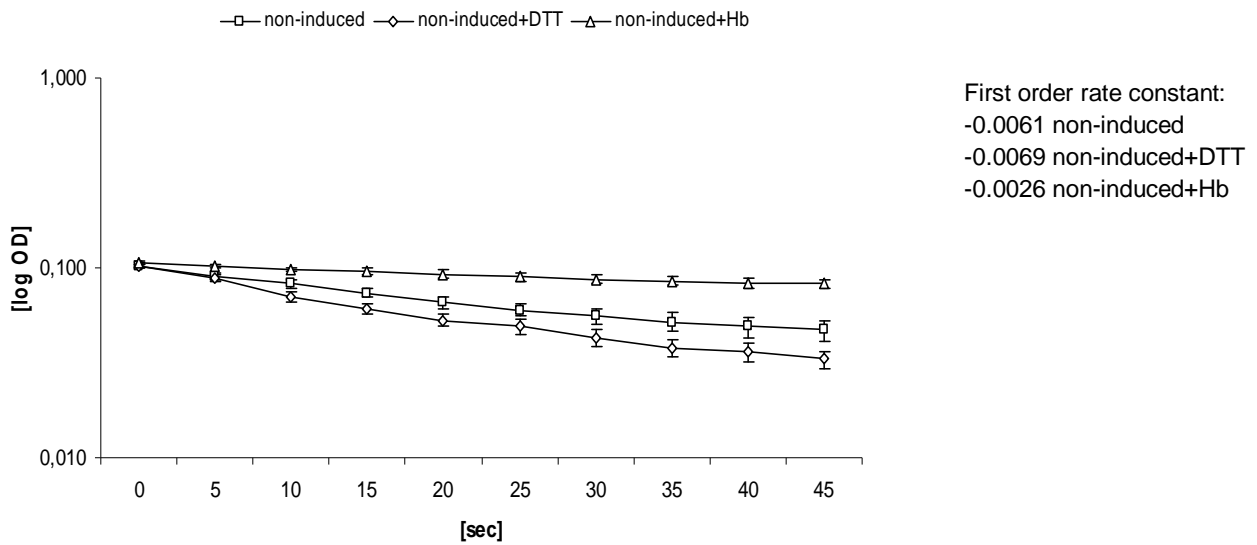
**Figure 44: Cytochrome c oxidase activity:****Figure 44 legend: Cytochrome c oxidase activity**

nNOS overexpression significantly suppressed cytochrome c oxidase activity ( $72.0 \pm 8.9$  units/ml in nNOS overexpressing mice vs.  $113.2 \pm 17.1$  units/ml in non-induced mice,  $n=12$ ,  $p < 0.01$ ).

**Figure 45: Cytochrome c oxidase rate of nNOS overexpressing mice:****Figure 45 legend: Cytochrome c oxidase rate of nNOS overexpressing mice**

DTT ( $50 \mu\text{M}$ ) or haemoglobin ( $4 \mu\text{M}$ ) was added and measurement of cytochrome c oxidase activity was started immediately. Application of DTT completely reversed the inhibiting effect of nNOS overexpression ( $-0.0041$  first order rate constant of nNOS overexpressing mice vs.  $-0.0061$  first order rate constant of nNOS overexpressing animals + DTT,  $n=7$ ,  $p < 0.05$ ).

In contrast application of haemoglobin further suppressed cytochrome c oxidase activity significantly ( $-0.0018$  first order rate constant vs.  $-0.0041$  first order rate constant,  $n=7$ ,  $p < 0.05$ ).

**Figure 46: Cytochrome c oxidase rate of non-induced mice:****Figure 46 legend: Cytochrome c oxidase rate of non-induced mice**

Application of DTT had no significant effect on cytochrome c oxidase activity in non-induced nNOS<sup>+</sup>/αMHC-tTA<sup>+</sup> mice (-0.0061 first order rate constant of non-induced mice vs. -0.0069 first order rate constant of non-induced animals + DTT, n=7).

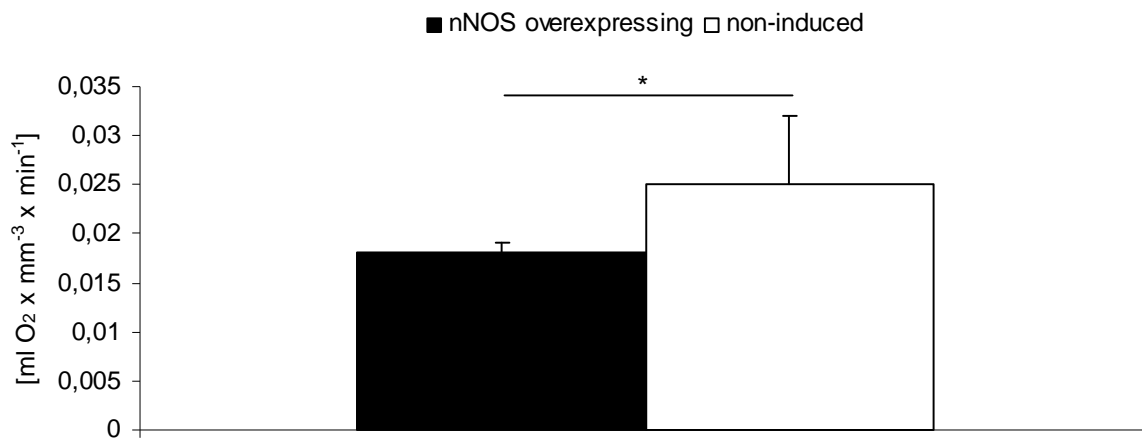
Again, application of haemoglobin suppressed cytochrome c oxidase activity significantly (-0.0026 first order rate constant vs. -0.0061 first order rate constant, n=7, p<0.05).

#### 4.6. Myocardial oxygen consumption (MVO<sub>2</sub>):

To investigate whether NO derived from nNOS directly affects MVO<sub>2</sub>, we examined the effects of conditional nNOS overexpression on MVO<sub>2</sub> in isolated muscle stripes. Already under resting conditions there was a significant inhibition of MVO<sub>2</sub> in isolated muscle stripes of nNOS overexpressing mice compared to non-induced animals ( $0.016 \pm 0.0015$  vs.  $0.024 \pm 0.006 \text{ ml}[\text{O}_2] \times \text{mm}^{-3} \times \text{min}^{-1}$ ,  $n=13$ ,  $p<0.05$ ) (figure 47). This effect was sustained during work (stimulation at 5Hz for 30min). O<sub>2</sub> consumption was given as ratio MVO<sub>2</sub>/FTI ( $69.0 \pm 11.0$  rel.% vs.  $100.0 \pm 14.0$  rel.%,  $n=14$ ,  $p<0.05$ ). MVO<sub>2</sub>/FTI was taken as 100% in the non-induced animals (figure 48).

nNOS mediated alterations of MVO<sub>2</sub> under rest indicate a direct inhibitory effect of nNOS on mitochondrial function, since the effect of crossbridge cycling kinetics under rest is negligible.

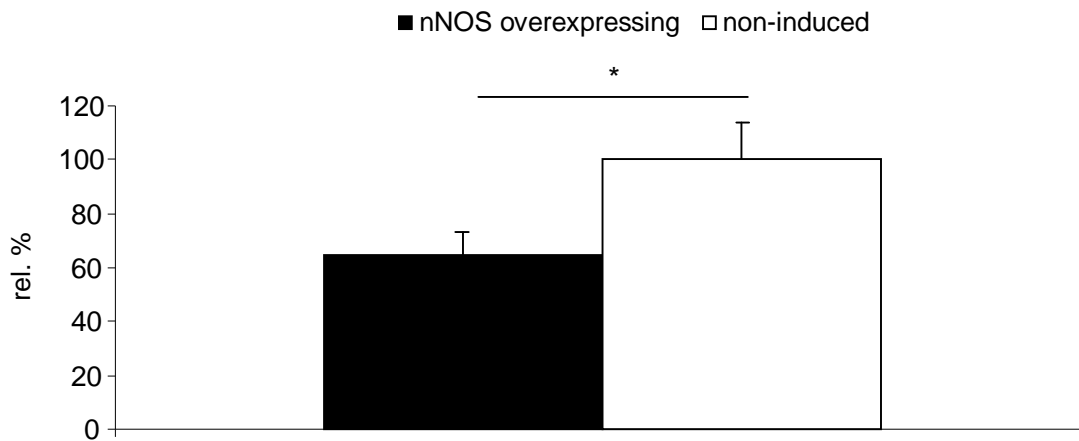
**Figure 47: Myocardial oxygen consumption at rest:**



**Figure 47 legend: Myocardial oxygen consumption at rest**

Specific oxygen consumption was significantly reduced in nNOS overexpressing mice already during rest ( $0.016 \pm 0.0015$  vs.  $0.024 \pm 0.006 \text{ ml}[\text{O}_2] \times \text{mm}^{-3} \times \text{min}^{-1}$ ,  $n=13$ ,  $p<0.05$ ).



**Figure 48: Myocardial oxygen consumption at work load****Figure 48 legend: Myocardial oxygen consumption at work load**

During stimulation with 5Hz nNOS overexpressing animals display also decreased  $O_2$  consumption. In this case  $O_2$  consumption is measured as ratio  $MVO_2/FTI$  and given in relative % ( $69.0 \pm 11.0$  rel.% vs.  $100.0 \pm 14.0$  rel.%,  $n=14$ ,  $p<0.05$ ).

#### 4.7. Generation of reactive oxygen species (ROS) and $O_2^-$ production:

Measurement of  $O_2^-$  production in isolated mitochondria showed a significant decrease in nNOS overexpressing mice compared to non-induced animals ( $0.34 \pm 0.01$  units vs.  $0.54 \pm 0.03$  units,  $n=5$ ,  $p<0.05$ ) (figure 49).

Reactive oxygen free radicals (ROS) have been implicated in cardiac dysfunction. Xanthine oxidoreductase (XOR) and reduced nicotinamide-adenine dinucleotide phosphate (NADPH) oxidase are known to be the major enzymes generating ROS in cardiac myocytes. In this study, we investigated ROS generation during nNOS overexpression compared to non-induced mice.

The total ROS concentration was significantly reduced in hearts of nNOS overexpressing mice compared to non-induced animals ( $6.14 \pm 0.685$  vs.  $14.53 \pm 1.7 \mu\text{M}$ ,  $n=8$ ,  $p < 0.01$ ) (figure 50).

To define whether the XOR or the NADPH oxidase generates ROS, different inhibitors were applied. We investigated the effect of allopurinol, an inhibitor of XOR, and apocynin, an inhibitor of NADPH oxidase in both nNOS overexpressing mice and non-induced animals.

The NADPH oxidase inhibitor apocynin ( $300 \mu\text{M}$ , 30min,  $37^\circ\text{C}$ ) caused an estimated decrease of the ROS concentration in both nNOS overexpressing mice and non-induced animals ( $14.53 \pm 1.7$  vs.  $7.4 \pm 3.15 \mu\text{mol}$ ,  $n=8$ ,  $p < 0.05$  in non-induced animals;  $6.14 \pm 0.685$  vs.  $3.23 \pm 0.5 \mu\text{M}$ ,  $n=8$ ,  $p < 0.05$  in nNOS overexpressing mice) (figure 51, 52), whereas application of the xanthine oxidoreductase inhibitor allopurinol ( $0.1 \text{mM}$ , 1min, room temperature) caused a significant decrease of the ROS production only in non-induced animals ( $14.53 \pm 1.7$  vs.  $2.35 \pm 0.45 \mu\text{M}$ ,  $n=8$ ,  $p < 0.05$  in non-induced animals;  $6.14 \pm 0.685$  vs.  $5.4 \pm 2.35 \mu\text{M}$ ,  $n=8$ , n.s. in nNOS overexpressing mice) (figure 51, 52).

This data indicate that conditional nNOS overexpression in cardiac myocytes decreases ROS generation by selectively inhibiting XOR while having no effect on NADPH oxidase activity.

**Figure 49:  $\text{O}_2^-$  production in isolated mitochondria:**

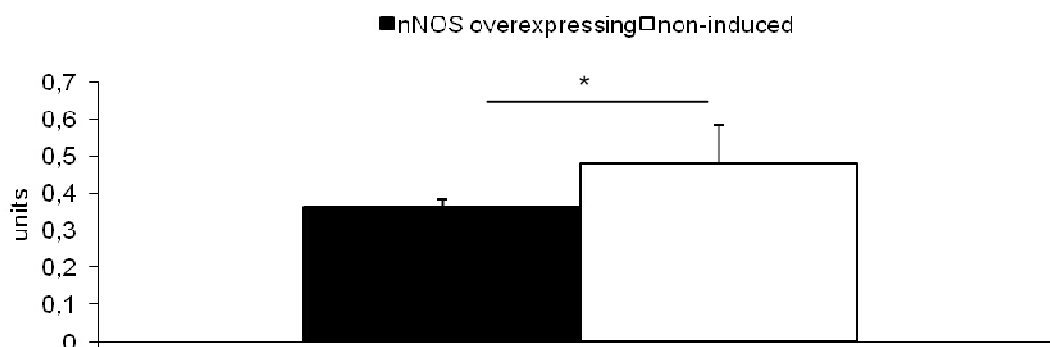


**Figure 49 legend:  $\text{O}_2^-$  production in isolated mitochondria**

$\text{O}_2^-$  production was measured in isolated mitochondria of nNOS overexpressing and non-induced mice.  $\text{O}_2^-$  production was significantly reduced in nNOS overexpressing mice ( $0.34 \pm 0.01$  units vs.  $0.54 \pm 0.03$  units,  $n=5$ ,  $p < 0.05$ ).

Figure 50: ROS concentration:

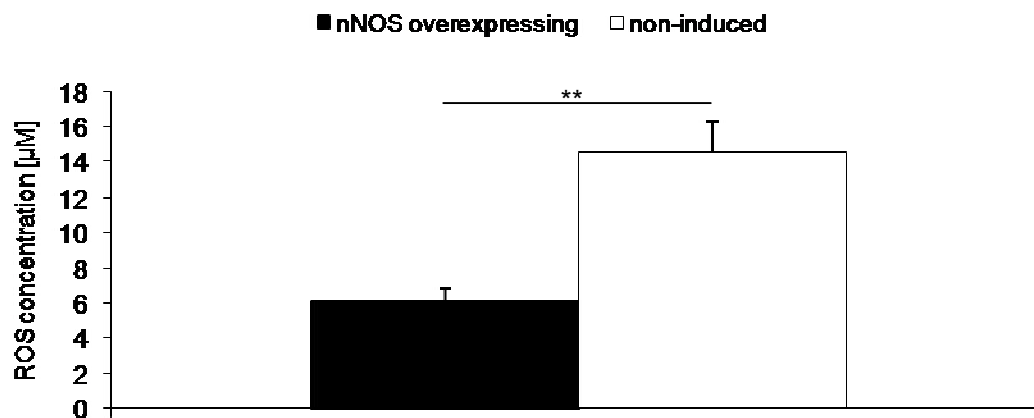


Figure 50 legend: ROS concentration

The ROS concentration was significantly decreased in hearts of nNOS overexpressing mice ( $6.14 \pm 0.685$  vs.  $14.53 \pm 1.7 \mu\text{M}$ ,  $n=8$ ,  $p < 0.01$ ).

Figure 51: ROS concentration in non-induced mice:

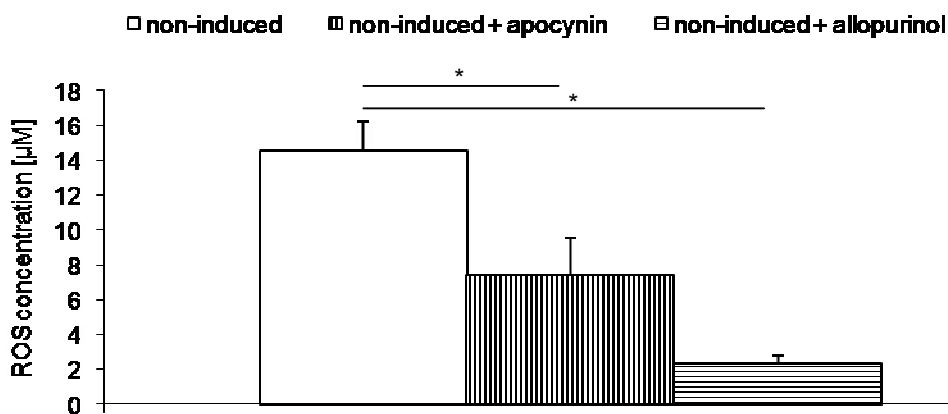


Figure 51 legend: ROS concentration in non-induced mice

In non-induced animals application of both apocynin ( $300 \mu\text{M}$ , 30min,  $37^\circ\text{C}$ ) ( $14.53 \pm 1.7$  vs.  $7.4 \pm 3.15 \mu\text{mol}$ ,  $n=8$ ,  $p < 0.05$ ) and allopurinol ( $0.1 \text{mM}$ , 1min, room temperature) caused a significant decline of ROS concentration ( $14.53 \pm 1.7$  vs.  $2.35 \pm 0.45 \mu\text{M}$ ,  $n=8$ ,  $p < 0.05$ ).

Figure 52: ROS concentration in nNOS overexpressing mice:

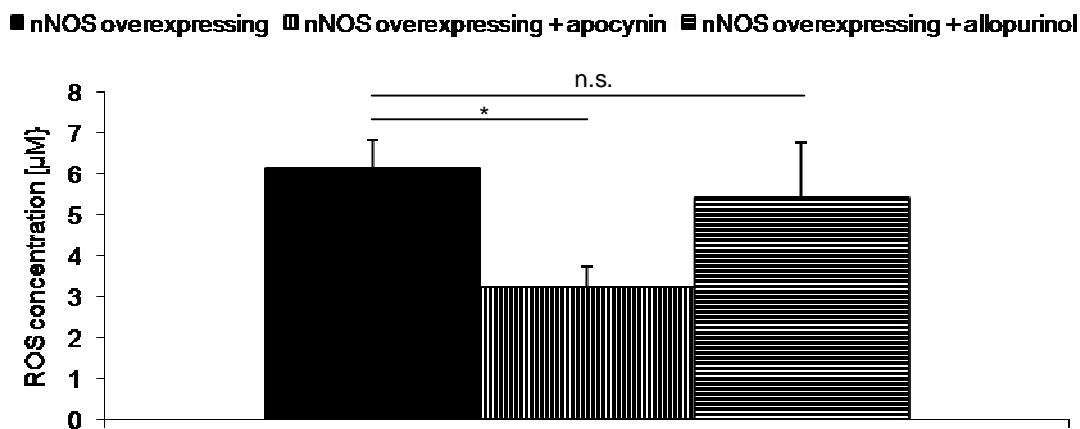


Figure 52 legend: ROS concentration in nNOS overexpressing mice

In nNOS overexpressing mice an application of apocynin also significantly inhibited ROS generation (6.14±0.685 vs. 3.23±0.5 $\mu\text{M}$ , n=8, p<0.05). In contrast to the non-induced animals, application of allopurinol had no significant inhibitory effect on ROS generation in nNOS overexpressing mice (6.14±0.685 vs. 5.4±2.35 $\mu\text{M}$ , n=8, n.s.).

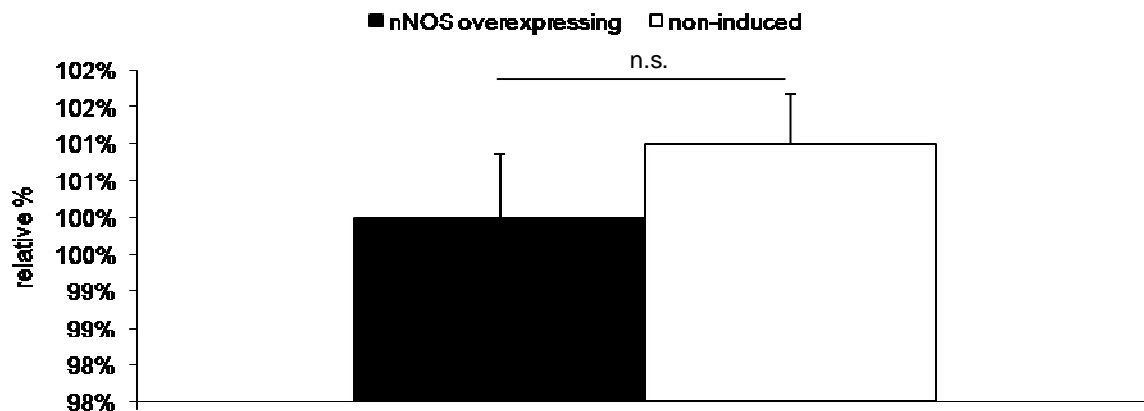
#### 4.8. NADPH oxidase activity and xanthine oxidoreductase activity:

To verify the results from the measurement of the ROS concentration, we investigated the NADPH oxidase and XOR activity.

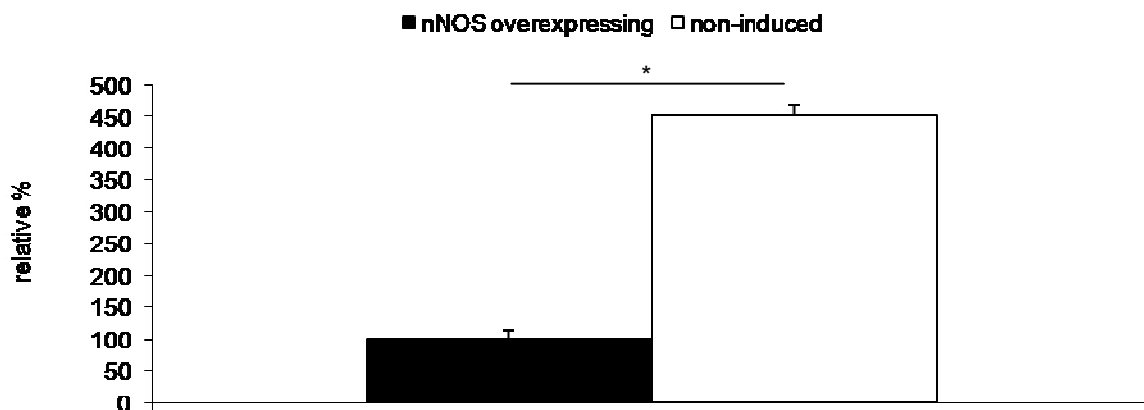
Measuring NADPH oxidase activity in hearts of nNOS overexpressing and non-induced animals showed no significant difference (100±0.01 vs. 101±0.01 relative %, n=7, n.s.) (figure 53).

XOR activity was significantly decreased in nNOS overexpressing mice (100±4.2 vs. 452±5.4 relative %, n=8, p<0.05) (figure 54).

These results were consistent with the results for the ROS generation.

**Figure 53: NADPH oxidase activity:****Figure 53 legend: NADPH oxidase activity**

There was no significant difference between non-induced and nNOS overexpressing animals concerning NADPH oxidase activity ( $100 \pm 0.01$  vs.  $101 \pm 0.01$  relative %,  $n=7$ , n.s.).

**Figure 54: Xanthine oxidoreductase activity:****Figure 54 legend: Xanthine oxidoreductase activity**

Measurement of xanthine oxidoreductase activity showed a significant decrease in nNOS overexpressing mice ( $100 \pm 4.2$  vs.  $452 \pm 5.4$  relative %,  $n=8$ ,  $p < 0.05$ ).

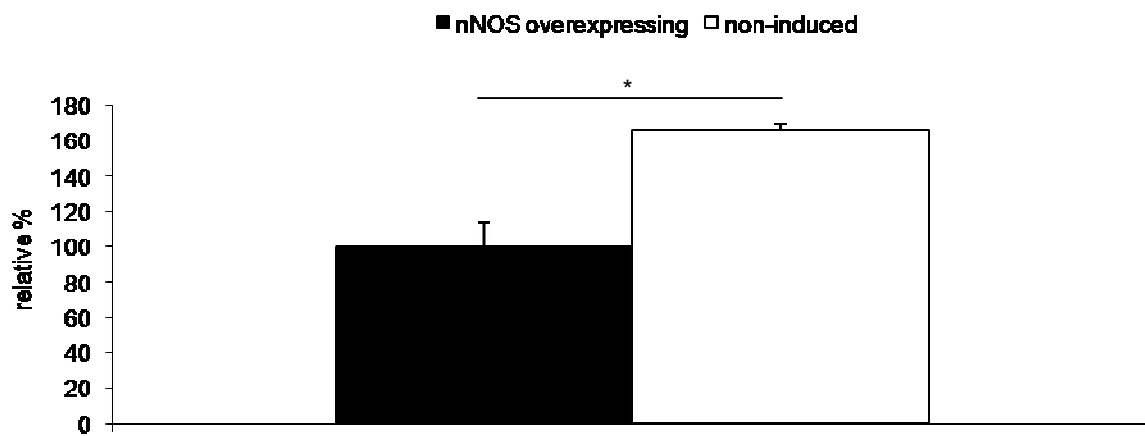
#### 4.9. NADPH oxidase subunits and XOR protein expression levels:

To investigate whether protein expression levels of NADPH oxidase and XOR were also affected, Western Blot analysis were performed.

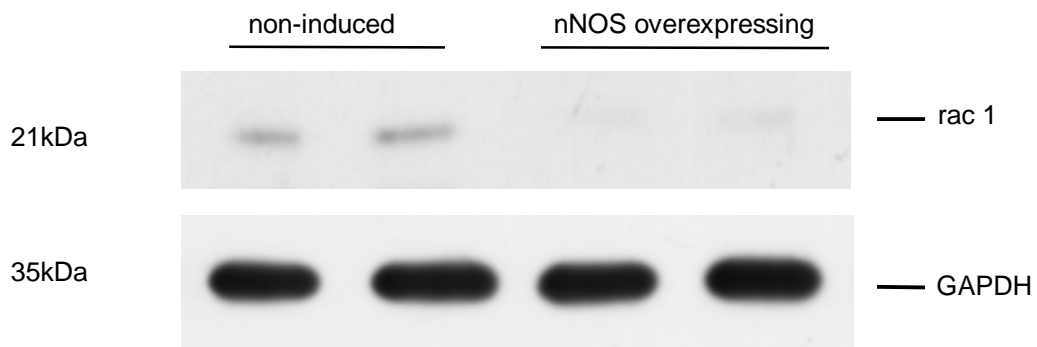
As mentioned before, NADPH oxidase is one major enzyme generating ROS. It catalyses the production of superoxide from oxygen and NADPH. It is a complex enzyme consisting of two membrane-bound elements (gp91<sup>PHOX</sup> and p22<sup>PHOX</sup>), three cytosolic components (p67<sup>PHOX</sup>, p47<sup>PHOX</sup> and p40<sup>PHOX</sup>) and a low molecular weight G protein (either rac 1 or rac 2).

Protein expression of p47<sup>PHOX</sup>, p67<sup>PHOX</sup> and rac 1 was investigated by Western Blot analysis. Only protein expression of rac 1 (important for activating the NADPH oxidase) was significantly reduced in nNOS overexpressing mice (166.4±3.1 vs. 100±13.9 relative %, n=10, p<0.05) (figure 55, 56), whereas protein expression of p47<sup>PHOX</sup> (100±71.9 relative % in nNOS overexpressing mice vs. 133.1±16.3 relative % in non-induced animals, n=10, n.s.) and p67<sup>PHOX</sup> (100±30.1 relative % in nNOS overexpressing mice vs. 133.4±16.5 relative % in non-induced animals, n=10, n.s.) was not significantly changed (figure 57, 58, 59, 60).

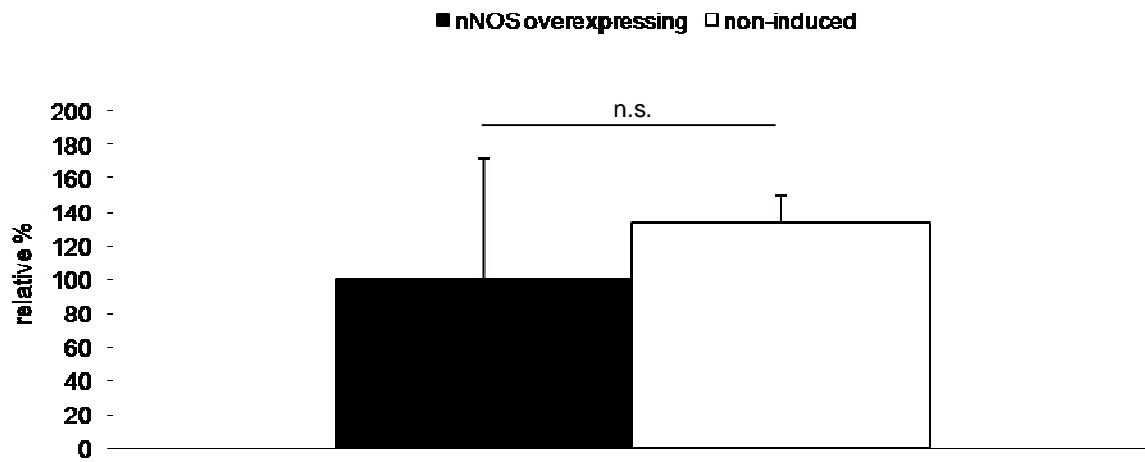
Western Blot analysis of XOR protein expression showed no significant difference concerning nNOS overexpressing mice and non-induced animals (100±15.5 vs. 107±4.45 relative %, n=7, n.s.) (figure 61, 62).

**Figure 55: Rac 1 protein expression:****Figure 55 legend: Rac 1 protein expression**

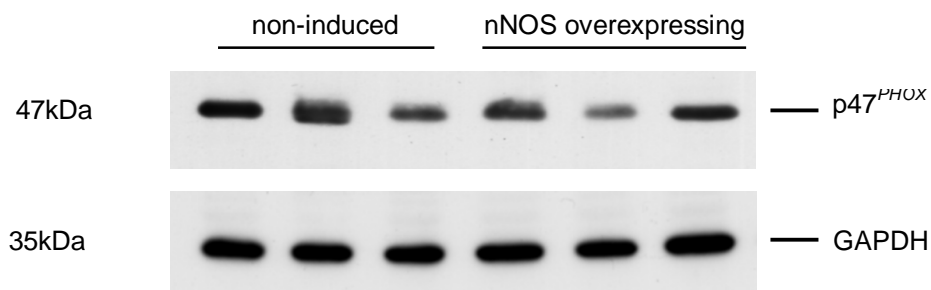
Western Blot analysis of rac 1 (a low-molecular-weight G protein, important for the activation of NADPH oxidase) protein expression showed a significant decrease in hearts of nNOS overexpressing mice compared to non-induced animals ( $166.4 \pm 3.1$  vs.  $100 \pm 13.9$  relative %,  $n=10$ ,  $p<0.05$ ).

**Figure 56: Representative Western Blot of rac 1 protein expression:****Figure 56 legend: Representative Western Blot of rac 1 protein expression**

GAPDH was used as loading control.

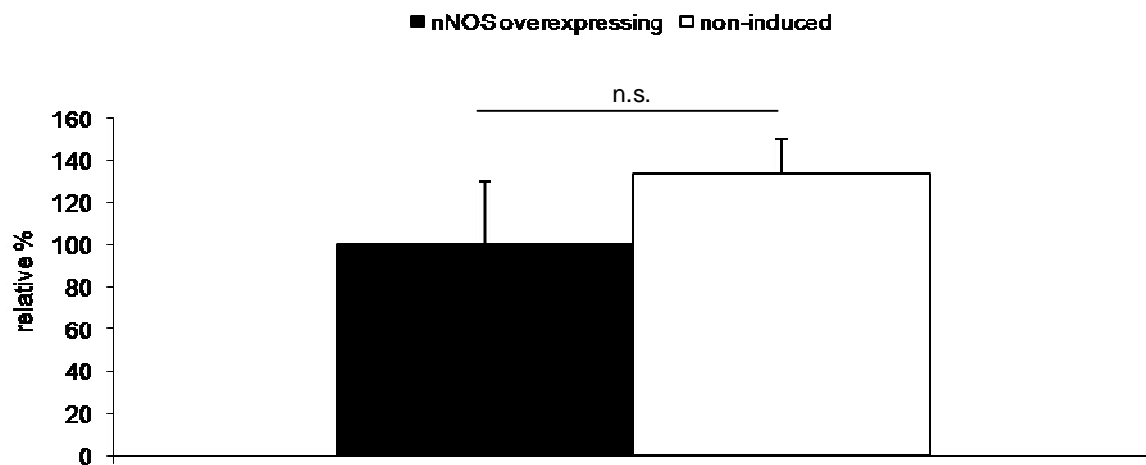
**Figure 57: p47<sup>PHOX</sup> protein expression:****Figure 57 legend: p47<sup>PHOX</sup> protein expression**

Western Blot analysis of p47<sup>PHOX</sup> (cytosolic component of NADPH oxidase) showed no significant difference between nNOS overexpressing and non-induced animals (100±71.9 vs. 133.1±16.3 relative %, n=10, n.s.).

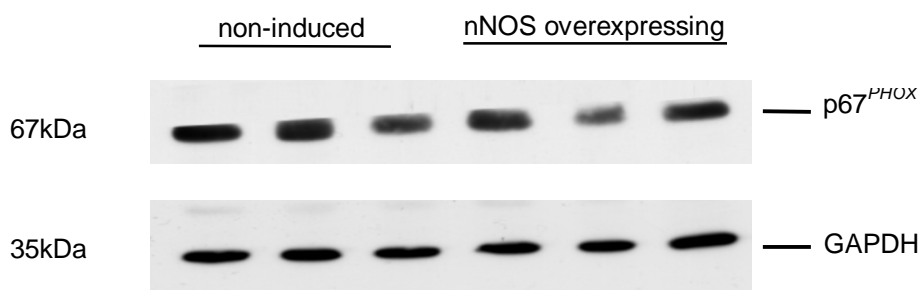
**Figure 58: Representative Western Blot of p47<sup>PHOX</sup> protein expression:****Figure 58 legend: Representative Western Blot of p47<sup>PHOX</sup> protein expression**

GAPDH was used as loading control.

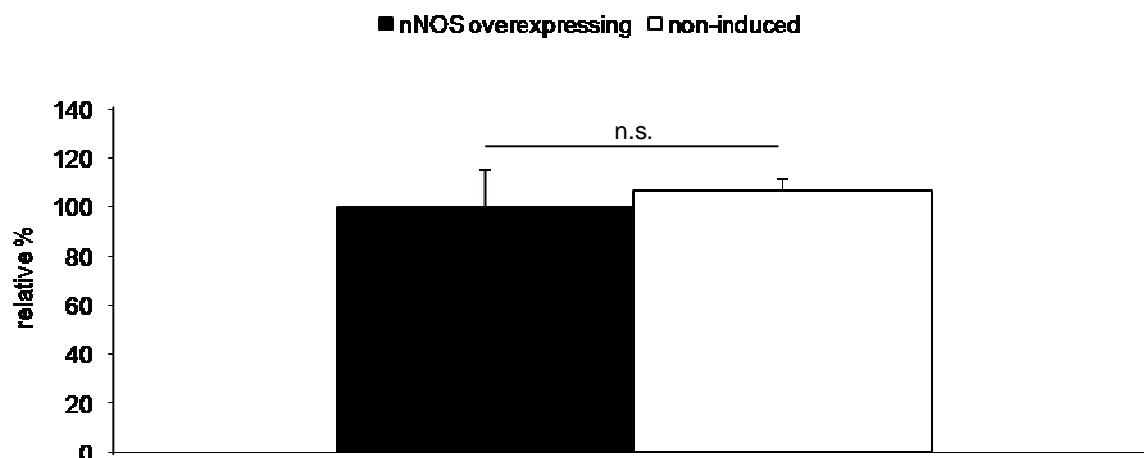


**Figure 59: p67<sup>PHOX</sup> protein expression:****Figure 59 legend: p67<sup>PHOX</sup> protein expression**

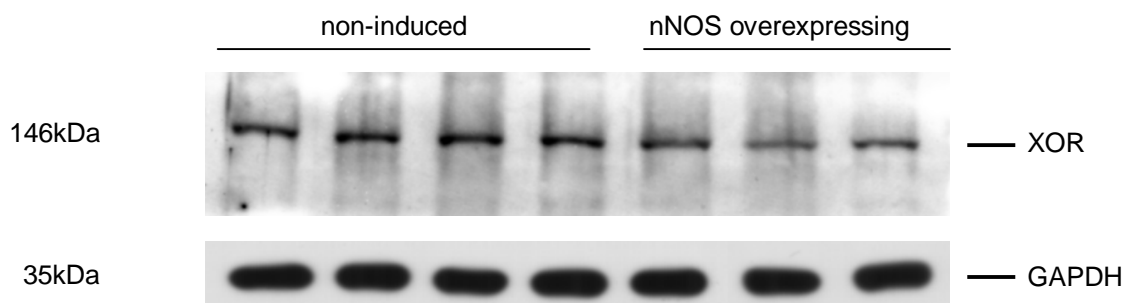
Western Blot analysis of p67<sup>PHOX</sup> (cytosolic component of NADPH oxidase) showed no significant difference between nNOs overexpressing and non-induced animals (100±30.1 vs. 133.4±16.5 relative %, n=10, n.s.).

**Figure 60: Representative Western Blot of p67<sup>PHOX</sup> protein expression:****Figure 60 legend: Representative Western Blot of p67<sup>PHOX</sup> protein expression**

GAPDH was used as loading control.

**Figure 61: XOR protein expression:****Figure 61 legend: XOR protein expression**

Western Blot analysis of XOR protein expression showed no significant difference between nNOS overexpressing and non-induced animals ( $100 \pm 15.5$  vs.  $107 \pm 4.45$  relative %,  $n=7$ , n.s.).

**Figure 62: Representative Western Blot of XOR protein expression:****Figure 62 legend: Representative Western Blot of XOR protein expression**

GAPDH was used as loading control.

These results showed that nNOS overexpression only influences the XOR activity but not the protein expression.

## 5. Discussion:

Recent studies consistently demonstrated that nNOS is cardioprotective in different disease states. An increase in myocardial nNOS protein levels was shown in postmyocardial infarction and spontaneously hypertensive rats<sup>195,196,197</sup>. An increase in NOS protein expression may not necessarily correlate with an increase in NO production, as it is becoming increasingly apparent that uncoupling of NOS activity in disease states may lead to NOS synthesis of ROS<sup>198</sup>. Damy et al.<sup>195</sup> and other studies would suggest that upregulation of nNOS may be protective, as an inhibition of nNOS worsened LV dysfunction<sup>195,199</sup>. For example, in isolated hearts the depression of LV developed pressure following 40min of global ischemia was greater in nNOS<sup>-/-</sup> mice than in WT mice<sup>199</sup>. In addition, the nNOS<sup>-/-</sup> hearts developed a larger infarct and a greater expression of tumor necrosis factor alpha (TNF- $\alpha$ )<sup>199</sup>. However, in another study of WT and nNOS<sup>-/-</sup> mice subjected to 20min of coronary artery occlusion and 120min of reperfusion, there was no difference in infarct size between the two groups, although hearts of nNOS<sup>-/-</sup> mice exhibited more infiltration of polymorphonuclear leucocytes than did hearts of WT mice<sup>200</sup>. nNOS inhibition with 1-(2-trimethylphenyl) imidazole (TRIM) increased heart rate significantly more in myocardial infarction rats than in sham-operated rats, suggesting that nNOS upregulation may be protective by enhancing vagal responsiveness after myocardial infarction<sup>201</sup>. However, perhaps surprisingly, there was no difference in the response to the muscarinic inhibitor atropine between the two groups<sup>201</sup>. Both, protective<sup>202,203</sup> and injurious effects<sup>204</sup> of eNOS-derived NO on myocardial ischemia-reperfusion injury have been shown. A finding that could prove to have physiological and clinical implications is that angiotensin II increases the protein expression of both nNOS and eNOS in the myocardium<sup>205</sup>. However, in hypertensive rats, treatment with an angiotensin-converting enzyme (ACE) inhibitor led to an increase of left ventricular eNOS and a decrease in iNOS expression<sup>206</sup>. So far there is no study on whether ACE inhibition has an effect on myocardial nNOS levels, the findings in healthy animals, can lead to speculate that cardiac upregulation of nNOS in disease state may protect the myocardium from catecholamine toxicity<sup>207,208</sup> and promote a

favourable sympatho-vagal balance<sup>209</sup>. Investigations of nNOS in disease models remain limited and further investigations of the role of nNOS in cardiac disease states may yield interesting findings. The precise molecular mechanisms of nNOS action in the myocardium during rest and after myocardial damage are still being discussed contradictory.

In a model with nNOS overexpression restricted to cardiac myocytes we recently demonstrated that nNOS decreased myocardial contractility via inhibition of the L-type calcium current ( $I_{Ca,L}$ ) amplitude and  $[Ca^{2+}]_i$  transients<sup>1</sup>. We now identified mitochondria and xanthine oxidoreductase as further targets for nNOS in this model. Since suppression of XOR activity by nNOS has been linked to an improved outcome after myocardial infarction we now hypothesise that nNOS also acts cardioprotective during ischemia-reperfusion injury. Indeed, we found preserved left ventricular developed pressure and a significant decrease in infarct size after ischemia-reperfusion injury in nNOS overexpressing animals.

In electronmicroscopical studies we also found a strong enrichment of overexpressed and endogenous nNOS at the mitochondria. Mitochondrial respiration and its regulation by NO are important in the heart for several reasons. Firstly, mitochondria generate almost all the ATP required for muscle contraction in the heart, so that inhibition of mitochondrial respiration results in an inhibition of contractility. Secondly, inhibition of mitochondrial respiration stimulates mitochondrial production of ROS which regulates signal transduction pathways within the heart. Thirdly, inhibition of mitochondrial respiration can cause necrosis or apoptosis within the heart. Endogenous NO interacts with the mitochondrial respiratory chain at several steps of the electron transfer. It was shown that NO modulates  $O_2$  consumption by competitive inhibition of the cytochrome c oxidase<sup>210</sup>. This modulation is transient as long as NO is generated in small quantities<sup>210</sup>. However, at higher NO concentrations, the inhibition of the respiratory chain at different levels leads to an increased rate of ROS production<sup>211</sup> which in turn may damage the mitochondria. Others have indicated that a sustained production of NO triggered by increased  $Ca^{2+}$

levels may release cytochrome c from mitochondria, an event implicated in cell apoptosis<sup>212</sup>. The cytochrome c oxidase reaction, the terminal step in the respiratory chain, is irreversible and therefore a potential control site. Although it was suggested that cytochrome c oxidase might be a site for allosteric regulation<sup>213</sup>, there were no known significant physiological effectors of cytochrome c oxidase activity. Now, NO has demonstrated its capacity as a modulator of cytochrome c oxidase activity<sup>210</sup>. NO does not stop, but rather slows the electron flow through the respiratory chain to achieve its inhibitory effect and thus avoids the complete reduction of respiratory chain components and the burst of ROS at lower NO/O<sub>2</sub> ratios. This makes the regulation of the respiratory chain possible without unintended damage to the mitochondria or the cell. NO slows the O<sub>2</sub> consumption in cells close to blood vessels, allowing O<sub>2</sub> to penetrate into the cells at the boundary of becoming hypoxic. Cells close to blood supply have the greatest supply of L-arginine and O<sub>2</sub>, which stimulate mitochondrial NOS (in this study nNOS) production of NO. NO, in turn, interacts with cytochrome c oxidase to decrease the O<sub>2</sub> consumption of the oxygenated cells, allowing the O<sub>2</sub> supply to diffuse further into the tissue<sup>214</sup>. In addition, NO, probably derived from eNOS, would help dilate blood vessels and potentially increase O<sub>2</sub> delivery to borderline hypoxic cells. Here, we demonstrated that nNOS overexpression potently inhibited myocardial oxygen consumption mainly due to inhibition of the cytochrome c oxidase. This is in line with earlier findings<sup>189,215</sup> but raises two questions: how is nNOS translocated into the mitochondria and how can nNOS produce NO in mitochondria where it is in competition for O<sub>2</sub> with other enzymes of the respiratory chain?

We now identified HSP90 as a carrier protein to translocate nNOS across the outer mitochondrial membrane to cytochrome c oxidase via the TOM complex. This could be specifically inhibited by the HSP90 inhibitor geldanamycin. Similarly, a recent study described HSP90 as a carrier responsible for translocation of connexin 43 into the mitochondria, which there protected from ischemia-reperfusion injury<sup>216</sup>. Dany et al. also reported an increased HSP90-nNOS interaction in failing human hearts<sup>217</sup>.

In a scenario with low oxygen tension (like ischemia) it has been demonstrated previously that haemoglobin and myoglobin can form NO from nitrite at low oxygen apart from NOS enzymes<sup>218,219</sup>. Clearly, nitrite had to be formed by abundant NO

before. NO from these nitrite sources might then inhibit cytochrome c oxidase during acute ischemia. After translocation of nNOS to the mitochondria, as it occurs in ischemia-reperfusion injury and during subsequent reperfusion with gradually increasing O<sub>2</sub> levels, NO that is generated from nNOS at the mitochondria might then take over and continue to inhibit cytochrome c oxidase (which might be easier now because cytochrome c oxidase was inhibited earlier and could therefore not compete for O<sub>2</sub>). Accordingly, we found increased nitrite levels in isolated mitochondria from nNOS overexpressing mice that are in favour of this mechanism.

Recent work already identified NO derived from the other NOS enzymes (eNOS and iNOS) as responsible factor for cardioprotection in ischemia and reperfusion. It was demonstrated that iNOS inhibited mitochondrial permeability transition (MPT) and the authors suggested that iNOS acts upstream of MPT<sup>220</sup>. Also in the case of eNOS overexpression, the protective effect has been consistently demonstrated by several studies<sup>202,221,222</sup>. An explanation for this effect might come from a study in eNOS overexpressing animals where Massion et al. showed that eNOS, targeted to caveolae in cardiomyocytes, attenuated the effect of high concentrations of catecholamines<sup>223</sup>. Therefore, all three NOS isoforms as a net effect decreased ischemic damage. However, it appears that the molecular and subcellular process behind this uniform protection are different for each case.

In further experiments with isolated muscle stripes we found that increased nNOS expression decreased myocardial contractility and simultaneously decreased myocardial oxygen consumption both, at work and rest. Especially from the decrease in MVO<sub>2</sub> at rest we concluded that an increase in nNOS expression might act as a preconditioning measure before ischemia-reperfusion.

During ischemia, ATP depletion leads to a rise in Ca<sup>2+</sup>, which further accelerates ATP depletion. The rise of Ca<sup>2+</sup> during ischemia and reperfusion leads to mitochondrial Ca<sup>2+</sup> accumulation, particularly during reperfusion when oxygen is reintroduced. This can result in opening of the mitochondrial permeability transition pore, which further

compromises cellular energetics. If downregulation of mitochondrial function occurs prior to ischemia, this may downregulate cellular energetics and prevent cell death.

However, to this end it is not fully clear whether this direct effect of nNOS on mitochondrial function is cardioprotective or rather detrimental since one would expect that inhibition of mitochondrial function cuts off the energy supply. In contrast and of particular interest, it was observed that GSNO treatment led to an increased S-nitrosylation of the mitochondrial F1-ATPase, which resulted in decreased activity. It has been reported that approximately half of the ATP generated during ischemia by glycolysis is consumed by reverse mode of the mitochondrial F1-ATPase. Therefore, inhibition of the F1-ATPase during ischemia would conserve ATP. Thus inhibition of the F1-ATPase could be beneficial by conserving cytosolic ATP and by reducing  $\text{Ca}^{2+}$  uptake into the mitochondria<sup>191</sup>.

Additional effectors of ischemia-reperfusion injury in cardiomyocytes are reactive oxygen species. Reduction of ROS was already reported to reduce ischemic injury<sup>233</sup>. In this study, we now showed that the overexpression of nNOS in cardiac tissue balances the production between ROS and NO. Decreased ROS production can be attributed to lower activity of both, XOR and NADPH oxidase. ROS production by the NADPH oxidase in smooth muscle and endothelial cells of the vessel wall has been implicated in the genesis of hypertensive vascular smooth muscle hypertrophy<sup>224,225,226</sup>, arteriosclerosis<sup>227</sup>, and endothelial dysfunction<sup>228</sup>. Importantly, NADPH oxidase is known to be activated by several stimuli of relevance to cardiovascular pathophysiology, including angiotensin II, noradrenaline, TNF- $\alpha$ , and increased mechanical forces<sup>232,119</sup>. Recent experimental studies suggest a role for NADPH oxidase in cardiac pathophysiology. Heymes et al. reported an increased myocardial expression of NADPH oxidase in experimental pressure-overload cardiac hypertrophy<sup>229</sup> and suggested a role for ROS derived from this oxidase in the genesis of cardiac contractile dysfunction in this setting<sup>230</sup>. The development of experimental angiotensin II-induced cardiac hypertrophy was found to be inhibited in mice lacking a functional NADPH oxidase<sup>231</sup>. Likewise, ROS production by NADPH oxidase was implicated in alpha-adrenergic agonist-induced cardiomyocyte hypertrophy<sup>232</sup>. Although the NADPH oxidase was shown to be a major source of ROS and plays a crucial role in cardiac pathophysiology, in our study, there was no evidence that the

NADPH oxidase activity was significantly influenced by nNOS overexpression. Only protein expression of rac 1 was significantly reduced in nNOS overexpressing mice. Rac is a small G protein which is an important molecular switch integrating diverse stimuli in the cardiovascular system and transducing key signaling functions such as superoxide production<sup>233,234</sup>, cytoskeletal organisation<sup>235,236</sup> and gene expression essential for cellular proliferation and hypertrophy<sup>237,238</sup>. The role of rac as a regulator of the NADPH oxidase complex was first described in phagocytes, where the isoform rac 1 and rac 2 control respiratory burst oxidation. Recently, an NADPH oxidase complex, regulated by rac 1, has been characterised in nonphagocytic cells, such as vascular smooth muscle, cardiac myocytes and endothelial cells<sup>232</sup>. Although it was shown that rac 1 regulates NADPH oxidase activity<sup>239</sup>, we could not observe a significant difference. A possible explanation for our results might be that rac 1 is differentially activated by cellular receptors coupled to distinct rac-activating adapter molecules, with each leading to pathway specific arrays of downstream effects. For example rac can rapidly be activated through the G<sub>i</sub>- and G<sub>q</sub>-coupled receptor ANG II but is sustained through 30min<sup>240</sup>. rac can also be activated by receptor tyrosine kinases<sup>241</sup>. Furthermore, the translocation of the cytosolic subunits (including rac 1) to the membrane is important for the activation of the NADPH oxidase<sup>239</sup> and in this study, we did not investigate the cellular localisation of rac 1. Thus it may be important to investigate not just whether rac is activated or downregulated but also where, how and for what effector.

We also investigated the XOR (another major source of ROS). Notably, it was previously shown that XOR activity was elevated at baseline in nNOS<sup>-/-</sup> relative to WT mice and remained persistently elevated, whereas WT mice exhibited a transient elevation that was restored to normal by 4 weeks after MI<sup>181</sup>. The mechanisms involved in increased XOR activity are complex and probably include nNOS-mediated posttranslational modification (e.g. S-nitrosylation) of XOR. This phenomenon is in accordance with our findings which showed decreased XOR activity, with unchanged XOR protein expression, in nNOS overexpressing mice, resulting in lower ROS levels.

The mechanisms underlying nNOS and eNOS mediated cardiac protection after myocardial infarction include the maintenance of an equilibrium between ROS and



RNS in different cellular compartments. In infarcted nNOS<sup>-/-</sup> mice, there is a clear mismatch between the increase in ROS, especially that due to XOR activity, and NO production. XOR activity is persistently up-regulated after MI in nNOS<sup>-/-</sup> mice, whereas it transiently increases in control mice after MI. The increased XOR activity was attributed to a diminished XOR inhibition in the absence of nNOS-derived NO. Therefore, the absence of nNOS within the myocardium creates a nitroso–redox imbalance shown to be sustained in both, acute and chronic MI<sup>181,242</sup>. We could now demonstrate that reducing ROS, possibly by overexpression of nNOS, reduced ischemic injury.

Recently, an additional mechanism for the protective effects of nNOS, translocation, was suggested in a study by Sun and colleagues<sup>10</sup> who examined male and female mice following ischemia-reperfusion. The L-type Ca<sup>2+</sup> channel appeared to be a major membrane target for nNOS following translocation. In female hearts there was increased S-nitrosylation of the L-type Ca<sup>2+</sup> channel. Functionally, this led to decreased  $I_{Ca,L}$  with reduced Ca<sup>2+</sup> entry into the cell, which in turn protected the cell from Ca<sup>2+</sup> overload injury<sup>10,191</sup>. This is in line with our previous studies<sup>1</sup>. The 30% decreased entry of Ca<sup>2+</sup> via  $I_{Ca,L}$  in nNOS overexpressing myocytes may directly contribute to the decreased performance we observed. Further to this it has been suggested that nNOS-derived NO increases the activity of the Na<sup>+</sup>-K<sup>+</sup>-ATPase pump<sup>243,244</sup> which may directly affect Ca<sup>2+</sup>-fluxes through an action on intracellular Na<sup>+</sup> levels and resultant change in activity of the Na<sup>+</sup>-Ca<sup>2+</sup>-exchanger. In agreement with our findings, Sears et al.<sup>183</sup> described an attenuation of L-type Ca<sup>2+</sup> currents by nNOS-derived NO. In contrast, others have observed unchanged L-type Ca<sup>2+</sup> current between nNOS<sup>-/-</sup> and WT<sup>8</sup> or an increase in L-type Ca<sup>2+</sup> current density in nNOS overexpressing animals<sup>179</sup>. The latter studies however did not focus on ischemia-reperfusion injury.

#### Conclusions:

In summary, conditional transgenic overexpression of nNOS is localised at the mitochondria and inhibits XOR resulting in a decrease of ROS formation. Mitochondrial respiration is also downregulated in response to nNOS accumulation at the mitochondria. Together with nNOS-mediated inhibition of L-type Ca<sup>2+</sup> currents

these multiple actions of nNOS potentially protect cardiomyocytes from ischemia-reperfusion injury. nNOS has versatile actions at multiple subcellular sites and it is modulated according to the type and state of cardiac disease. This versatility may be responsible for the controversial results in different animal models and suggest a fine regulation of nNOS function depending on the respective subcellular localisation and type of disease.

---

## 6. References:

1. **Burkard N., Rokita A.G., Kaufmann S., Hallhuber M., Wu R., Hu K., Hofmann U., Bonz A., Frantz S., Cartwright E., Neyses L., Maier L.S., Maier S.K.G., Renné T., Schuh K., Ritter O.** (2007). Conditional neuronal nitric oxide synthase overexpression impairs myocardial contractility. *Circ Res* **100**, 32-44
2. **Ignarro L.J.** (1989). Biological actions and properties of endothelium derived nitric oxide formed and released from artery and vein. *Circ Res* **65**(1), 1-21
3. **Ignarro L.J., Fukuto J.M., Griscavage J.M., Rogers N.E., Byrns R.E.** (1993). Oxidation of nitric oxide in aqueous solution to nitrite but not to nitrate: Comparison with enzymatically formed nitric oxide from L-arginine. *Proc Natl Acad Sci USA* **90**(17), 8103-8107
4. **Subczynski W.K., Lomnicka M., Hyde J.S.** (1996). Permeability of nitric oxide through lipid bilayer membranes. *Free Radic Res* **24**(5), 343-349
5. **Zioli M.T.** (2008). The fork in the nitric oxide road: cyclic GMP or nitrosylation? *Nitric oxide* **18**(3), 153-165
6. **Stamler J.S., Lamas S., Fang F.C.** (2001). Nitrosylation: the prototypic redox-based signaling mechanism. *Cell* **106**(6), 675-683
7. **Vila-Petroff M.G., Younes A., Egan J., Lakatta E.G., Sollot S.J.** (1999). Activation of distinct cAMP-dependent and cGMP-dependent pathways by nitric oxide in cardiac myocytes. *Circ Res* **84**(9), 1020-1031
8. **Barouch L.A., Harrison R.W., Skaf M.W., Rosas G.O., Cappola T.P., Kobeissi Z.A.** (2002). Nitric oxide regulates the heart by spatial confinement of nitric oxide synthase isoforms. *Nature* **416**(6878), 337-339
9. **Ziolo M.T., Bers D.M.** (2003). The real estate of NOS signaling: location, location, location. *Circ Res* **92**(12), 1279-1281
10. **Sun J., Picht E., Ginsburg K.S., Bers D.M., Steenbergen C., Murphy E.** (2006). Hypercontractile female hearts exhibit increased S-nitrosylation of the L-type Ca<sup>2+</sup> channel alpha1 subunit and reduced ischemia/reperfusion injury. *Circ Res* **98**(3), 403-411
11. **Katori D., Donzelli S., Tochetti C.G., Miranda K.M., Cormaci G., Thomas D.D.** (2006). Peroxynitrite and myocardial contractility: in vivo versus in vitro effects. *Free Radic Biol Med* **41**(10), 1606-1618
12. **Walsh E.K., Huang H., Wang Z., Williams J., de Crom R., van Haperen R.** (2004). Control of myocardial oxygen consumption in transgenic mice overexpressing vascular eNOS. *Am J Physiol Heart Circ Physiol* **287**(5), H2115-H2121

13. Kohr M.J., Wang H., Wheeler D.G., Velayutham M., Zweier J.L., Ziolo M.T. (2008). Targeting of phospholamban by peroxynitrite decreases {beta}-adrenergic stimulation in cardiomyocytes. *Cardiovasc Res* **77**(2), 353-361
14. Ziolo M.T., Katoh H., Bers D.M. (2001). Positive and negative effects of nitric oxide on Ca(2+) sparks: influence of beta-adrenergic stimulation. *Am J Physiol Heart Circ Physiol* **281**(6), H2295-H2303
15. Tochetti G.C., Wang W., Froehlich J.P., Huke S., Aon M.A., Wilson G.M. (2007). Nitroxyl improves cellular heart function by directly enhancing cardiac sarcoplasmic reticulum Ca<sup>2+</sup> cycling. *Circ Res* **100**(1), 96-104
16. Kojda G., Kottenberg K., Nix P., Schluter K.D., Piper H.M., Noack E. (1996). Low increase in cGMP induced by organic nitrates and nitrovasodilators improves contractile response of rat ventricular myocytes. *Circ Res* **78**(1), 91-101
17. Nakane M., Schmidt H.H., Pollock J.S., Forstermann U., Murad F. (1993). Cloned human brain nitric oxide synthase is highly expressed in skeletal muscle. *FEBS Lett.* **316**, 175-180
18. Hall A.V., Antoniou H., Wang Y., Cheung A.H., Arbus A.M., Olson S.L., Lu W.C., Marsden P.A. (1994). Structural organization of the human neuronal nitric oxide synthase gene (NOS1). *J. Biol. Chem.* **269**, 33082-33090
19. Geller D.A., Lowenstein C.J., Shapiro R.A., Nussler A.K., Di Silvio M., Wang S.C., Nakayama D.K., Simmons R.L., Snyder S.H., Billar T.R. (1993). Molecular cloning and expression of inducible nitric oxide synthase from human hepatocytes. *Proc. Natl. Acad. Sci. U.S.A.* **90**, 3491-3495
20. Sherman P.A., Laubach V.E., Reep B.R., Wood E.R. (1993). Purification and cDNA sequence of an inducible nitric oxide synthase from a human tumor cell line. *Biochemistry* **32**, 11600-11605
21. Charles I.G., Palmer R.M., Hickery M.S., Bayliss M.T., Chubb A.P., Moss D.W., Moncada S. (1993). Cloning, characterization and expression of a cDNA encoding and inducible nitric oxide synthase from the human chondrocyte. *Proc. Natl. Acad. Sci. U.S.A.* **90**, 11419-11423
22. Janssens S.P., Shimouchi A., Quertermous T., Bloch D.B., Bloch K.D. (1992). Cloning and expression of a cDNA encoding human endothelium-derived relaxing factor/nitric oxide synthase. *J. Biol. Chem.* **267**, 14519-14522
23. Marsden P.A., Schappert K.T., Chen H.S., Flowers M., Sundell C.L., Wilcox J.N., Lamas S., Michel T. (1992). Molecular cloning and characterization of human endothelial nitric oxide synthase. *FEBS Lett.* **307**, 287-293
24. Abu-Soud H.M., Presta A., Mayer B., Stuehr D.J. (1997). Analysis of neuronal NO synthase under single-turnover conditions: conversion of N<sup>ω</sup>-hydroxyarginine to nitric oxide and citrulline. *Biochemistry* **36**, 10811-10816

- 
25. **Stuehr D.J., Kwon N.S., Nathan C.F.** (1991). N $\omega$ -Hydroxy-L-arginine is an intermediate in the biosynthesis of nitric oxide from L-Arginine. *J. Biol. Chem.* **266**, 6259-6263
26. **Ghosh D.K., Stuehr D.J.** (1995). Macrophage NO synthase: characterization of isolated oxygenase and reductase domains reveals a head-to head subunit interaction. *Biochemistry.* **34**, 801-807
27. **Klatt P., Schmidt K., Uray G., Mayer B.** (1993). Multiple catalytic functions of brain nitric oxide synthase. Biochemical characterization, cofactor-requirement and role of N<sup>G</sup>-hydroxy-L-arginine as an intermediate. *J. Biol. Chem.* **268**, 14781-14787
28. **Abu-Soud H.M., Yoho L.L., Stuehr D.J.** (1994). Calmodulin controls neuronal nitric-oxide synthase by a dual mechanism: Activation of intra- and interdomain electron transfer. *J. Biol. Chem.* **269**, 32047-3205
29. **Bredt D.S., Hwang P.M., Glatt C.E.** (1991). Cloned and expressed nitric oxide synthase structurally resembles cytochrom P450 reductase. *Nature* **351**, 714-718
30. **Xie Q., Cho H., Kashiwabara Y.** (1994). Carboxyl terminus of inducible nitric oxide synthase: Contribution to NADPH binding and enzymatic activity. *J. Biol. Chem.* **269**, 28500-28505
31. **Zhang J.L., Patel J.M., Li Y.D., Block E.R.** (1996). Reductase domain cysteines 1048 and 1114 are critical for catalytic activity of human endothelial cell nitric oxide synthase as probed by site-directed mutagenesis. *Biochem. Biophys. Res Commun.* **226**, 293-300
32. **Gachhui R., Gosh D.K., Wu C.** (1997). Mutagenesis of acidic residues in the oxygenase domain of inducible nitric-oxide synthase identifies a glutamate involved in arginine binding. *Biochemistry* **36**, 5097-5103
33. **Chen P.F., Tsai A.L., Berka V., Wu K.K.** (1997). Mutation of Glu-361 in human endothelial nitric-oxide synthase selectively abolishes L-arginine binding without perturbing the behavior of heme and other redox centers. *J. Biol. Chem.* **272**, 6114-6118
34. **Crane B.R., Arvai A.S., Ghosh D.K.** (1998). Structure of nitric oxide synthase oxygenase dimer with pterin and substrate. *Science* **279**, 2121-2126
35. **Abu-Soud H.M., Feldman P.L., Clark P., Stuehr D.J.** (1994). Electron transfer in nitric-oxide synthases. Characterization of L-arginine analogs that block heme iron reduction. *J. Biol. Chem.* **269**, 32318-26
36. **Siddhanta U., Presta A., Fan B., Wolan D., Rousseau D.L., Stuehr D.J.** (1998). Domain swapping in inducible nitric-oxide synthase. Electron transfer occurs between flavin and heme groups located on adjacent subunits in the dimer. *J. Biol. Chem.* **273**, 18950-58

- 
37. **Kishimoto J., Spurr N., Liao M., Lizhi L., Emson P., Xu W.** (1992). Localization of brain nitric oxide synthase (NOS) to human chromosome 12. *Genomics* **14**, 802-804
38. **Xu W., Gorman P., Sheer D., Bates G., Kishimoto J., Liu L., Emson P.** (1993) Regional localization of the gene coding for human brain nitric oxide synthase (NOS1) to 12q24.2→24.31 by fluorescent in situ hybridization. *Cytogene Cell Genet.* **64**, 62-63
39. **Xu W., Charles I.G., Moncada S., Gorman P., Sheer D., Liu L., Emson P.** (1994). Mapping of the genes encoding human inducible and endothelial nitric oxide synthase (NOS2 and NOS3) to the pericentric region of chromosome 17 and to chromosome 7, respectively. *Genomics* **21**(2), 419-422
40. **Boissel JP., Ohly D., Bros M., Godtel-Armbrust U., Forstermann U., Frank S.** (2004). The neuronal nitric oxide synthase is upregulated in mouse skin repair and in response to epidermal growth factor in human HaCaT keratinocytes. *J. Invest. Dermatol.* **123**, 132-39
41. **Wang Y., Kodani E., Wang J., Zhang S.X., Takano H.** (2004). Cardioprotection during the final stage of the late phase of ischemic preconditioning is mediated by neuronal NO synthase in concert with cyclooxygenase-2. *Circ. Res.* **95**(1), 84-91
42. **Dekker R.J., vans Soest S., Fontijn R.D., Salamanca S., de Groot P.G.** (2002). Prolonged fluid shear stress induces a distinct set of endothelial cell genes, most specifically lung Kruppel-like factor (KLF2). *Blood* **100**, 1689-98
43. **SenBanerjee S., Lin Z., Atkins G.B., Grief D.M., Rao R.M.** (2004). Identification of KLF2 as a novel transcriptional regulator of endothelial proinflammatory activation. *J. Exp. Med.* **199**, 1305-15
44. **Laufs U., Liao J.K.** (2000). Targeting rho in cardiovascular disease. *Circ. Res.* **87**, 526-28
45. **Takemoto M., Sun J., Hiroki J., Shirnokawa H., Liao J.K.** (2002). Rho-kinase mediated hypoxia-induced downregulation of endothelial nitric oxide synthase. *Circulation* **106**, 57-65
46. **Lee G.C., Gregg A.R., O'Brian W.E.** (1995). Localization of the neuronal form of nitric oxide synthase to mouse chromosome 5. *Mamm Genome* **6**(1), 56-57
47. **Deng A.Y., Rapp J.P., Kato H., Bihoreau M.T.** (1995). Linkage mapping of the neuronal nitric oxide synthase gene (NOS1) to rat chromosome 12. *Mamm Genome* **6**(11), 824
48. **Silvagno F., Xia H., Bredt D.S.** (1996). Neuronal nitric-oxide synthase mu, an alternatively spliced isoform expressed in differentiated skeletal muscle. *J Biol Chem* **271**(19), 11204-11208

- 
49. **Magee T., Fuentes A.M., Garban H., Rajavashisth T., Marquez D., Rodriguez J.A.** (1996). Cloning of a novel neuronal nitric oxide synthase expressed in penis and lower urinary tract. *Biochem Biophys Res Commun* **226**(1), 145-151
  50. **Brenman J.E., Chao D.S., Gee S.H., McGee A.W., Craven S.E., Santillano D.R.** (1996). Interaction of nitric oxide synthase with the postsynaptic density protein PSD-95 and alpha1-synthropin mediated by PDZ domains. *Cell* **84**(5), 757-767
  51. **Takahashi Y., Makayama T., Soma M., Izumi Y., Kanmatsuse K.** (1997). CA repeat polymorphism of the neuronal nitric oxide synthase gene. *Hum Hered* **47**(1), 58-59
  52. **Jennings R.B., Sommers H.M., Smyth G.A., Flack H.A., Linn H.** (1960). Myocardial necrosis induced by temporary occlusion of a coronary artery in the dog. *Arch Pathol* **70**, 68-78
  53. **Braunwald E., Kloner R.A.** (1982). The stunned myocardium: prolonged, postischemic ventricular dysfunction. *Circulation* **66**, 1146-1149
  54. **Krug A., Du Mesnil de Rochemont R., Korb G.** (1966). Blood supply of the myocardium after temporary coronary occlusion. *Circ Res* **19**, 57-62
  55. **Ito H.** (2006). No-flow phenomenon and prognosis in patients with acute myocardial infarction. *Nat Clin Pract Cardiovasc Med* **3**, 499-506
  56. **Manning A.S., Hearse D.J.** (1984). Reperfusion-induced arrhythmias: mechanism of myocardial infarction. *J Mol Cell Cardiol* **16**, 497-518
  57. **Bolli R., Marbán E.** (1999). Molecular and cellular mechanism of myocardial stunning. *Physiol Rev* **79**, 609-634
  58. **Kloner R.A.** (1993). Does reperfusion injury exist in human? *J Mol Cell Cardiol* **21**, 537-545
  59. **Piper H.M., Garcia-Dorado D., Ovize M.** (1998). A fresh look at reperfusion injury. *Cardiovasc Res* **38**, 291-300
  60. **Yellon D.M., Baxter G.F.** (1999). Reperfusion injury revisited: is there a role for growth factor signaling in limiting lethal reperfusion injury? *Trends Cardiovasc Med* **9**, 245-249
  61. **Zweier J.L.** (1988). Measurement of superoxide-derived free radicals in the reperfused heart: evidence for a free radical mechanism of reperfusion injury. *J Biol Chem* **263**, 1353-1357
  62. **Zweier J.L., Talukeder M.A.** (2006). The role of oxidants and free radicals in reperfusion injury. *Cardiovasc Res* **70**, 181-190
  63. **Weyrich A.S., Ma X.L., Lefer A.M.** (1992). The role of L-arginine in ameliorating reperfusion injury after myocardial ischemia in the cat. *Circulation* **86**, 279-288

- 
64. **Droge W.** (2003). Oxidative stress and aging. *Adv Exp Med Biol* **543**, 191-200
65. **Nichols D.G., Budd S.L.** (2000). Mitochondria and neuronal survival. *Physiol Rev* **80**, 315-360
66. **Nichols D.G., Ward M.W.** (2000). Mitochondrial membrane potential and neuronal glutamate excitotoxicity: mortality and millivolts. *Trends Neurosci* **23**, 166-174
67. **Droge W.** (2002). Free radicals in the physiological control of cell function. *Physiol Rev* **82**, 47-95
68. **Chen Q., Vazquez E.J., Moghaddas S., Hoppel C.L., Lesnefsky E.J.** (2003). Production of reactive oxygen species by mitochondria: central role of complex III. *J Biol Chem* **278**, 36027-36031
69. **Turrens J.F.** (2003). Mitochondrial formation of reactive oxygen species. *J Physiol* **552**, 335-344
70. **Turrens J.F., Alexandre A., Lehninger A.L.** (1985). Ubisemiquinone is the electron donor for superoxide formation by complex III of heart mitochondria. *Arch Biochem Biophys* **237**, 408-414
71. **Kushnareva Y., Murphy A.N., Andreyev A.** (2002). Complex I-mediated reactive oxygen species generation: modulation by cytochrome c and (NAD(P)<sup>+</sup> oxidation-reduction state. *Biochem J* **368**, 545-553
72. **Aon M.A., Cortassa S., O'Rourke B.** (2004). Percolation and criticality in a mitochondrial network. *Proc Natl Acad Sci USA* **101**, 4447-4452
73. **Aon M.A., Cortassa S., Marban E., O'Rourke B.** (2003). Synchronized whole cell oscillation in mitochondrial metabolism triggered by a local release of reactive oxygen species in cardiac myocytes. *J Biol Chem* **278**, 44735-44744
74. **Camello-Almarez M.C., Pozo M.J., Murphy M.P., Camello P.J.** (2006). Mitochondrial production of oxidants is necessary for physiological calcium oscillations. *J Cell Physiol* **206**, 487-494
75. **Dawson T.L., Gores G.J., Nieminen A.L., Herman B., Lemasters J.J.** (1993). Mitochondria as a source of reactive oxygen species during reductive stress in rat hepatocytes. *Am J Physiol Cell Physiol* **264**, C961-C967
76. **Gonzales A., Granados M.P., Salido G.M., Pariente J.A.** (2003). Changes in mitochondrial activity evoked by cholecystokinin in isolated mouse pancreatic acinar cells. *Cell Signal* **15**, 1039-1048
77. **Hajnoczky G., Robb-Gaspers L.D., Seitz M.B., Thomas A.P.** (1995). Decoding of cytosolic calcium oscillations in the mitochondria. *Cell* **82**, 415-424
78. **Spat A., Pitter J.G.** (2004). The effect of cytoplasmic Ca<sup>2+</sup> signal on the redox state of mitochondrial pyridine nucleotides. *Mol Cell Endocrinol* **215**, 115-118



- 
79. **Voronina S., Sukhomlin T., Johnson P.R., Erdemli G., Peterson O.H., Tepikin A.** (2002). Correlation of NADH and  $Ca^{2+}$  signals in mouse pancreatic acinar cells. *J Physiol* **539**, 41-52
80. **Cortassa A., Aon M.A., Winslow R.L., O'Rourke B.** (2004). A mitochondrial oscillator dependent on reactive oxygen species. *Biophys J* **87**, 2060-2073
81. **Hsieh T.J., Zhang S.L., Filep J.G., Tang S.S., Ingelfinger J.R., Chan J.S.** (2002). High glucose stimulates angiotensinogen gene expression via reactive oxygen species generation in rat kidney proximal tubular cells. *Endocrinology* **143**, 2975-2985
82. **Izeradjene K., Douglas L., Tillman D.M., Delaney A.B., Houghton J.A.** (2005). Reactive oxygen species regulate caspase activation in tumor necrosis factor-related apoptosis-inducing ligand-resistant human colon carcinoma cell lines. *Cancer Res* **65**, 7436-7445
83. **Kimura S., Zhang G.X., Nishiyama A., Shokoji T., Yao L., Fan Y.Y., Rahman M., Abe Y.** (2005). Mitochondria-derived reactive oxygen species and vascular MAP kinases: comparison of angiotensin II and diazoxide. *Hypertension* **45**, 438-444
84. **Kimura S., Zhang G.X., Nishiyama A., Shokoji T., Yao L., Fan Y.Y., Rahman M., Suzuki T., Maeta H., Abe Y.** (2005). Role of NAD(P)H oxidase- and mitochondria-derived reactive oxygen species in cardioprotection of ischemic reperfusion injury by angiotensin II. *Hypertension* **45**, 860-866
85. **Pueyo M.E., Gonzalez W., Nicoletti A., Savoie F., Arnal J.F., Michel J.B.** (2000). Angiotensin II stimulates endothelial vascular cell adhesion molecule-1 via nuclear factor-kB activation induced by intracellular oxidative stress. *Arterioscler Thromb Vasc Biol* **20**, 645-651
86. **Waypa G.B., Marks J.D., Mack M.M., Boriboun C., Mungai P.T., Schumacker P.T.** (2002). Mitochondrial reactive oxygen species trigger calcium increases during hypoxia in pulmonary arterial myocytes. *Circ Res* **91**, 719-726
87. **Waypa G.B., Schumacker P.T.** (2005). Hypoxic pulmonary vasoconstriction: redox events in oxygen sensing. *J Appl Physiol* **98**, 404-414
88. **Xi Q., Cheranov S.Y., Jagger J.H.** (2005). Mitochondria-derived reactive oxygen species dilate cerebral arteries by activating  $Ca^{2+}$  sparks. *Circ Res* **97**, 354-362
89. **Brown G.C., Cooper C.E.** (1994). Nanomolar concentrations of NO reversibly inhibit synaptosomal respiration by competing with oxygen at cytochrome oxidase. *FEBS Lett* **356**, 295-298
90. **Cleeter M.W.J., Cooper J.M., Darley-Usmar V.M., Moncada S., Schapira A.H.V.** (1994). Reversible inhibition of cytochrome oxidase, the terminal enzyme of the mitochondrial respiratory chain by NO. *FEBS Lett* **345**, 50-54

- 
- 91. Sarti P., Forte E., Mastronicola D., Barone M.C., Brunori M.** (2000). Nitric oxide and cytochrome oxidase: mechanisms of inhibition and NO degradation. *Biochem Biophys Res Commun* **274**, 183–187
- 92. Cooper C.E.** (2002). Nitric oxide and cytochrome oxidase: substrate, inhibitor or effector? *Trends Biochem Sci* **27**, 33–39
- 93. Mason M.G., Nicholls P., Wilson M.T., Cooper C.E.** (2006). Nitric oxide inhibition of respiration involves both competitive (heme) and noncompetitive (copper) binding to cytochrome c oxidase. *Proc Natl Acad Sci U S A* **103**, 708–713
- 94. Juhaszova M., Zorov D.B., Kim S.H., Pepe S., Fu Q., Fishbein K.W.** (2004). Glycogen synthase kinase-3 $\beta$  mediates convergence of protection signaling to inhibit the mitochondrial permeability transition pore. *J Clin Invest* **113**, 1535–1549
- 95. Shiva S., Brookes P.S., Patel R.P., Anderson P.G., Darley-Usmar V.M.** (2001). Nitric oxide partitioning into mitochondrial membranes and the control of respiration at cytochrome c oxidase. *Proc Natl Acad Sci U S A* **98**, 7212–7217
- 96. Poderoso J.J., Peralta J.G., Lisdero C.L., Carreras M.C., Radisic M., Schopfer F.** (1998). NO regulates oxygen uptake and hydrogen peroxide release by the isolated beating rat heart. *Am J Physiol* **274**, C112–C119
- 97. Poderoso J.J., Carreras M.C., Lisdero C., Riobo N., Schopfer F., Boveris A.** (1996). NO inhibits electron transfer and increases superoxide radical production in rat heart mitochondria and submitochondrial particles. *Arch Biochem Biophys* **328**, 85–92
- 98. Borutaite V., Brown G.C.** (2003). Nitric oxide induces apoptosis via hydrogen peroxide, but necrosis via energy and thiol depletion. *Free Radic Biol Med* **35**, 1457–1468
- 99. Poderoso J.J., Carreras M.C., Schopfer F., Lisdero C.L., Riobo A.N., Giulivi C.** (1999). The reaction of nitric oxide with ubiquinol: kinetic properties and biological significance. *Free Radic Biol Med* **26**, 925–935
- 100. Dahm C.C., Moore K., Murphy M.P.** (2006). Persistent S-nitrosation of complex I and other mitochondrial membrane proteins by S-nitrosothiols but not nitric oxide or peroxynitrite: implications for the interaction of nitric oxide with mitochondria. *J Biol Chem* **281**, 10056–10065
- 101. Borutaite V., Brown G.C.** (2006). S-nitrosothiol inhibition of mitochondrial complex I causes a reversible increase in mitochondrial hydrogen peroxide production. *Biochim Biophys Acta* **1757**, 562–566
- 102. Riobo N.A., Clementi E., Melani M., Boveris A., Cadenas E., Moncada S.** (2001). Nitric oxide inhibits mitochondrial NADH: ubiquinone reductase activity through peroxynitrite formation. *Biochem J* **359**, 139–145

- 
103. **Ignarro L.J.** (2000). Nitric oxide: biology and pathobiology. *San Diego: Academic Press*
104. **Packer M.A., Murphy M.P.** (1994). Peroxynitrite causes calcium efflux from mitochondria which is prevented by cyclosporin A. *FEBS Lett* **345**, 237–240
105. **Borutaite V., Morkuniene R., Brown G.C.** (1999). Release of cytochrome c from heart mitochondria is induced by high calcium and peroxynitrite and is responsible for calcium-induced inhibition of substrate oxidation. *Biochim Biophys Acta* **1453**, 41–48
106. **Vieira H.L., Belzacq A.S., Haouzi D., Bernassola F., Cohen I., Jacotot E.** (2001). The adenine nucleotide translocator: a target of nitric oxide, peroxynitrite, and 4-hydroxynonenal. *Oncogene* **20**, 4305–4316
107. **Balakirev M.Y., Khramtsov V.V., Zimmer G.** (1997). Modulation of the mitochondrial permeability transition by nitric oxide. *Eur J Biochem* **246**, 710–718
108. **Brookes P.S., Salinas E.P., Darley-Usmar K., Eiserich J.P., Freeman B.A., Darley-Usmar V.M.** (2000). Concentration-dependent effects of nitric oxide on mitochondrial permeability transition and cytochrome c release. *J Biol Chem* **275**, 20474–20479
109. **Costa A.D.T., Garlid K.D., West I.C., Lincoln T.M., Downey J.M., Cohen M.V.** (2005). Protein kinase G transmits the cardioprotective signal from cytosol to mitochondria. *Circ Res* **97**, 329–336
110. **Takuma K., Phuagphong P., Lee E., Mori K., Baba A., Matsuda T.** (2001). Anti-apoptotic effect of cGMP in cultured astrocytes: inhibition by cGMP-dependent protein kinase of mitochondrial permeable transition pore. *J Biol Chem* **276**, 48093–48099
111. **Davidson S.M., Duchon M.R.** (2006). Effects of NO on mitochondrial function in cardiomyocytes: pathophysiological relevance. *Cardiovasc Res* **71**, 10–21
112. **Ago T., Nuno H., Ito T., Sumimoto H.** (1999). Mechanism for phosphorylation-induced activation of the phagocyte NADPH oxidase protein p47(phox). Triple replacement of serines 303, 304, and 328 with aspartates disrupts the sh3 domain-mediated intramolecular interaction in p47(phox), thereby activating the oxidase. *J. Biol. Chem.* **274**, 33644–33653
113. **Batot G., Martel C., Capdeville N., Wientjes F., Morel F.** (1995). Characterization of neutrophil NADPH oxidase activity reconstituted in a cell-free assay using specific monoclonal antibodies raised against cytochrome *b*<sub>558</sub>. *Eur. J. Biochem.* **234**, 208–215
114. **Segal A.W., Garcia R., Goldstone A.H., Cross A.R., Jones O.T.G.** (1981). Cytochrome *b*-245 of neutrophils is also present in human monocytes, macrophages and eosinophils. *Biochem. J.* **196**, 363–367

- 
115. **Arbiser J.L., Petros J., Klafter R., Govindajaran B., McLaughlin E.R., L.F. Brown L.F., Cohen C., Moses M., Kilroy S., Arnold R.S., Lambeth J.D.** (2002). Reactive oxygen generated by Nox1 triggers the angiogenic switch. *Proc. Natl. Acad. Sci. USA* **99**, 715–720
116. **Cheng G., Cao Z., Xu X., van Meir E.G., Lambeth J.D.** (2001). Homologs of gp91phox: cloning and tissue expression of Nox 3, Nox4, and Nox5. *Gene* **269**, 131–140
117. **Coffman R.L., Seymour B.W.P., Hudak S., Jackson J., Rennick D.** (1989). Antibody to interleukin-5 inhibits helminth-induced eosinophilia in mice. *Science* **245**, 308–310
118. **Fridovich I.** (1975). Superoxide dismutases. *Annu. Rev. Biochem.* **44**, 147–159
119. **Babior B.M.** (1999). NADPH oxidase: an update. *Blood* **93**, 1464–1476
120. **Weiss S.J., Test S.T., Eckmann C.M., Roos D., Regiani S.** (1986). Brominating oxidants generated by human eosinophils. *Science* **234**, 200–202
121. **Arlandson M., Decker T., Roongta V.A., Bonilla L., Mayo K.H., MacPherson J.C., Hazen S.L., Slungaard A.** (2001). Eosinophil peroxidase oxidation of thiocyanate. Characterization of major reaction products and a potential sulfhydryl-targeted cytotoxicity system. *J. Biol. Chem.* **276**, 215–224
122. **Steinbeck M.J., Khan A.U., Karnovsky M.J.** (1992). Intracellular singlet oxygen generation by phagocytosing neutrophils in response to particles coated with a chemical trap. *J. Biol. Chem.* **267**, 13425–13433
123. **Steinbeck M.J., Khan A.U., Karnovsky M.J.** (1993). Extracellular production of singlet oxygen by stimulated macrophages quantified using 9,10-diphenylanthracene and perylene in a polystyrene film. *J. Biol. Chem.* **268**, 15649–15654
124. **Babior B.M., Takeuchi C., Ruedi J.M., Gutierrez A., Wentworth P.** (2003). Investigating antibody-catalyzed ozone generation by human neutrophils. *Proc. Natl. Acad. Sci. USA* **100**, 3031–3034
125. **Lerner R.A., Eschenmoser A.** (2003). Ozone in biology. *Proc. Natl. Acad. Sci. USA* **100**, 3013–3015
126. **Wentworth P., Jr. McDunn J.E., Wentworth A.D., Takeuchi C., Nieva J., Jones T., Bautista C., Ruedi J.M., Gutierrez A., Janda K.D.** (2002). Evidence for antibody-catalyzed ozone formation in bacterial killing and inflammation. *Science* **298**, 2195–2199
127. **Wink D.A., Nims R.W., Saavedra J.E., Utermahlen W.E., Ford P.C.** (1994). The Fenton oxidation mechanism: reactivities of biologically relevant substrates with two oxidizing intermediates differ from those predicted for the hydroxyl radical. *Proc. Natl. Acad. Sci. USA* **91**, 6604–6608

- 
128. Gardner P.R., Fridovich I. (1991). Superoxide sensitivity of the *Escherichia coli* 6-phosphogluconate dehydratase. *J. Biol. Chem.* **266**, 1478–1483
129. Gardner P.R., Fridovich I. (1991). Superoxide sensitivity of the *Escherichia coli* aconitase. *J. Biol. Chem.* **266**, 19328–19333
130. Hausladen A., Fridovich I. (1994). Superoxide and peroxyxynitrite inactivate aconitases, but nitric oxide does not. *J. Biol. Chem.* **269**, 29405–29408
131. Schalk I., Zeng K., Wu S.K., Stura E.A., Matteson J., Huang M., Tandon A., Wilson I.A., Balch W.E. (1996). Structure and mutational analysis of Rab GDP-dissociation inhibitor. *Nature* **381**, 42–48
132. Han C.H., Lee M.H. (2000). Expression and characterization of the flavoprotein domain of gp91<sup>PHOX</sup>. *J Vet Sci* **1**, 19-26
133. Cross A.R., Rae J., Curnutte J.T. (1995). Cytochrome b<sub>245</sub> of the neutrophil superoxide-generating system contains two nonidentical hemes. Potentiometric studies of a mutant form of gp91phox. *J. Biol. Chem.* **270**, 17075–17077
134. Fujii H., Finnegan M.G., Miki T., Crouse B.R., Kakinuma K., Johnson M.K. (1995). Spectroscopic identification of the heme axial ligation of Cytochrome b<sub>558</sub> in the NADPH oxidase of porcine neutrophils. *FEBS Lett.* **377**, 345–348
135. Fujii H., Finnegan M.G., Johnson M.K. (1999). The active form of the ferric heme in neutrophil Cytochrome b(558) is low-spin in the reconstituted cell-free system in the presence of amphophil. *J. Biochem. (Tokyo)* **126**, 708–714
136. Smith R.M., Curnutte J.T., Mayo L.A., Babior B.M. (1989). Use of an affinity label to probe the function of the NADPH binding component of the respiratory burst oxidase of human neutrophils. *J. Biol. Chem.* **264**, 12243–12248
137. Smith R.M., Curnutte J.T., Babior B.M. (1989). Affinity labeling of the cytosolic and membrane components of respiratory burst oxidase by the 2',3'-dialdehyde derivative of NADPH. Evidence for a cytosolic location of the nucleotide-binding site in the resting cell. *J. Biol. Chem.* **264**, 1958–1962
138. Smith R.M., Connor J.A., Chen L.M., Babior B.M. (1996). The cytosolic subunit p67phox contains an NADPH-binding site that participates in catalysis by the leukocyte NADPH oxidase. *J. Clin. Invest.* **98**, 977–983
139. Dang P.M.C., Babior B.M., Smith R.M. (1999). NADPH dehydrogenase activity of p67<sup>PHOX</sup>, a cytosolic subunit of the leukocyte NADPH oxidase. *Biochemistry* **38**, 5746–5753
140. Freeman J.L., Lambeth J.D. (1996). NADPH oxidase activity is independent of p47phox *in vitro*. *J. Biol. Chem.* **271**, 22578–22582
141. Pagano P.J., Tornheim K., Cohen R.A. (1993). Superoxide anion production by rabbit thoracic aorta: effect of endothelium-derived nitric oxide. *Am J Physiol* **265**, H707-H712

- 
142. **Griendling K.K., Minieri C.A., Ollerenshaw J.D., Alexander R.W.** (1994). Angiotensin II stimulates NADH and NADPH oxidase activity in cultured vascular smooth muscle cells. *Circ Res* **74**, 1141-1148
143. **Pagano P.J., Clark J.K., Cifuentes-Pagano M.E., Clark S.M., Callis G.M., Quinn M.T.** (1997). Localization of a constitutively active, phagocyte-like NADPH oxidase in rabbit aortic adventitia: enhancement by angiotensin II. *Proc Natl Acad Sci USA* **94**, 14438-14488
144. **Rajagopalan S., Kurz S., Münzel T., Tarpey M., Freeman B.A., Griendling K.K., Harrison D.G.** (1996). Angiotensin II mediated hypertension in the rat increases vascular superoxide production via membrane NADH/NADPH oxidase activation: contribution to alterations of vasomotor tone. *J Clin Invest* **97**, 1916-1923
145. **Meier B.** (1996). Regulation of the superoxide releasing system in human fibroblasts. *Adv Exp Med Biol* **387**, 113-116
146. **De Keulenaer G.W., Alexander R.W., Ushio-Fukai M., Ishizaka N., Griendling K.K.** (1998). Tumor necrosis factor- $\alpha$  activates a p22phox-based NADH oxidase in vascular smooth muscle cells. *Biochem J* **329**, 653-657
147. **Fukui T., Ishizaka N., Rajagopalan S., Laursen J.B., Caspers Q., Taylor W.R., Harrison D.G., de Leon H., Wilcox J.N., Griendling K.K.** (1997). p22phox mRNA expression and NADPH oxidase activity are increased in aortas from hypertensive rats. *Circ Res* **80**, 45-51
148. **Pagano P.J., Chanock S.J., Siwik D.A., Colucci W.S., Clark J.K.** (1998). Angiotensin II induces p67phox mRNA expression and NADPH oxidase superoxide generation in rabbit aortic adventitial fibroblasts. *Hypertension* **32**, 331-337
149. **Schardinger F.** (1902). Über das Verhalten der Kuhmilch gegen Methylenblau und seine Verwendung zur Unterscheidung von ungekochter und gekochter Milch. *Untersuch Nahrungs Genussmittel* **5**, 1113–1121
150. **Kisker C., Schindelin H., Rees D.C.** (1997). Molybdenum cofactor-containing enzymes: structure and mechanism. *Annu Rev Biochem* **66**, 233–267
151. **Stirpe F., Della Corte E.** (1969). The regulation of rat liver xanthine oxidase – conversion in vitro of the enzyme activity from dehydrogenase (type D) to oxidase (type O). *J Biol Chem* **244**, 3855–3863
152. **Waud W.R., Rajagopalan K.V.** (1976b). The mechanism of conversion of rat liver xanthine dehydrogenase from an NAD<sup>+</sup>-dependent form (Type D) to an O<sub>2</sub>-dependent form (Type O). *Arch Biochem Biophys* **172**, 365–379
153. **Hille R., Nishino T.** (1995). Xanthine oxidase and xanthine dehydrogenase. *FASEB J* **9**, 995–1003

- 
154. Xu P., Huecksteadt T., Hoidal J.R. (1996). Molecular cloning and characterization of the human xanthine dehydrogenase gene (XDH). *Genomics* **34**, 173–180
155. Ichida K., Amaya Y., Noda K., Minoshima S., Hosoya T., Sakai O., Shimizu N., Nishino T. (1993). Cloning of the cDNA encoding human xanthine dehydrogenase (oxidase): structural analysis of the protein and chromosomal location of the gene. *Gene* **133**, 279–284
156. Xu P., Zhu X.L., Huecksteadt T., Brothman A.R., Hoidal J.R. (1994). Assignment of human xanthine dehydrogenase gene to chromosome 2p22. *Genomics* **23**, 289–291
157. Ichida K., Amaya Y., Noda K., Minoshima S., Hosoya T., Sakai O., Shimizu N., Nishino T. (1993). Cloning of the cDNA encoding human xanthine dehydrogenase (oxidase): structural analysis of the protein and chromosomal location of the gene. *Gene* **133**, 279–284
158. Xu P., Huecksteadt T., Harrison R., Hoidal J.R. (1995). Molecular cloning, tissue expression of human xanthine dehydrogenase. *Biochem Biophys Res Commun* **215**, 429
159. Terao M., Kurosaki M., Demontis S., Zanotta S., Garattini E. (1998). Isolation and characterization of the human aldehyde oxidase gene: conservation of intron/exon boundaries with the xanthine oxidoreductase gene indicates a common origin. *Biochem J* **332**, 383–393
160. Terao M., Kurosaki M., Zanotta S., Garattini E. (1997). The xanthine oxidoreductase gene: structure and regulation. *Biochem Soc Trans* **25**, 791–796
161. Turner N.A., Doyle W.A., Ventom A.M., Bray R.C. (1995). Properties of rabbit liver aldehyde oxidase and the relationship of the enzyme to xanthine oxidase and dehydrogenase. *Eur J Biochem* **232**, 646–657
162. Krenitsky T.A., Spector T., Hall W.W. (1986). Xanthine oxidase from human liver: purification and characterization. *Arch Biochem Biophys* **247**, 108–119
163. Enroth C., Eger B.T., Okamoto K., Nishino T., Nishino T., Pai E.F. (2000). Crystal structures of bovine milk xanthine dehydrogenase and xanthine oxidase: structure-based mechanism of conversion. *Proc Natl Acad Sci U S A* **97**, 10723–10728
164. Romão M.J., Archer M., Moura I., Moura J.J.G., LeGall J., Engh R., Schneider M., Hof P., Huber R. (1995). Crystal structure of the xanthine oxidase-related aldehyde oxidoreductase from *D. gigas*. *Science* **270**, 1170–1176
165. Huber R., Hof P., Duarte R.O., Moura J.J.G., Moura I., Liu M., LeGall J., Hille R., Archer M., Romao M. (1996). A structure-based catalytic mechanism for the xanthine oxidase family of molybdenum enzymes. *Proc Natl Acad Sci U S A* **93**, 8846–8851

- 
166. Hancock J.T., Salisbury V., Ovejero-Boglione M.C., Cherry R., Hoare C., Eisenthal R., Harrison R. (2002). Antimicrobial properties of milk: dependence on presence of xanthine oxidase and nitrite. *Antimicrob Agents Chemother* **46**, 3308–3310
167. Stevens C.R., Millar T.M., Clinch J.G., Kanczler J., Bodamyali T., Blake D.R. (2000). Antibacterial properties of xanthine oxidase in human milk. *Lancet* **356**, 829–830
168. Segal B.H., Sakamoto N., Patel M., Maemura K., Klein A.S., Holland S.M., Bulkley G.B. (2000). Xanthine oxidase contributes to host defense against *Burkholderia cepacia* in the p47<sup>phox</sup><sup>-/-</sup> mouse model of chronic granulomatous disease. *Infect Immun* **68**, 2374–2378
169. Harrison R. (2002). Structure and function of xanthine oxidoreductase: where are we now? *Free Radic Biol Med* **33**, 774–797
170. Becker B.F. (1993). Towards the physiological function of uric acid. *Free Radic Biol Med* **14**, 615–631
171. Usuda N., Reddy M.K., Hashimoto T., Rao M.S., Reddy J.K. (1988). Tissue specificity and species differences in the distribution of urate oxidase in peroxisomes. *Laboratory Invest* **58**, 100–111
172. Watanabe S., Kang D., Feng L., Nakagawa T., Kanellis J., Lan H., Mazzali M., Johnson R.J. (2002). Uric acid, hominoid evolution, and the pathogenesis of salt-sensitivity. *Hypertension* **40**, 355–360
173. Ames B.N., Cathcart R., Schwiers E., Hochstein P. (1981). Uric acid provides antioxidant defense in humans against oxidant- and radical-caused aging and cancer: a hypothesis. *Proc Natl Acad Sci* **78**, 6858–6862
174. Weiss S.J. (1986). Oxygen, ischemia, and inflammation. *Acta Physiol Scand* **548**, 9–37
175. Kehrer J.P. (2000). The Haber-Weiss reaction and mechanisms of toxicity. *Toxicology* **149**, 43–50
176. Granger D.N., Rutili G., McCord J.M. (1981). Role of superoxide in feline intestinal ischemia. *Gastroenterology* **81**, 22–29
177. McCord J.M. (1985). Oxygen-derived free radicals in postischemic tissue injury. *N Engl J Med* **312**, 159–163
178. Granger D.N., Hollwarth M.E., Parks D.A. (1986). Ischemia-reperfusion injury: role of oxygen-derived free radicals. *Acta Physiol Scand* **548**(Suppl), 47–63
179. Loyer X., Gomez A.M., Milliez P., Fernandez-Velasco M., Vangheluwe P., Heymes C. (2008). Cardiomyocyte overexpression of neuronal nitric oxide synthase delays transition toward heart failure in response to pressure overload. *Circulation* **117**, 3187–3198



- 
- 180. Dawson D., Lygate C.A., Zhang M.H., Hulbert K., Neubauer S., Casadei B.** (2005). nNOS gene deletion exacerbates pathological remodeling and functional deterioration after myocardial infarction. *Circulation* **112**, 3729-3737
- 181. Saraiva R.M., Minhas K.M., Raju S.V., Barouch L.A., Pitz E., Hare J.M.** (2005). Deficiency of neuronal nitric oxide synthase increases mortality and cardiac remodeling after myocardial infarction: role of nitroso-redox equilibrium. *Circulation* **112**, 3415-3422
- 182. Xu K.Y., Huso D.L., Dawson T.M., Bredt D.S., Becker L.C.** (1999). Nitric oxide synthase in cardiac sarcoplasmic reticulum. *Proc Natl Acad Sci USA* **96**, 657-662
- 183. Sears C.E., Bryant S.M., Ashley E.A., Lygate C.A., Rakovic S., Casadei B.** (2003). Cardiac nitric neuronal nitric oxide synthase isoform regulates myocardial contraction and calcium handling. *Circ Res* **92**, e52-59
- 184. Zhang Y.H., Zhang M.H., Sears C.E., Emanuel K., Redwood C., Casadei B.** (2008). Reduced phospholamban phosphorylation is associated with impaired relaxation in left ventricular myocytes from neuronal NO-synthase deficient mice. *Circ Res* **102**, 242-249
- 185. Kahn S.A., Lee K., Minhas K.M., Gonzales D.R., Raju S.V., Hare J.M.** (2004). Neuronal nitric oxide synthase negatively regulates xanthine oxidoreductase inhibition of cardiac excitation-contraction coupling. *Proc Natl Acad Sci USA* **101**, 15944-15948
- 186. Kinugawa S., Huang H., Wang Z., Kaminski P.M., Wolin M.S., Hintze T.H.** (2005). A defect of neuronal nitric oxide synthase increases xanthine oxidase-derived superoxide anion and attenuates the control of myocardial oxygen consumption by nitric oxide derived from endothelial nitric oxide synthase. *Circ Res* **96**, 355-362
- 187. Giulivi C., Poderoso J.J., Boveris A.** (1998). Production of nitric oxide by mitochondria. *J Biol Chem* **273**, 11038-11043
- 188. Kanai A.J., Pearce L.L., Clemens P.R., Birder L.A., VanBibber M.M., Peterson J.** (2001). Identification of a neuronal nitric oxide synthase in isolated cardiac mitochondria using electrochemical detection. *Proc Natl Acad Sci USA* **98**, 14126-14131
- 189. Brown G.C., Borutaite V.** (2007). Nitric oxide and mitochondrial respiration in the heart. *Cardiovasc Res* **75**, 283-290
- 190. Kahn S.A., Lee K., Minhas K.M., Gonzales D.R., Raju S.V., Hare J.M.** (2004). Neuronal nitric oxide synthase negatively regulates xanthine oxidoreductase inhibition of cardiac excitation-contraction coupling. *Proc Natl Acad Sci USA* **101**, 15944-15948

- 
191. Sun J., Morgan M., Shen R.F., Steenbergen C., Murphy E. (2007). Preconditioning results in S-nitrosylation of proteins involved in regulation of mitochondrial energetic and calcium transport. *Circ Res* **101**, 1155-1163
192. Frantz S., Calvillo L., Tillmanns J., Elbing I., Dienesch C., Bischoff H., Ertl G., Bauersachs J. (2005). Repetitive postprandial hyperglycemia increases cardiac ischemia/reperfusion injury: prevention by the alpha-glucosidase inhibitor acarbose. *Faseb J.* **19**, 591-593
193. Han H., Neubauer S., Braeker B., Ertl G. (1994). Endothelin-1 Contributes to Ischemia/Reperfusion Injury in Isolated Rat Heart-Attenuation of Ischemic Injury by the Endothelin-1 Antagonists BQ123 and BQ610. *J Mol Cell Cardiol* **27**, 761-766
194. Hofmann U, Domeier E, Frantz S, Laser M, Weckler B, Bonz AW. (2003). Increased myocardial oxygen consumption by TNF-alpha is mediated by sphingosine signalling pathway. *Am J Physiol Heart Circ Physiol* **284**, H2100-2105
195. Damy T., Ratajczak P., Robidel E., Bendall J.K., Oliviero P., Boczkowski J., Ebrahimian T., Marotte F., Samuel J.L., Heymes C. (2003). Upregulation of cardiac nitric oxide synthase 1-derived nitric oxide after myocardial infarction in senescent rats. *FASEB J* **17**, 1934-1936
196. Piech A., Dessy C., Havaux X., Feron O., Balligand J.L. (2003). Differential regulation of nitric oxide synthases and their allosteric regulators in heart and vessels of hypertensive rats. *Cardiovasc Res* **57**, 456-467
197. Takimoto Y., Aoyama T., Keyamura R., Shinoda E., Hatori R., Yui Y., Sasayama S. (2000). Differential expression of three types of nitric oxide synthase in both infarcted and non-infarcted left ventricles after myocardial infarction in the rat. *Int J Cardiol* **76**, 135-145
198. Kojda G., Harrison D. (1999). Interactions between NO and reactive oxygen species: pathophysiological importance in atherosclerosis, hypertension, diabetes and heart failure. *Cardiovasc Res* **43**, 562-571
199. Song X., Vaage J., Valen G. (2001). The role of neuronal nitric oxide synthase in ischemia-reperfusion injury of the isolated mouse heart. *Acta Physiol Scand* **172**, 291-295
200. Jones S.P., Girod W.G., Huang P.L., Lefler D.J. (2000). Myocardial reperfusion injury in neuronal nitric oxide synthase deficient mice. *Coron Artery Dis* **11**, 593-597
201. Takimoto Y., Aoyama T., Tanaka K., Keyamura R., Yui Y., Sasayama S. (2002). Augmented expression of neuronal nitric oxide synthase in the atria parasympathetically decreases heart rate during acute myocardial infarction in rats. *Circulation* **105**, 490-496

- 
202. Brunner F., Maier R., Andrew P., Wolkart G., Zechner R., Mayer B. (2003). Attenuation of myocardial ischemia/reperfusion injury in mice with myocyte-specific over-expression of endothelial nitric oxide synthase. *Cardiovasc Res* **57**, 55-62
203. Jones S.P., Girod W.G., Palazzo A.J., Granger D.N., Grisham M.B., Jourdain D., Huang P.L., Lefer D.J. (1999). Myocardial ischemia-reperfusion injury exacerbated in absence of endothelial cell nitric oxide synthase. *Am J Physiol* **276**, H1567-H1573
204. Wang P., Zweier J.L. (1996). Measurement of nitric oxide and peroxynitrite in the postischemic heart. Evidence for peroxynitrite-mediated reperfusion injury. *J Biol Chem* **271**, 29223-29230
205. Tambascia R.C., Fonseca P.M., Corat P.D., Moreno Jr H., Saad M.J., Franchini K.G. (2001). Expression and distribution of NOS1 and NOS3 in the myocardium of angiotensin II-infused rats. *Hypertension* **37**, 1423-1428
206. Kobayashi N., Higashi T., Hara K., Shirataki H., Matsuoka H. (1999). Effects of imidapril on NOS expression and myocardial remodelling in failing heart of Dahl salt-sensitive hypertensive rats. *Cardiovasc Res* **44**, 518-526
207. Ashley E.A., Sears C.E., Bryant S.M., Watkins H.C., Casadei B. (2002). Cardiac nitric oxide synthase 1 regulates basal and beta-adrenergic contractility in murine ventricular myocytes. *Circulation* **105**, 120-125
208. Sears C.E., Zhang Y. H., Ashley E.A., Lygate C.A., Kim Y.M., Neubauer S., Casadei B. (2003). Myocardial NOS1 controls the lusitropic response to beta-adrenergic stimulation *in vivo* and *in vitro*. *Circulation* **108**(Suppl), 1173
209. Mohan R.M., Heaton D.A., Danson E.J., Krishnan S.P., Cai S., Channon K.M., Paterson D.J. (2002). Neuronal nitric oxide synthase gene transfer promotes cardiac vagal gain of function. *Circ Res* **91**, 1089-1091
210. Giulivi C. (2003). Characterization and function of mitochondrial nitric oxide synthase. *Free Radical Biology & Medicine* **34**, 397-408
211. Sarkela T. M., Berthiaume J., Elfering S., Gybina A.A., Giulivi C. (2001). The modulation of oxygen radical production by nitric oxide in mitochondria. *J Biol Chem* **276**, 6945-6949
212. Ghafourifar P., Schenk U., Klein S.D., Richter C. (1999). Mitochondrial nitric-oxide synthase stimulation causes cytochrome c release from isolated mitochondria. Evidence for intramitochondrial peroxynitrite formation. *J Biol Chem* **274**, 31185-31188
213. Kadenbach B. (1986). Regulation of respiration and ATP synthesis in higher organism: hypothesis. *J Bioenerg Biomembr* **18**, 39-54

- 
214. **Thomas D.D., Liu X., Kantrow S.P., Lancaster J. Jr.** (2001). The biological lifetime of nitric oxide: implications of the perivascular dynamics of NO and O<sub>2</sub>. *Proc Natl Acad Sci USA* **98**, 355-360
215. **Larson S.K., Dwyer D., Lo H.H., Ghafourifar P.** (2006). Mitochondrial cytochrome c reacts with nitric oxide via S-nitrosation. *Biochem Biophys Res Commun* **342**, 991-995
216. **Rodriguez-Sinovas A., Boengler K., Cabestrero A., Gres P., Morente M., Ruiz-Meana M., Konietzka I., Miro E., Totzeck A., Heusch G., Schulz R., Garcia-Dorado D.** (2006). Translocation of connexin 43 to the inner mitochondrial membrane of cardiomyocytes through the heat shock protein 90-dependent TOM pathway and its importance for cardioprotection. *Circ Res* **99**, 93-101
217. **Damy T., Ratajczak P., Shah A.M., Camors E., Marty I., Hasenfuss G., Marotte F., Samuel J.L., Heymes C.** (2004). Increased neuronal nitric oxide synthase-derived NO production in the failing human heart. *Lancet* **363**, 1365-1367
218. **Lundberg J.O., Weitzberg E., Gladwin M.T.** (2008). The nitrate-nitrite-nitric oxide pathway in physiology and therapeutics. *Nat Rev Drug Discov* **7**, 156-167
219. **Shiva S., Huang Z., Grubina R., Sun J., Ringwood L.A., MacArthur P.H., Xu X., Murphy E., Darley-Usmar V.M., Gladwin M.T.** (2007). Deoxymyoglobin is a nitrite reductase that generates nitric oxide and regulates mitochondrial respiration. *Circ Res* **100**, 654-661
220. **West M.B., Rokosh G., Obal D., Velayutham M., Xuan Y.T., Hill B.G., Keith R.J., Schrader J., Guo Y., Conklin D.J., Prabhu S.D., Zweier J.L., Bolli R., Bhatnagar A.** (2008). Cardiac Myocyte-Specific Expression of Inducible Nitric Oxide Synthase Protects Against Ischemia/Reperfusion Injury by Preventing Mitochondrial Permeability Transition. *Circulation* **118**, 1915-9
221. **Elrod J.W., Greer J.J., Bryan N.S., Langston W., Szot J.F., Gebregzlabher H., Janssen S., Feelisch M., Lefer D.J.** (2006). Cardiomyocyte-specific overexpression of NO synthase-3 protects against myocardial ischemia-reperfusion injury. *Arterioscler Thromb Vasc Biol* **26**, 1517-1523
222. **Jones S.P., Greer J.J., Kakkar A.K., Ware P.D., Turnage R.H., Hicks M., van Haperen R., de Crom R., Kawashima S., Yokohama M., Lefer D.J.** (2004). Endothelial nitric oxide synthase overexpression attenuates myocardial reperfusion injury. *Am J Physiol Heart Circ Physiol* **286**, H276-282
223. **Massion P.B., Dessy C., Desjardin F., Pelat M., Havaux X., Belge C., Moulin P., Guiot Y., Feron O., Janssen S., Balligand J.L.** (2004). Cardiomyocyte-restricted overexpression of endothelial nitric oxide synthase (NOS3) attenuates beta-adrenergic stimulation and reinforces vagal inhibition of cardiac contraction. *Circulation* **110**, 2666-2672

- 
- 224. Griendling K.K., Sorescu D., Ushio-Fukai M.** (2000). NAD(P)H oxidase. Role in cardiovascular biology and disease. *Circ Res* **86**, 494-501
- 225. Rajagoplan S., Kurz S., Munzel T.** (1996). Angiotensin II-mediated hypertension in the rat increases vascular superoxide production via membrane NADH/NADPH oxidase activation. Contribution to alterations of vasomotor tone. *J Clin Invest* **97**, 1916-1923
- 226. Wang H.D., Xu S., Johns D.G.** (2001). Role of NADPH oxidase in the vascular hypertrophic and oxidative stress response to angiotensin II in mice. *Circ Res* **88**, 947-953
- 227. Barry-Lane P.A., Patterson C., van der Merwe M.** (2001). p47phox is required for atherosclerotic lesion progression in ApoE<sup>-/-</sup> mice. *J Clin Invest* **108**, 1513-1522
- 228. Guzik T.J., West N.E.J., Black E.** (2000). Vascular superoxide production by NAD(P)H oxidase: association with endothelial dysfunction and clinical risk factors. *Circ Res* **86**, e85-90
- 229. Li J.M., Gall N.P., Grieve D.G., Chen M.A., Shah A.M.** (2002). Activation of NADPH oxidase during progression of cardiac hypertrophy to failure. *Hypertension* **40**, 477-484
- 230. MacCarthy P.A., Grieve D.G., Li M.J., Dunster C., Kelly F.J., Shah A.M.** (2001). Impaired endothelial regulation of ventricular relaxation in cardiac hypertrophy. Role of reactive oxygen species and NADPH oxidase. *Circulation* **104**, 2967-2974
- 231. Bendall J.K., Cave A.C., Heymes C., Gall N., Shah A.M.** (2002). Pivotal role of gp91<sup>phox</sup>-containing NADPH oxidase in angiotensin II-induced cardiac hypertrophy in mice. *Circulation* **105**, 293-296
- 232. Xiao L., Pimentel D.R., Wang J., Singh K., Colucci W.S., Sawyer D.B.** (2002). Role of reactive oxygen species and NAD(P)H oxidase in  $\alpha_1$ -adrenoceptor signalling in adult rat cardiac myocytes. *Am J Physiol* **282**, C926-934
- 233. Abo A., Pick E., Hall A., Totty N., Teahan C.G., Segal A.W.** (1999). Activation of the NADPH oxidase involves the small GTP-binding protein p21rac1. *Nature* **353**, 668-670
- 234. Diekmann D., Abo A., Johnston C., Segal A.W., Hall A.** (1994). Interaction of Rac with p67phox and regulation of phagocytic NADPH oxidase activity. *Science* **265**, 531-533
- 235. Ridley A.J.** (2001). Rho family proteins: coordinating cell responses. *Trends Cell Biol* **11**, 471-477
- 236. Ridley A.J., Paterson H.F., Johnston C.L., Diekmann D., Hall A.** (1992). The small GTP-binding protein rac regulates growth factor-induced membrane ruffling. *Cell* **70**, 401-410

- 
237. **Coso O.A., Chiariello M., Yu J.C., Teramoto H., Crespo P., Xu N., Miki T., Gutkind J.S.** (1995). The small GTP-binding proteins Rac1 and Cdc42 regulate the activity of the JNK/SAPK signaling pathway. *Cell* **81**, 1137-1146
238. **Minden A., Lin A., Claret F.X., Abo A., Karin M.** (1995). Selective activation of the JNK signaling cascade and c-Jun transcriptional activity by the small GTPases Rac and Cdc42Hs. *Cell* **81**, 1147-1157
239. **Maack C., Kartes T., Kilter H., Schäfers H.J., Nickenig G., Böhm M., Laufs U.** (2003). Oxygen free radical release in human failing myocardium is associated with increased activity of rac1-GTPase and represents a target for statin treatment. *Circulation* **108**, 1567-1574
240. **Seshiah P.N., Weber D.S., Rocic P., Valppu L., Taniyama Y., Griending K.K.** (2002). Molecular cloning of cDNAs encoding the GAP-associated protein p190: implications for a signaling pathway from ras to the nucleus. *Cell* **69**, 539-549
241. **Gregg D., Rauscher F.M., Goldschmidt-Clermont P.J.** (2003). Rac regulates cardiovascular superoxide through diverse molecular interactions: more than a binary GTP switch. *Am J Physiol Cell Physiol* **285**, C723-C734
242. **Murphy E., Steenbergen C.** (2008). Mechanism underlying acute protection from cardiac ischemia-reperfusion injury. *Physiol Rev* **88**, 581-609
243. **Xu K.Y., Kuppusamy S.P., Wang J.Q., Li H., Cui H., Dawson T.M., Huang P.L., Burnett A.L., Kuppusamy P., Becker L.C.** (2003). Nitric oxide protects cardiac sarcolemmal membrane enzyme function and ion active transport against ischemia-induced inactivation. *J Biol Chem* **155**, 201-205
244. **Zhou L., Burnett A.L., Huang P.L., Becker L.C., Kuppusamy P., Kass D.A., Donahue K., Proud D., Sham J.S., Dawson T.M., Xu K.Y.** Lack of nitric oxide synthase depresses ion transporting enzyme function in cardiac muscle. *Biochem Biophys Res Commun* **294**, 1030-1035
245. **Zielonka J, Srinivasan S, Hardy M, Ouari O, Lopez M, Vasquez-Vivar J, Avadhani NG, Kalyanaraman B.** (2008). Cytochrome c-mediated oxidation of hydroethidine and mito-hydroethidine in mitochondria: identification of homo- and heterodimers. *Free Radic Biol Med.* **44**, 835-46.

---

## 7. Abbreviations:

ABAP:	2,2'-azobis(2-amidinopropane)
ACE:	angiotensin-converting enzyme
AO:	aldehyde oxidase
BDM:	2,3-butandion monoxim
BH <sub>4</sub> :	tetrahydrobiopterin
CaM:	calmodulin
cAMP:	cyclic adenosine monophosphate
cGMP:	cyclic guanosine monophosphate
e <sup>-</sup> :	electron
ECC:	excitation-contraction coupling
eNOS:	endothelial nitric oxide synthase
ETC:	electron transport chain
FAD:	flavin adenine dinucleotide
Fe <sub>2</sub> -S <sub>2</sub> :	iron-sulphur center
FMN:	flavin mononucleotide
FTI:	force-time integral
H <sub>2</sub> O <sub>2</sub> :	hydrogen peroxide
HRP:	horseradish peroxidase
<i>I</i> <sub>Ca,L</sub> :	L-type calcium current
ICAM 1:	intracellular adhesion molecule 1
iNOS:	inducible nitric oxide synthase
KHS:	Krebs-Henseleit buffer
LAD:	left coronary artery
LH•:	luminol radical
LH <sub>2</sub> :	luminol
LPS:	lipopolysaccharide
LVDP:	left ventricular developed pressure
MI:	myocardial infarction

---

Mo-Co:	molybdopterin
MTP:	mitochondrial permeability transition pore
MVO <sub>2</sub> :	myocardial oxygen consumption
Myr:	myristoylation site
NADPH:	reduced nicotinamide dinucleotide phosphate
nNOS:	neuronal nitric oxide synthase
NO:	nitric oxide
NO <sub>2</sub> <sup>-</sup> :	nitrite
NOS:	nitric oxide synthase
O <sub>2</sub> <sup>-</sup> :	superoxide anion
OH•:	hydroxyl radical
ONNO <sup>-</sup> :	peroxynitrite
Palm:	palmitoylation site
PBS:	phosphate buffered saline
PCI:	percutaneous coronary intervention
PDE:	phosphodiesterase
PDZ:	postsynaptic density protein 95/discs-large/zona occludens-1
PFA:	paraformaldehyde
PKG:	protein kinase G
PLN:	phospholamban
P <sub>minCMV</sub> :	minimal immediate early promoter of cytomegalovirus
PTP:	permeability transition pore
QH•:	ubisemiquinone
QH <sub>2</sub> :	ubiquinol
RNS:	reactive nitrogen species
ROS:	reactive oxygen species
RyR2:	ryanodine receptor 2
SERCA:	sarcoplasmic reticulum calcium ATPase
SH3:	Src homology 3
SO:	sulphite oxidase
SOD:	superoxide dismutase



---

TNF- $\alpha$ :	tumor necrosis factor alpha
TRE:	tetracycline-response element
tTA:	tetracycline-controlled transactivator
TTC:	triphenyl-tetrazolium-chlorid
TRIM:	1-/2-trimethylphenyl
UA:	uric acid
VSMC:	vascular smooth muscle cells
XDH:	xanthine dehydrogenase
XO:	xanthine oxidase
XOR:	xanthine oxidoreductase

## 8. Acknowledgments:

First, I would like to adress my gratitude to **Prof. Dr. med. Georg Ertl** for giving me the opportunity to do my PhD work at his institute.

Additionally, I thank **Prof. Dr. Thomas Dandekar**, my custodian from the faculty of biology. Without him, my external PhD study would not have been possible.

Especially, I want to thank **PD Dr. med. Oliver Ritter** for giving me the possibility to do my PhD study in his group and supporting me in critical situations. It was he, who gave me the opportunity to start my study in biomedicine while working as MTA in his group. Thank you.

A lot of thanks to my colleagues **Matthias Hallhuber, Claudia Gebhardt, Melanie Mühlfelder, Tatjana Williams, Paula Arias Loza, Martin Czolbe and Torsten Volkmar** for their motivating discussions and their help with technical assistance.

My very special thanks to **Jenny Muck**, who “has to” sit right beside me, for her support in difficult situations, not only in the lab but also in her leisure time. Thank you.

Moreover, I thank the following members of other research groups: **Prof. Georg Krohne, Nadja Blömer, Stefan Frantz, Ulrich Hofmann, Martin Link and Constanze Blume** for their help and cooperation.

I also thank **Evi Reichert** who was in charge of the animals, for her committed assignment to the mice in the animal house.

Very special thanks are adressed to my beloved husband **Martin**, who was extremely patient with me and accepted and supported my work whenever it was possible.

## 9. Curriculum Vitae:

### Personal Information

Name: Natalie Burkard  
Nationality: German  
Marital status: married  
Date of birth: 23.12.1977  
Place of birth: Würzburg, Germany  
Address of correspondence: Eduard-Buchner-Strasse 6  
97080 Würzburg  
e-mail: [Burkard\\_N@klinik.uni-wuerzburg.de](mailto:Burkard_N@klinik.uni-wuerzburg.de)  
[miraa@gmx.de](mailto:miraa@gmx.de)

### School Education

1984-1988 primary school Höchberg  
1988-1997 Röntgen Gymnasium Würzburg  
Diploma from German secondary school qualification for university admission (Abitur)

### Professional Education

1997-2000 Staatliche Berufsfachschule für technische Assistenten in der Medizin in Würzburg  
State examination

### **Occupational Activity**

2000-2008 working as MTA at the Clinic of the University of Wuerzburg, Department of Medicine I, Molecular Cardiology, working group PD Dr. med. Oliver Ritter

### **Academic studies**

WS 2003-SS 2006 study in Biomedicine at the Bayerischen Julius-Maximilians University of Wuerzburg

Certificate: Bachelor of Science

WS 2006-01/2008 study in Biomedicine at the Bayerischen Julius-Maximilians University of Wuerzburg

Certificate: Master of Science

Master thesis supervised by PD Dr. med. Oliver Ritter: The role of the neuronal NO synthase in the myocardium: conditional and cardiac specific nNOS overexpression decreases myocardial contractility

Since 02/2008 PhD student at the Bayerischen Julius-Maximilians University of Wuerzburg, Department of Medicine I, Molecular Biology; working group PD Dr. med. Oliver Ritter

Würzburg,

Natalie Burkard

---

**10. Publication list:**

1. **Burkard N, Williams T, Czolbe M, Blömer N, Panther F, Link M, Fraccarollo D, Widder J, Hu K, Han H, Hofmann U, Frantz F, Schuh K, Ritter O.** Conditional nitric oxide synthase is cardioprotective in ischemia-reperfusion. *Circulation* 2010 conditionally accepted
2. **Hofmann U, Burkard N, Vogt C, Thoma A, Frantz S, Ertl G, Ritter O, Bonz A.** Protective effects of sphingosin-1-phosphate receptor agonist treatment after myocardial ischemia-reperfusion. *Cardiovasc Res* 2009. **83(2):285-93**
3. **Burkard N, Rokita AG, Kaufmann SG, Hallhuber M, Wu R, Hu K, Hofmann U, Bonz A, Frantz S, Cartwright EJ, Neyses L, Maier LS, Maier SK, Renne T, Schuh K, Ritter O.** Conditional neuronal nitric oxide synthase overexpression impairs myocardial contractility. *Circ Res.* 2007 Feb 16; **100(3):e32-44**
4. **Smul TM, Lange M, Redel A, Burkard N, Roewer N, Kehl F.** Desflurane-induced preconditioning against myocardial infarction is mediated by nitric oxide. *Anesthesiology* 2006 Oct; **105(4):719-25**
5. **Hallhuber M, Burkard N, Wu R, Buch MH, Engelhardt S, Hein L, Neyses L, Schuh K, Ritter O.** Inhibition of nuclear import of calcineurin prevents myocardial hypertrophy. *Circ Res.* 2006 Sep 15; **99(6):626-35**
6. **Burkard N, Becher J, Heindl C, Neyses L, Schuh K, Ritter O.** Targeted proteolysis sustains calcineurin activation. *Circulation.* 2005 Mar 1; **111(8):1045-54**
7. **Ritter O, Schuh K, Brede M, Rothlein N, Burkard N, Hein L, Neyses L.** AT2 receptor activation regulates myocardial eNOS expression via the calcineurin-NF-AT pathway. *FASEB J.* 2003 Feb; **17(2):283-5**
8. **Ritter O, Bottez N, Burkard N, Schulte HD, Neyses L.** A molecular mechanism improving the contractile state in human myocardial hypertrophy. *Exp and clin cardiol.* 2002; **7(2): 151-57**